

NEW ALGEBRAIC FAST ALGORITHMS FOR N -BODY PROBLEMS IN TWO AND THREE DIMENSIONS

RITEESH KHAN* AND SIVARAM AMBIKASARAN†

Abstract. We present two new **algebraic** multilevel hierarchical matrix algorithms to perform fast matrix-vector product (MVP) for N -body problems in d dimensions, namely efficient \mathcal{H}_*^2 (fully nested algorithm, i.e., \mathcal{H}^2 matrix-like algorithm) and $(\mathcal{H}^2 + \mathcal{H})_*$ (semi-nested algorithm, i.e., cross of \mathcal{H}^2 and \mathcal{H} matrix-like algorithms). The efficient \mathcal{H}_*^2 and $(\mathcal{H}^2 + \mathcal{H})_*$ hierarchical representations are based on our recently introduced *weak admissibility* condition in higher dimensions [25], where the admissible clusters are the far-field and the **vertex-sharing** clusters. Due to the use of nested form of the bases, the proposed hierarchical matrix algorithms are more efficient than the non-nested algorithms (\mathcal{H} matrix algorithms). We rely on purely algebraic low-rank approximation techniques (e.g., ACA [5] and NCA [6, 36, 19]) and develop both algorithms in a black-box (kernel-independent) fashion. The initialization time of the proposed algorithms scales quasi-linearly¹. Using the proposed hierarchical representations, one can perform the MVP that scales at most quasi-linearly. Another noteworthy contribution of this article is that we perform a comparative study of the proposed algorithms with different **algebraic** (NCA or ACA-based compression) fast MVP algorithms (e.g., \mathcal{H}^2 , \mathcal{H} , etc) in 2D and 3D ($d = 2, 3$). The fast algorithms are tested on various kernel matrices and applied to get fast iterative solutions of a dense linear system arising from the discretized integral equations and radial basis function interpolation. The article also discusses the scalability of the algorithms and provides various benchmarks. Notably, all the algorithms are developed in a similar fashion in C++ and tested within the same environment, allowing for *meaningful comparisons*. The numerical results demonstrate that the proposed algorithms are competitive to the NCA-based standard \mathcal{H}^2 matrix algorithm [6, 36, 19] (where the admissible clusters are the far-field clusters) with respect to the memory and time. The C++ implementation of the proposed algorithms is available at <https://github.com/riteshkhan/H2weak/>.

Key words. N -body problems, Hierarchical matrices, Weak admissibility, \mathcal{H}^2 -matrices, ACA, Nested Cross Approximation

AMS subject classifications. 65F55, 65D12, 65R20, 65D05, 65R10

1. Introduction. Kernel matrices are frequently encountered in many fields such as PDEs [17, 23, 27], Gaussian processes [29], machine learning [16, 33], inverse problems [31], etc. These kernel matrices are usually large and dense. A direct evaluation of the product of a $N \times N$ kernel matrix with vector is prohibitive as its time and space complexity scale as $\mathcal{O}(N^2)$. However, these matrices possess block low-rank structures, which can be leveraged to store and perform matrix operations. The literature on the block low-rank matrices is vast, and we do not intend to review it here. Instead, we refer to a few selected articles [11, 9, 22, 35] and the books by Hackbusch [20] and Bebendorf [4].

In the past decades, various algorithms have been developed to perform the matrix-vector product efficiently. One of the first works in this area was the Barnes-Hut algorithm [3] or Tree code, which reduces the matrix-vector product complexity from $\mathcal{O}(N^2)$ to $\mathcal{O}(N \log(N))$. Greengard and Rokhlin propose the Fast Multipole Method (from now on abbreviated as FMM) [17, 18], which further reduces the matrix-vector product cost to $\mathcal{O}(N)$. After that, various FMM-like kernel-independent algorithms [34] were proposed, primarily based on analytic expansions. Hackbusch and collaborators [9, 8] are the pioneers in interpreting certain sub-blocks (sub-matrices) of the matrices arising from N -body problems as low-rank and provide an important theoretical framework. In [9, 8, 15], they discuss the standard (or strong) admissibility condition, i.e., where the separation distance between two clusters exceeds the diameter of either cluster. It is to be noted that the FMM (equivalent to \mathcal{H}^2 matrix with standard admissibility) and the Tree code (equivalent to \mathcal{H} matrix with standard admissibility) are based on the standard or strong admissibility condition. In their subsequent work [21], they introduce the notion of weak admissibility condition for one-dimensional problems. This article shows that the rank of interaction between the neighboring intervals in 1D does not scale as a positive power of N , and consequently, the neighboring or non-overlapping intervals are admissible. HODLR [1, 2], HSS [32, 11] and HBS [14] matrices belong to the category of \mathcal{H} matrix based on this weak admissibility condition. However, the work [21] does not discuss the notion of weak admissibility condition in higher dimensions. A straightforward extension of this idea, i.e., compressing all the non-self interactions, does not result in a quasi-linear matrix-vector product algorithm in d dimensions ($d > 1$) since the rank of the nearby clusters grows as $\mathcal{O}(N^{(d-1)/d} \log(N))$ [23, 24, 25].

*Department of Mathematics, IIT Madras, Chennai, India. khanritesh28@gmail.com

† Department of Data Science & Artificial Intelligence, Wadhvani School of Data Science & Artificial Intelligence, Department of Mathematics and IIT Madras, Chennai, India. sivaambi@alumni.stanford.edu

¹ $\mathcal{O}(N \log^\alpha(N))$, $\alpha \geq 0$ and small.

In our recent work [25], we have shown that the rank of the far-field and the vertex-sharing interactions do not scale with any positive power of N . Hence, admissibility of the far-field and the vertex-sharing clusters *could be* a way to extend the notion of *weak admissibility* condition in higher dimensions. Based on this *weak admissibility* condition, we developed a matrix-vector product algorithm in d dimensions with quasi-linear complexity, namely the hierarchically off-diagonal low-rank matrix in d dimensions or HODLR d D. HODLR d D is a special type of \mathcal{H} matrix, and in this article, we denote it as \mathcal{H}_* from now on.

*Our main focus in this article is to develop nested bases algorithms in a **purely algebraic** way, which are based on our weak admissibility condition (admissible clusters are the far-field and vertex-sharing clusters).*

In this article, we present two new hierarchical matrix algorithms with **nested bases** for fast MVP in d dimensions. The first algorithm we propose is efficient \mathcal{H}_*^2 , which is a *special* subclass of the \mathcal{H}^2 matrices. Due to the use of nested form of the bases, the time and space complexities are reduced compared to the \mathcal{H}_* algorithm. The numerical experiments in 2D and 3D show that the efficient \mathcal{H}_*^2 algorithm is competitive to the NCA-based standard \mathcal{H}^2 matrix algorithm [36, 19] with respect to the MVP time and space complexity. The second algorithm we develop in this article is a *semi-nested*¹ algorithm, denoted as $(\mathcal{H}^2 + \mathcal{H})_*$. The $(\mathcal{H}^2 + \mathcal{H})_*$ algorithm can be thought of as a cross of \mathcal{H}^2 and \mathcal{H} like matrices. We develop all the algorithms in this article using purely algebraic techniques (ACA [5] or NCA [36, 19]), making them kernel-independent.

2. Related works and novelty of our work. The kernel matrices arising out of N -body problems usually possess block low-rank structure, i.e., certain sub-blocks of these matrices can be approximated by a low-rank representation. The construction of the low-rank approximation has been studied extensively. One can categorize the low-rank approximation techniques into two classes: (i) Analytic techniques (Analytic series expansions [17, 18], Interpolation [13], etc.) and (ii) Algebraic techniques (SVD, RRQR [12], RRLU [28], ACA [5], etc.). Both the analytic and algebraic techniques have their advantages and disadvantages.

The popular FMM algorithms [17, 18, 34, 13] and the widely used FMM libraries (FMM3D, bbFMM [13], PVFMM [26]) are mainly based on analytic techniques. All these analytic FMM algorithms require very minimal pre-computation/initialization/assembly time for translation invariant and homogeneous kernels. The majority of their time is spent on performing the MVP. Also, for the translation invariant and homogeneous kernels the storage requirement is less. However, in higher dimensions with a general kernel function, the storage requirement becomes high since the analytic compression rank is high. In this case, the translation matrices/operators need special attention (further compression using algebraic techniques like SVD) to reduce the storage, resulting in an increase in initialization time.

On the other hand, algebraic techniques are popular due to their wide range of applicability (in terms of domain and problem specification) and better compression than their purely analytic counterparts. If the algebraic techniques are employed to construct the standard \mathcal{H}^2 matrix, the \mathcal{H}^2 matrix-vector product can be viewed as an algebraic variant of the FMM. Since the algebraic compression rank is usually lower than the purely analytic compression rank, algebraic \mathcal{H}^2 MVP is faster than a purely analytic FMM. However, the downside of algebraic techniques is that they usually have a longer \mathcal{H}^2 matrix initialization time than the analytic techniques for translation invariant and homogeneous kernels. Nevertheless, the algebraic \mathcal{H}^2 matrix is more effective when performing multiple MVPs for a wide range of problems.

We want to summarize the reasons for choosing algebraic techniques.

1. Algebraic techniques only require access to the matrix entries and can be used in a kernel-independent (black-box) fashion; they neither need any series expansions of the underlying kernel function nor the knowledge of the kernel function.
2. The rank of the compressed blocks obtained using algebraic techniques is usually lower than that obtained from purely analytic techniques, as algebraic techniques are domain and problem-specific.
3. Algebraic techniques are more efficient than analytical techniques when dealing with data sets of higher dimensions.
4. This article focuses on developing efficient nested hierarchical matrix representations based on a *weak admissibility* condition [25], where the distance between two admissible clusters can be zero. Algebraic techniques are useful in this case.

The main focus of this article is to develop *new* nested hierarchical MVP algorithms in

¹We term it semi-nested because nested bases are employed for the **partial** interaction list of a cluster, while non-nested bases are used for the remaining interaction list

a *purely algebraic way*. Hence, we believe that it would be fair to compare the proposed algorithms with the related algebraic \mathcal{H}^2 MVP algorithms [6, 36, 19].

This section discusses some existing works that study different algebraic techniques and those that are in line with this article.

The \mathcal{H} -matrix [21, 20] is one of the most commonly used frameworks to handle the large dense matrices arising from the N -body problems. Though the \mathcal{H} matrix algorithm is fast, it can be further accelerated using the nested form of the bases, which leads to \mathcal{H}^2 matrix algorithm [7, 8]. It has been demonstrated that the \mathcal{H}^2 matrix is a more efficient framework than the \mathcal{H} matrix regarding time and storage. Several kernel-independent algorithms have been developed to construct the \mathcal{H}^2 matrix efficiently. Börm [7] proposes an $\mathcal{O}(N \log(N))$ algorithm to construct \mathcal{H}^2 matrix in a purely algebraic way without storing the entire matrix. The projection-based algebraic Nested Cross Approximation (NCA) was introduced in [6]. The NCA is a variant of the Adaptive Cross Approximation (ACA) [5] that gives the nested basis for the \mathcal{H}^2 matrix. Bebendorf et al. [6] choose indices of points close to the Chebyshev grids and perform ACA upon them to obtain the pivots in a top-bottom fashion, leading to complexity $\mathcal{O}(N \log(N))$. However, [6] required the geometrical information of clusters to find the pivots. Zhao et al. [36] develop two **purely algebraic** NCA algorithms. They first propose an $\mathcal{O}(N \log(N))$ algorithm to find the pivots, which involves a similar approach (top-bottom tree traversal) like [6] but without the geometrical information of clusters. They also develop another algorithm that involves a bottom-top tree traversal to find the local pivots followed by a top-bottom tree traversal to find the global pivots. The overall complexity of this algorithm reduces to $\mathcal{O}(N)$. Gujjula et al. [19] propose a NCA with complexity $\mathcal{O}(N)$, where they show that one can eliminate the global pivots selection step in [36], i.e., only the bottom-top traversal is sufficient (local pivots are enough), the subsequent top-bottom tree traversal could be redundant (which finds global pivots) without substantial change in the relative error. This makes their NCA slightly computationally faster than the [36]. They also compare their NCA algorithm with [6, 36] and present various benchmarks. We use similar NCAs as in [36, 19] to construct our algorithms, but directly applying them on our *weak admissibility* condition in higher dimensions [25] (far-field and vertex-sharing clusters are the admissible clusters) will not produce an **efficient** nested bases algorithm.

The most important difference between the existing works and ours is that in d dimensions ($d > 1$), the existing algorithms convert the \mathcal{H} matrix based on the strong/standard admissibility condition to the \mathcal{H}^2 matrix with the same strong/standard admissibility condition or directly construct the \mathcal{H}^2 matrix. In comparison, this article presents an efficient way to construct a hierarchical matrix algorithm with nested bases (\mathcal{H}_*^2), which is based on a *weak admissibility* condition in higher dimensions [25] (the admissible clusters include the vertex-sharing clusters and the distance between two clusters sharing a vertex is zero). It is by no means a trivial task to construct such a nested hierarchical representation efficiently. We have shown in [25] that a *weak admissibility*-based \mathcal{H}_* representation is competitive with the strong admissibility-based standard \mathcal{H} representation (ACA-based compression). This article will also investigate whether the proposed efficient \mathcal{H}_*^2 representation is competitive with the NCA-based standard \mathcal{H}^2 representation. Furthermore, we present a semi-nested hierarchical representation, $(\mathcal{H}^2 + \mathcal{H})_*$, which is also based on our *weak admissibility* condition in higher dimensions [25].

Main highlights of the article: The following are the main highlights of this article.

1. We propose a fully nested **efficient** hierarchical matrix algorithm based on our *weak admissibility* condition in higher dimensions [25]. To construct it, we use a combination of NCA with bottom-top and top-bottom pivot selection with an appropriate partitioning of the interaction list. We refer to this algorithm as efficient $\mathcal{H}_*^2 / \mathcal{H}_*^2(\text{b+t})$. The numerical results show that the $\mathcal{H}_*^2(\text{b+t})$ algorithm performs much better than the \mathcal{H}_* algorithm [25] and is competitive to the NCA-based standard \mathcal{H}^2 matrix [36] in d dimensions with respect to the memory and MVP time.
2. The second hierarchical matrix algorithm we propose is the $(\mathcal{H}^2 + \mathcal{H})_*$, which is a **semi-nested** algorithm based on our *weak admissibility* condition in higher dimensions [25]. The $(\mathcal{H}^2 + \mathcal{H})_*$ could be considered as a cross of \mathcal{H}^2 and \mathcal{H} matrix-like algorithms. We rely on the NCA and ACA to build the $(\mathcal{H}^2 + \mathcal{H})_*$ representation. The numerical results show that the $(\mathcal{H}^2 + \mathcal{H})_*$ algorithm performs

better than the \mathcal{H}_* algorithm, and in 3D, it is competitive to the NCA-based standard \mathcal{H}^2 matrix [36] with respect to the memory and MVP time.

3. We report the performance of the proposed algorithms for various kernel matrix-vector products. In 2D, we choose the single-layer Laplacian. In 3D, we choose the single-layer Laplacian, Matérn covariance kernel and Helmholtz kernel (wave number $k = 1$).
4. We apply the proposed fast MVP algorithms to solve integral equations and radial basis function (RBF) interpolation in 2D and 3D using fast iterative solver. In each experiment, we compare the performance of the proposed algorithms with standard \mathcal{H}^2 matrix algorithm [36, 19] and discuss their scalability. Additionally, in 3D, we report the performance of the proposed algorithms for various non-translation invariant kernels. All the algorithms are implemented in the same fashion using C++ and tested within the same environment, allowing for meaningful comparisons.
5. Finally, as a part of this article, we would also like to release the C++ implementation of the proposed algorithms made available at <https://github.com/riteshkhan/H2weak/>.

Outline of the article. The rest of the article is organized as follows. In Section 3, we discuss different hierarchical representations used in this article with a summary of NCA. In Section 4, we discuss the applicability of NCA with various pivot selection strategies on our *weak admissibility* condition. The Section 5 discusses the proposed hierarchical matrix algorithms to perform fast MVP and their complexity analysis. In Section 6, we perform various numerical experiments in 2D and 3D and compare the performance of the proposed algorithms with related purely algebraic hierarchical matrix algorithms. Finally, we conclude in Section 7.

3. Preliminaries. In this section, we describe the tree data structure used to build the different hierarchical matrix algorithms and briefly discuss various hierarchical representations used in this article. A brief discussion on Nested Cross Approximation (NCA) to construct \mathcal{H}^2 matrices is also included.

3.1. Construction of the 2^d tree. Let $C \subset \mathbb{R}^d$ be a compact hyper-cube, which contains the N particles. To exploit the hierarchical representations, we need to subdivide the hyper-cube C (computational domain). Depending upon the particle distribution or requirement, one can use different trees like 2^d uniform tree (or balanced tree), adaptive 2^d tree, level restricted 2^d tree, K-d tree, etc. **But for simplicity, we consider the 2^d uniform tree (for $d = 1, 2$ and 3, it is binary, quad and oct tree, respectively) in this article.** At level 0 of the tree is the hyper-cube C itself (root level). A hyper-cube at a level l is subdivided into 2^d finer hyper-cubes belonging to level $(l + 1)$ of the tree. The former is called the parent of the latter, and the latter (finer hyper-cubes) are the children of the former (coarser hyper-cube). We define cluster $\mathcal{C}^{(l)}$ as containing all the particles inside a hyper-cube at level l . In Figure 1, we illustrate the uniform quad tree at different levels in 2D. We stop the sub-division at a level κ of the tree when each finest hyper-cube contains at most n_{max} particles, where n_{max} is a user-specified threshold that defines the maximum number of particles at each finest hyper-cube. The total $2^{d\kappa}$ finest hyper-cubes at level κ are called the leaves. Note that, $N \leq n_{max}2^{d\kappa} \implies \kappa = \lceil \log_{2^d}(N/n_{max}) \rceil$.

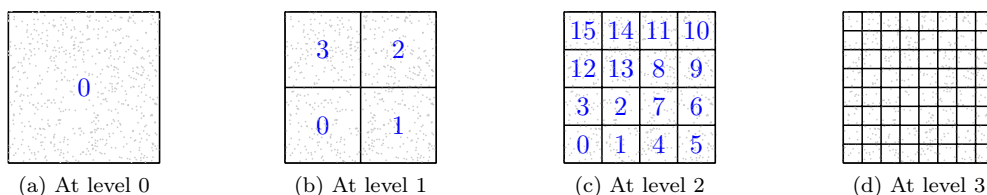


FIG. 1. Hierarchical subdivision of the computational domain C using 2^d uniform tree and the numbering convention followed in this article at different levels ($d = 2$).

3.2. Definition. The diameter of a cluster and the distance between two clusters are defined as follows:

- The diameter of a cluster X is given by

$$(3.1) \quad \text{diam}(X) = \sup\{\|u - v\|_2 : u, v \in X\}$$

- The distance between two clusters X and Y is given by

$$(3.2) \quad \text{dist}(X, Y) = \inf\{\|x - y\|_2 : x \in X, y \in Y\}$$

3.3. \mathcal{H} -matrix based on the standard/strong admissibility condition. The \mathcal{H} -matrix with strong admissibility condition is the hierarchical low-rank representation whose admissible clusters are the far-field or well-separated clusters (at least one box/cluster away).

Standard/strong admissibility condition. Two clusters X and Y at the same level of the 2^d tree are admissible iff

$$(3.3) \quad \min(\text{diam}(X), \text{diam}(Y)) \leq \eta \text{ dist}(X, Y) \implies \frac{\min(\text{diam}(X), \text{diam}(Y))}{\text{dist}(X, Y)} \leq \eta$$

In this article, we set $\eta = \sqrt{d}$ in the admissibility condition (3.3), where d is the underlying dimension. Specifically, $\eta = \sqrt{2}$ and $\sqrt{3}$ for 2D and 3D, respectively. **The \mathcal{H} and \mathcal{H}^2 matrices discussed in this article are the standard \mathcal{H} and \mathcal{H}^2 matrices, denoted as $\mathcal{H}_{\sqrt{d}}$ and $\mathcal{H}^2_{\sqrt{d}}$, respectively.** We use the number “ \sqrt{d} ” in the subscript to indicate that the hierarchical representation is based on the standard/strong admissibility condition (3.3) with $\eta = \sqrt{d}$. We denote the interaction list of a cluster \mathcal{C} in $\mathcal{H}_{\sqrt{d}}$ and $\mathcal{H}^2_{\sqrt{d}}$ representations as $\mathcal{IL}_{\sqrt{d}}(\mathcal{C})$, which contains the far-field clusters (at least one box away). For a cluster \mathcal{C} , the self cluster and its neighbors clusters collectively form the near-field list, denoted by $\mathcal{N}_{\sqrt{d}}(\mathcal{C})$ in $\mathcal{H}_{\sqrt{d}}$ and $\mathcal{H}^2_{\sqrt{d}}$ representations. Note that the $\mathcal{H}^2_{\sqrt{d}}$ matrix is identical to the balanced FMM structure. The neighbors and the interaction list for $\eta = \sqrt{d}$ (in 2D, $d = 2$) at different levels of the tree are illustrated in Figure 2. The $\mathcal{H}_{\sqrt{d}}$ matrix in 2D at different levels is depicted in Figure 3.

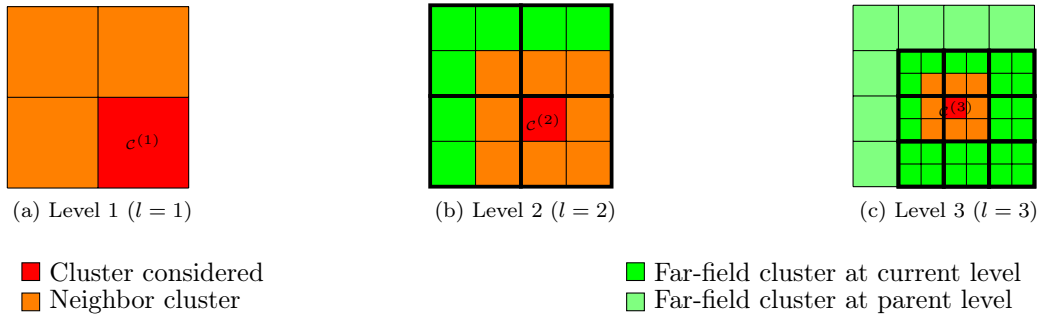


FIG. 2. The neighbors and the interaction list of cluster $\mathcal{C}^{(l)}$ ($\mathcal{IL}_{\sqrt{d}}(\mathcal{C}^{(l)})$ consists of the far-field clusters) for $\eta = \sqrt{d}$ in (3.3) at level l (in 2D, $d = 2$). The superscript “ l ” denotes the level of the uniform quad tree. The admissible clusters are the green colored clusters enclosed within a noticeable **black** border. The lighter shade colors represent the admissible clusters at the coarser levels (no admissible cluster at the level 1).

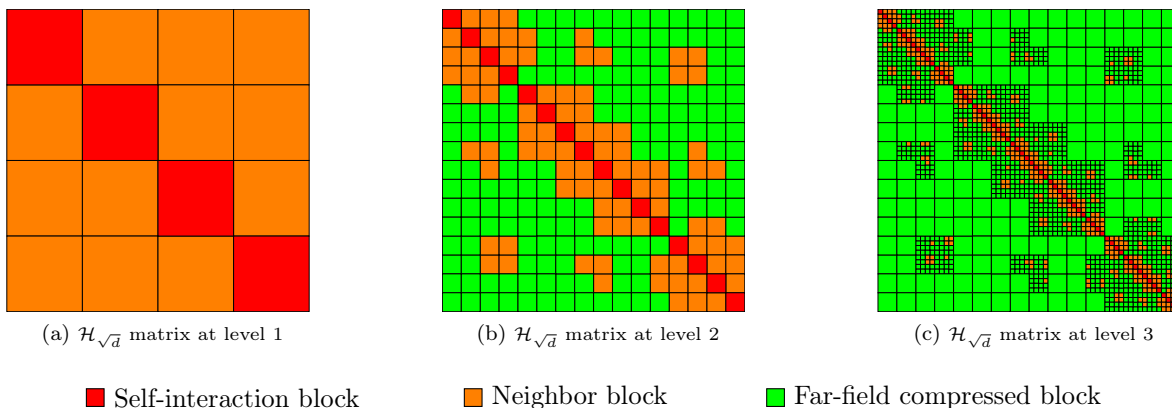


FIG. 3. $\mathcal{H}_{\sqrt{d}}$ in 2D at the level l , where $l = 1, 2, 3$ (no compression at the level 1).

3.4. \mathcal{H} -matrix based on Hackbusch’s weak admissibility condition. Hackbusch et al. [21] first introduced the notion of weak admissibility for one-dimensional problems, where they compress the sub-matrices corresponding to the adjacent intervals (clusters). This notion of weak admissibility doesn’t look at the distance between the clusters; rather, it is defined as two non-overlapping clusters being admissible. To be more precise, in terms of matrix setting, this represents all the off-diagonal sub-matrices as low-rank. HODLR (non-nested) [1, 2], HSS (nested) [32, 11] and HBS [14] belong to the category of the hierarchical matrix based on Hackbusch’s weak admissibility condition.

The article [21] discusses the notion of weak admissibility only for one-dimensional problems. It does not discuss the notion of weak admissibility in higher dimensions ($d > 1$) (though they mention in [21] that higher dimensional/multi-dimensional case will be considered later and refer to an article in the bibliography. However, to the best of our knowledge and searches, the article was never published or is available to the public). A straightforward extension of the notion of weak admissibility discussed in [21, 20] to higher dimensions ($d > 1$), i.e., compressing all the off-diagonal sub-matrices, will not result in a quasi-linear complexity hierarchical matrix algorithm. This is because, in higher dimensions, except for the vertex-sharing interaction sub-matrix, the rank of all other adjacent interactions sub-matrices grows with some positive power of N [23, 24, 25]. Therefore, the notion of weak admissibility introduced by Hackbusch is fine for the one-dimensional problems but needs to be revised for the higher-dimensional problems.

3.5. \mathcal{H} -matrix based on our *weak admissibility* condition in higher dimensions. The article [24] by our group shows that for the 2D Green’s function, the rank of not just the far-field but also the *vertex-sharing* interaction sub-matrices do not scale with any positive power of N and introduces HODLR2D hierarchical representation based on it. In our recent article [25], we generalize this for any non-oscillatory translation invariant kernel function in d dimensions and propose that the admissibility of *far-field* and *vertex-sharing* clusters could be considered a way to extend the notion of *weak admissibility* in higher dimensions. We also develop a hierarchical representation, namely HODLR d D [25], based on our proposed *weak admissibility* condition. The HODLR d D is a non-nested algorithm, i.e., clusters’ bases are non-nested with complexity $\mathcal{O}(pN \log(N))$, where $p \in \mathcal{O}(\log(N) \log^d(\log(N)))$. As mentioned earlier, we refer to HODLR d D as \mathcal{H}_* in this article. We use the subscript “*” to indicate that the hierarchical representation is based on our *weak admissibility* condition in higher dimensions, i.e., the admissible clusters are *far-field* and *vertex-sharing* clusters.

Let’s discuss the interaction list of a cluster $\mathcal{C}^{(l)}$ at level l of the 2^d tree, denoted as $\mathcal{IL}_*(\mathcal{C}^{(l)})$. We consider the 2D case for its simplicity in pictorial representation, but it is important to note that this article also considers the 3D case. We classify three different sets of clusters at the same level l :

(i) set of far-field/well-separated clusters (at least one cluster away from $\mathcal{C}^{(l)}$) denoted as $\mathcal{F}(\mathcal{C}^{(l)})$, (ii) set of clusters share a vertex with $\mathcal{C}^{(l)}$ denoted as $\mathcal{V}(\mathcal{C}^{(l)})$ and (iii) set of clusters share an edge with $\mathcal{C}^{(l)}$ denoted as $\mathcal{E}(\mathcal{C}^{(l)})$.

Let $child(\mathcal{C}^{(l)})$, $siblings(\mathcal{C}^{(l)})$ and $parent(\mathcal{C}^{(l)})$ denote the child, siblings and parent of the cluster $\mathcal{C}^{(l)}$, respectively. We also define the clan set of the cluster $\mathcal{C}^{(l)}$ as follows:

$$(3.4) \quad \mathit{clan}(\mathcal{C}^{(l)}) = \{siblings(\mathcal{C}^{(l)})\} \cup \{child(P) : P \in \mathcal{E}(parent(\mathcal{C}^{(l)}))\}$$

For the \mathcal{H}_* representation in 2D, the interaction list of the cluster $\mathcal{C}^{(l)}$ is given by

$$(3.5) \quad \mathcal{IL}_*(\mathcal{C}^{(l)}) = \mathit{clan}(\mathcal{C}^{(l)}) \cap (\mathcal{V}(\mathcal{C}^{(l)}) \cup \mathcal{F}(\mathcal{C}^{(l)}))$$

and the neighbors set of the cluster $\mathcal{C}^{(l)}$ is given by $\mathcal{E}(\mathcal{C}^{(l)})$.

The neighbors and the self cluster, i.e., the inadmissible clusters, collectively form the near-field list of $\mathcal{C}^{(l)}$, which is given by

$$(3.6) \quad \mathcal{N}_*(\mathcal{C}^{(l)}) = \mathcal{E}(\mathcal{C}^{(l)}) \cup \mathcal{C}^{(l)}$$

The Figure 4, illustrates the neighbors and the interaction list at different levels of the tree for our *weak admissibility* condition in 2D. The \mathcal{H}_* matrix in 2D at different levels is depicted in Figure 5.

In article [25], we extend the notion of *weak admissibility* condition to any dimension d as follows:

Weak admissibility condition in d dimensions. *Two clusters X and Y at the same level of the 2^d tree are admissible iff they share at the most a vertex, or equivalently, they do not share d' hyper-surface ($d' > 0$).*

The interaction list and the near-field list for this *weak admissibility* condition in d dimensions are given in Table 3.

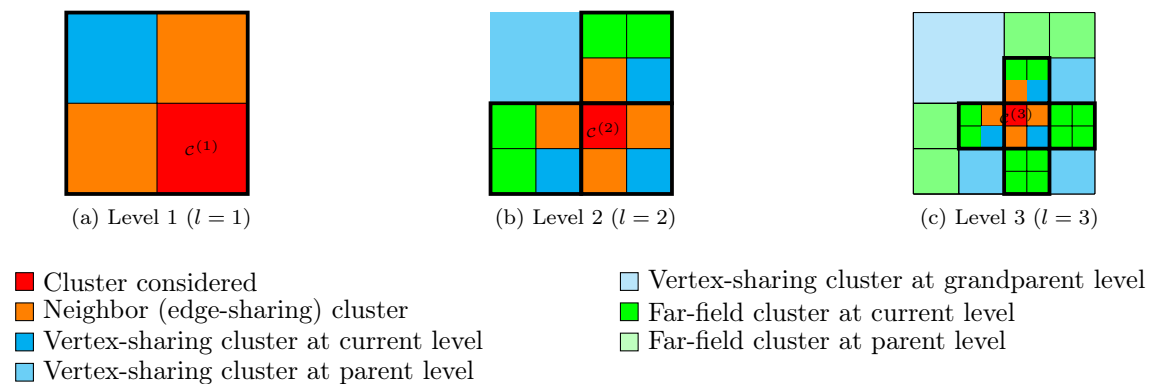


FIG. 4. The neighbors and the interaction list of cluster $\mathcal{C}^{(l)}$ ($\mathcal{IL}_*(\mathcal{C}^{(l)})$ consists of vertex-sharing and far-field clusters) for our *weak admissibility* condition in 2D at level l . The superscript “ l ” denotes the level of the uniform quad tree. The admissible clusters are the green and cyan colored clusters enclosed within a noticeable **black** border. The lighter shade colors represent the admissible clusters at the coarser levels.

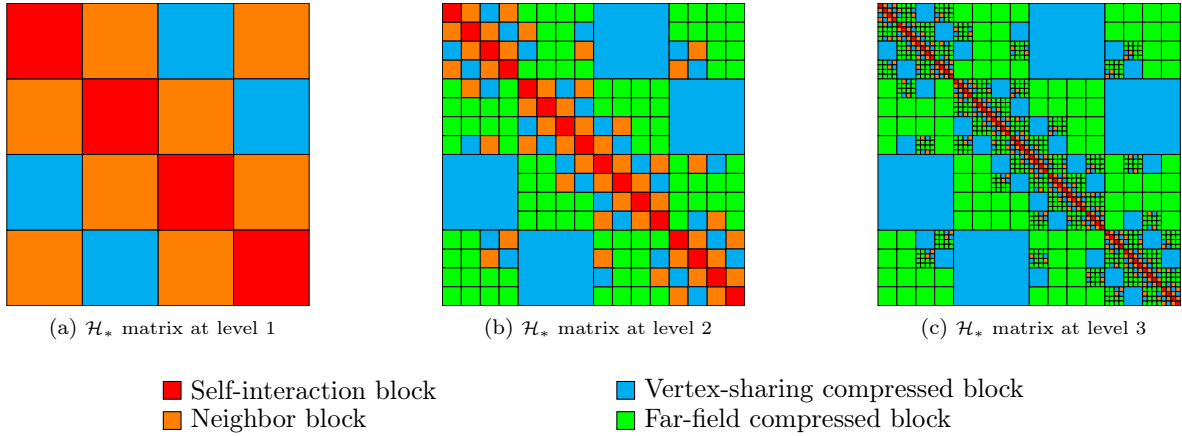


FIG. 5. The \mathcal{H}_* matrix in 2D at the level l , where $l = 1, 2, 3$ (no far-field compression at the level 1).

It is to be noted that the \mathcal{H}_* representation does not satisfy the standard/strong admissibility condition (3.3) because the distance (3.2) between two vertex-sharing clusters (admissible clusters include vertex-sharing clusters) is zero as they share a common point. To be more precise, let X and Y be two clusters at the same level of the tree with $Y \in \mathcal{IL}_*(X)$. If X and Y share a vertex, then $\text{dist}(X, Y) = 0$. Given that the $\text{dist}(X, Y) = 0$, no real value of η would generate the \mathcal{H}_* representation from (3.3).

Maximum size of interaction list ($\mathcal{IL}_*(\mathcal{C})$) and near-field list ($\mathcal{N}_*(\mathcal{C})$). Let us find the maximum possible size of the interaction list and the near-field list (neighbors + self) of a cluster \mathcal{C} for the \mathcal{H}_* representation.

In 2D, a square can have maximum 4 edges. Therefore, the maximum size of the near-field list is

$$(3.7) \quad \#\mathcal{N}_*(\mathcal{C}) = (\#\text{edges} + \#\text{self}) = 4 + 1 = 5$$

Note that $\#\text{self}$ denotes the number of self-interaction or the cluster considered, which is 1.

The maximum size of the interaction list corresponding \mathcal{C} is

$$(3.8) \quad \#\mathcal{IL}_*(\mathcal{C}) = (2^2 \times \#\mathcal{N}_*(\mathcal{C})) - \#\mathcal{N}_*(\mathcal{C}) = (4 \times 5) - 5 = 15$$

Out of a total of 15 interactions, 3 are vertex-sharing interactions, and 12 are far-field interactions (Figure 4c).

Similarly, in 3D, a cube can have maximum 12 edges and 6 faces. Therefore, the maximum size of the near-field list is

$$(3.9) \quad \#\mathcal{N}_*(\mathcal{C}) = (\#\text{edges} + \#\text{faces} + \#\text{self}) = 12 + 6 + 1 = 19$$

The maximum size of the interaction list corresponding \mathcal{C} is

$$(3.10) \quad \#\mathcal{IL}_*(\mathcal{C}) = (2^3 \times \#\mathcal{N}_*(\mathcal{C})) - \#\mathcal{N}_*(\mathcal{C}) = (8 \times 19) - 19 = 133$$

Out of a total of 133 interactions, 7 are the vertex-sharing interactions, and 126 are the far-field interactions.

One can get a closed-form formula for the maximum possible size of the interaction list and the near-field list of a cluster in d dimensions for the \mathcal{H}_* representation. The maximum size of the near-field list is

$$(3.11) \quad \#\mathcal{N}_*(\mathcal{C}) = (3^d - 2^d)$$

and the maximum size of the interaction list is

$$(3.12) \quad \#\mathcal{IL}_*(\mathcal{C}) = (2^d \times \#\mathcal{N}_*(\mathcal{C})) - \#\mathcal{N}_*(\mathcal{C}) = (3^d - 2^d)(2^d - 1) = 6^d - 4^d - 3^d + 2^d$$

Out of a total of $(6^d - 4^d - 3^d + 2^d)$ interactions, $(2^d - 1)$ are the vertex-sharing interactions and remaining $(6^d - 4^d - 3^d + 1)$ are the far-field interactions.

Remark 3.1. The \mathcal{H}_* matrix (Figure 5) has a couple of advantages compared to the $\mathcal{H}_{\sqrt{d}}$ matrix (Figure 3), as given below.

1. In the \mathcal{H}_* matrix, the maximum possible size of the interaction list corresponding to a cluster is $(6^d - 4^d - 3^d + 2^d)$, whereas for the $\mathcal{H}_{\sqrt{d}}$ matrix, the maximum possible size of the interaction list is $(6^d - 3^d)$. Therefore, the size of the interaction list of the \mathcal{H}_* is slightly smaller than that of the $\mathcal{H}_{\sqrt{d}}$ matrix. This is visible from Figure 4c and Figure 2c.
2. \mathcal{H}_* and $\mathcal{H}_{\sqrt{d}}$ matrices perform $(3^d - 2^d)$ and 3^d dense matrix computations at leaf level, respectively. Therefore, \mathcal{H}_* performs less dense matrix computations than the $\mathcal{H}_{\sqrt{d}}$ at the leaf level.

3.6. The Nested Cross Approximation (NCA) for \mathcal{H}^2 -matrices. The \mathcal{H} matrix algorithm can be further accelerated using the nested form of the cluster bases, which leads to the \mathcal{H}^2 matrix algorithm. As we rely on the algebraic techniques in this article, this subsection briefly discusses algebraic ways called NCA to construct \mathcal{H}^2 matrix. Let X and Y be two clusters (hyper-cubes) which belong to the 2^d tree. Let t^X and s^Y be the index sets that store the indices of points $x(\in X)$ and $y(\in Y)$, respectively.

$$(3.13) \quad t^X = \{i : x_i \in X\} \text{ and } s^Y = \{j : y_j \in Y\}$$

Let K_{t^X, s^Y} be the matrix sub-block that captures the interaction between the clusters, whose $(i, j)^{th}$ entry is given by $K_{t^X, s^Y}(i, j) = K(t^X(i), s^Y(j))$. If the cluster Y is in the interaction list of the cluster X , i.e., $Y \in \mathcal{IL}_\eta(X)$ ($\mathcal{IL}_\eta(X)$ denotes the interaction list of X generated from (3.3) for a value $\eta > 0$), then K_{t^X, s^Y} is called admissible sub-block. The admissible sub-block K_{t^X, s^Y} can be approximated by ACA [5, 6] as follows:

$$(3.14) \quad K_{t^X, s^Y} \approx K_{t^X, s^Y}^{(p)} = UV^* = K_{t^X, \sigma^Y} (K_{\tau^X, \sigma^Y})^{-1} K_{\tau^X, s^Y}$$

where $\tau^X \subset t^X$ and $\sigma^Y \subset s^Y$ are called the *row* and *column* pivots, respectively and the matrix $K_{t^X, s^Y}^{(p)}$ is the p^{th} update of the original matrix K_{t^X, s^Y} . Here, we use the partially pivoted ACA algorithm [5], where for a user-specified tolerance ϵ , the iteration stops if the following condition is true

$$(3.15) \quad \|u_p\|_2 \|v_p\|_2 \leq \epsilon \left\| K_{t^X, s^Y}^{(p)} \right\|_F$$

where u_p and v_p are the p^{th} column vectors of the matrices U and V , respectively. The ACA-based \mathcal{H} matrix-like fast algorithm leads to a complexity of $\mathcal{O}(N \log(N))$. One needs an algorithm that exploits the nestedness among the admissible clusters to achieve a lower complexity, so the NCA was proposed [6, 36, 19]. The validation of NCA, along with numerical error analysis, is presented in [6]. Let $\mathcal{A}(\mathcal{C})$ denote the union of all the clusters forming the interaction list ($\mathcal{IL}_\eta(\mathcal{C})$) at the same level and the clusters that form the interaction list with \mathcal{C} 's ancestors at the lower (coarser) level of the tree. The low-rank approximation via NCA takes the following form [6, 36, 19]

$$(3.16) \quad K_{t^X, s^Y} \approx \underbrace{K_{t^X, s^{X,i}} (K_{t^X, i, s^{X,i}})^{-1}}_{U_X} \underbrace{K_{t^X, i, s^{Y,o}} (K_{t^Y, o, s^{Y,o}})^{-1}}_{T_{X,Y}} \underbrace{K_{t^Y, o, s^Y}}_{V_Y^*}$$

where $t^{X,i} \subset t^X$, $s^{X,i} \subset \mathcal{A}^{X,i}$ and $t^{Y,o} \subset \mathcal{A}^{Y,o}$, $s^{Y,o} \subset s^Y$. The sets $\mathcal{A}^{X,i}$ and $\mathcal{A}^{Y,o}$ are defined as

$$(3.17) \quad \mathcal{A}^{X,i} = \{s^{X'} : X' \in \mathcal{A}(X)\} \text{ and } \mathcal{A}^{Y,o} = \{t^{Y'} : Y' \in \mathcal{A}(Y)\}$$

$t^{X,i}$ and $s^{X,i}$ are termed as *incoming row pivots* and *incoming column pivots* of X , respectively. $t^{Y,o}$ and $s^{Y,o}$ are termed as *outgoing row pivots* and *outgoing column pivots* of Y , respectively. The U_X and V_Y^* in Equation (3.16) are the column basis of X and the row basis of Y , respectively.

It is to be noted that if the matrix K_{t^X, s^Y} is admissible, then so is K_{t^Y, s^X} and the low-rank approximation via NCA takes the form

$$(3.18) \quad K_{t^Y, s^X} \approx \underbrace{K_{t^Y, s^{Y,i}} (K_{t^Y, i, s^{Y,i}})^{-1}}_{U_Y} \underbrace{K_{t^Y, i, s^{X,o}} (K_{t^X, o, s^{X,o}})^{-1}}_{T_{Y,X}} \underbrace{K_{t^X, o, s^X}}_{V_X^*}$$

where $t^{Y,i} \subset t^Y$, $s^{Y,i} \subset \mathcal{A}^{Y,i}$ and $t^{X,o} \subset \mathcal{A}^{X,o}$, $s^{X,o} \subset s^X$.

Therefore, a cluster X has four sets of pivots: (i) $t^{X,i} \subset t^X$, (ii) $s^{X,i} \subset \mathcal{A}^{X,i}$, (iii) $t^{X,o} \subset \mathcal{A}^{X,o}$ and (iv) $s^{X,o} \subset s^X$ with the bases U_X and V_X^* .

3.6.1. Various pivots selection strategies. The efficiency (accuracy) of NCA depends on the strategy employed for selecting the pivots that represent the blocks at a specific level of the tree.

Bebendorf et al. [6] first introduce projection-based algebraic NCA. They choose indices of points close to the predefined Chebyshev grids and perform ACA upon it to obtain the pivots, and this involves a top to bottom (T2B) traversal of the 2^d tree. The overall complexity to generate \mathcal{H}^2 matrix representation using this method is $\mathcal{O}(N \log(N))$.

Zhao et al. [36] avoid the geometrical projection to find the pivots and propose two purely algebraic NCAs based on different pivot selection strategies. They first discuss an $\mathcal{O}(N \log(N))$ NCA algorithm to generate \mathcal{H}^2 matrix representation. In this algorithm, the pivots are obtained by traversing the 2^d tree from top to bottom (Algorithm 1, [36]).

They also discuss an $\mathcal{O}(N)$ NCA algorithm, which is done through a two-step procedure. The first step involves a bottom to top (B2T) tree traversal to find the *local pivots* (Algorithm 2, [36]), and the second step involves a top to bottom (T2B) tree traversal to find the *global pivots* (Algorithm 3, [36]). The overall complexity of this algorithm is $\mathcal{O}(N)$.

Gujjula et al. [19] propose a purely algebraic NCA of complexity $\mathcal{O}(N)$, which is similar to the Algorithm 2 of [36]. It also involves a bottom to top (B2T) tree traversal to find the *local pivots*. But after that, it does not traverse the tree top to bottom (T2B) like the $\mathcal{O}(N)$ NCA algorithm of [36] for the *global pivots*. They construct the operators based on the *local pivots*. They show that to construct the standard \mathcal{H}^2 matrix representation *local pivots* are enough. To be more precise, [19] shows that for a purely algebraic construction of the standard \mathcal{H}^2 matrix, the bottom to top (B2T) tree traversal is sufficient; the subsequent top to bottom (T2B) tree traversal could be redundant without substantial change in the relative error. Therefore, the single bottom to top (B2T) tree traversal is sufficient, i.e., *local pivots* are sufficient for a good approximation, and the second step of $\mathcal{O}(N)$ NCA algorithm of [36], which finds the *global pivots* could be omitted without compromising on accuracy. Since [19] follows a single tree traversal procedure than the two tree traversal procedure of [36], this makes the NCA reported in [19] slightly computationally faster than the $\mathcal{O}(N)$ NCA algorithm of [36]. The article [19] compares their new NCA algorithm with the existing NCA algorithms ([6, 36]) and validates their claim numerically for different kernels. We refer the readers to [19] for more details.

We denote the NCA with B2T pivot selection as B2T NCA and the NCA with T2B pivot selection as T2B NCA. The standard $\mathcal{H}^2/\mathcal{H}_{\sqrt{d}}^2$ matrix can be formed using both B2T NCA and T2B NCA.

3.6.2. $\mathcal{H}_{\sqrt{d}}^2(\mathbf{b})$: B2T NCA to construct $\mathcal{H}_{\sqrt{d}}^2$ matrix. In the B2T NCA, the pivots of a cluster at a parent level are obtained from the pivots at its child level. Therefore, one needs to traverse the 2^d uniform tree from the B2T direction. Once the pivots of all the clusters are available, we construct all the required operators (P2M/M2M, M2L, L2L/L2P) as described in [Subsection 3.6.4](#). The cost of initializing the $\mathcal{H}_{\sqrt{d}}^2$ matrix representation using the B2T NCA is $\mathcal{O}(N)$ [36, 19].

The $\mathcal{H}_{\sqrt{d}}^2$ MVP is performed by following the upward, transverse and downward tree traversal. Since the B2T NCA is applied to get the $\mathcal{H}_{\sqrt{d}}^2$ representation, we denote this algorithm as $\mathcal{H}_{\sqrt{d}}^2(\mathbf{b})$. We use this algorithm many times for benchmarking with the proposed algorithms. Thus, for the convenience of the reader, we present it in the [Appendix A](#) by using similar notations to those used in this article. We also refer the reader to Algorithm 2 of [36], and [19] for more details.

3.6.3. $\mathcal{H}_{\sqrt{d}}^2(\mathbf{t})$: T2B NCA to construct $\mathcal{H}_{\sqrt{d}}^2$ matrix. In the T2B NCA, the pivots of a cluster at a child level are obtained from its own index set and the pivots at its parent level. Therefore, one needs to traverse the 2^d tree from the T2B direction. Once the pivots of all the clusters are available, we construct all the required operators as described in [Subsection 3.6.4](#). The cost of initializing the $\mathcal{H}_{\sqrt{d}}^2$ matrix representation using the T2B NCA is $\mathcal{O}(N \log(N))$ [36].

The $\mathcal{H}_{\sqrt{d}}^2$ MVP is performed by following the upward, transverse and downward tree traversal. Since we apply T2B NCA to get the \mathcal{H}^2 matrix, we denote this algorithm as $\mathcal{H}_{\sqrt{d}}^2(\mathbf{t})$. We also use this algorithm for

benchmarking with the proposed algorithms. Thus, for the convenience of the reader, we present it in the [Appendix B](#) by using similar notations to those used in this article. We refer the reader to Algorithm 1 of [\[36\]](#) for more details.

Remark 3.2. It is worth noting that the search spaces of pivots in $\mathcal{H}_{\sqrt{d}}^2(\text{b})$ ([Figure 18](#)) are smaller than that of $\mathcal{H}_{\sqrt{d}}^2(\text{t})$ ([Figure 19](#)). The initialization cost of $\mathcal{H}_{\sqrt{d}}^2(\text{b})$ is $\mathcal{O}(N)$, while the initialization cost of $\mathcal{H}_{\sqrt{d}}^2(\text{t})$ is $\mathcal{O}(N \log(N))$ (refer to [\[36\]](#)). Therefore, in terms of initialization time, $\mathcal{H}_{\sqrt{d}}^2(\text{b})$ is a faster/better algorithm.

3.6.4. Construction of operators. Once all the pivots ($t^{X,i}$, $s^{X,i}$, $t^{X,o}$ and $s^{X,o}$) corresponding to a cluster X are available, the operators can be constructed as follows:

- **L2P and P2M operators.** For a *leaf* cluster X , the matrices U_X and V_X^* are given by

$$(3.19) \quad U_X = K_{t^{X},s^{X},i} \left(K_{t^{X},i,s^{X},i} \right)^{-1}$$

The matrix U_X is called **L2P** (local to particles) operator.

$$(3.20) \quad V_X^* = \left(K_{t^{X},o,s^{X},o} \right)^{-1} K_{t^{X},o,s^{X}}$$

The matrix V_X^* is called **P2M** (particles to multipole) operator.

- **L2L and M2M operators.** For a *non-leaf* cluster $X = \bigcup_{c=1}^{2^d} X_c$, where X_c is a child of X .

$$(3.21) \quad U_X = \begin{bmatrix} U_{X_1} & 0 & \dots & 0 \\ 0 & U_{X_2} & & 0 \\ \vdots & & \ddots & \vdots \\ 0 & 0 & \dots & U_{X_{2^d}} \end{bmatrix} \begin{bmatrix} \tilde{U}_{X_1 X} \\ \tilde{U}_{X_2 X} \\ \vdots \\ \tilde{U}_{X_{2^d} X} \end{bmatrix}$$

where

$$(3.22) \quad \tilde{U}_{X_c X} = K_{t^{X_c},i,s^{X_c},i} \left(K_{t^{X_c},i,s^{X_c},i} \right)^{-1}, \quad 1 \leq c \leq 2^d$$

The matrices $\tilde{U}_{X_c X}$ are called the **L2L** (local to local) operators.

$$(3.23) \quad V_X = \begin{bmatrix} V_{X_1} & 0 & \dots & 0 \\ 0 & V_{X_2} & & 0 \\ \vdots & & \ddots & \vdots \\ 0 & 0 & \dots & V_{X_{2^d}} \end{bmatrix} \begin{bmatrix} \tilde{V}_{X X_1}^* \\ \tilde{V}_{X X_2}^* \\ \vdots \\ \tilde{V}_{X X_{2^d}}^* \end{bmatrix}$$

where

$$(3.24) \quad \tilde{V}_{X X_c}^* = \left(K_{t^{X_c},o,s^{X_c},o} \right)^{-1} K_{t^{X_c},o,s^{X_c},o}, \quad 1 \leq c \leq 2^d$$

The matrices $\tilde{V}_{X X_c}^*$ are called the **M2M** (multipole to multipole) operators.

- **M2L operators.** For any cluster X , the **M2L** (multipole to local) operator is given by

$$(3.25) \quad T_{X,Y} = K_{t^{X},i,s^{Y},o}, \quad Y \in \mathcal{IL}(X)$$

Remark 3.3. If the kernel matrix is symmetric, the P2M or M2M operators can be obtained simply by taking the transpose of L2P or L2L operators, respectively.

4. Various pivots selection strategies on weak admissibility condition. The NCAs [\[6, 36, 19\]](#) are primarily used to construct the nested hierarchical representations based on the **strong admissibility condition** [\(3.3\)](#), i.e., the admissible clusters are the far-field/well-separated clusters. To be more precise, all the existing literature on NCA discusses mainly strong admissibility-based \mathcal{H}^2 matrices. In this article, we want to construct nested bases algorithms based on our *weak admissibility* condition in higher dimensions ([Subsection 3.5](#)), where the admissible clusters are the far-field and the *vertex-sharing* clusters. Therefore, exploring the effectiveness of B2T NCA and T2B NCA on this *weak admissibility* condition is worthwhile.

4.1. B2T NCA on our *weak admissibility* condition. The B2T pivot selection selects the leaf clusters' global row and column indices and applies ACA to get the pivots. To obtain the pivots of a non-leaf cluster, ACA is applied to the pivots from the children-level clusters. This process recursively goes from bottom to top of the 2^d tree. Further explanation regarding the B2T NCA on our *weak admissibility* condition in higher dimensions (Subsection 3.5) is given below.

- If X is a leaf cluster (childless), then construct the following four sets

$$(4.1) \quad \tilde{t}^{X,i} := t^X \quad \text{and} \quad \tilde{s}^{X,i} := \bigcup_{Y \in \mathcal{IL}_*(X)} s^Y$$

$$(4.2) \quad \tilde{t}^{X,o} := \bigcup_{Y \in \mathcal{IL}_*(X)} t^Y \quad \text{and} \quad \tilde{s}^{X,o} := s^X$$

- If X is a non-leaf cluster, then construct the following four sets

$$(4.3) \quad \tilde{t}^{X,i} := \bigcup_{X_c \in \text{child}(X)} t^{X_c,i} \quad \text{and} \quad \tilde{s}^{X,i} := \bigcup_{Y \in \mathcal{IL}_*(X)} \bigcup_{Y_c \in \text{child}(Y)} s^{Y_c,o}$$

$$(4.4) \quad \tilde{t}^{X,o} := \bigcup_{Y \in \mathcal{IL}_*(X)} \bigcup_{Y_c \in \text{child}(Y)} t^{Y_c,i} \quad \text{and} \quad \tilde{s}^{X,o} := \bigcup_{X_c \in \text{child}(X)} s^{X_c,o}$$

To obtain the pivots $t^{X,i}$, $s^{X,i}$, $t^{X,o}$ and $s^{X,o}$, one needs to perform ACA [5]. We perform ACA on the matrix $K_{\tilde{t}^{X,i}, \tilde{s}^{X,i}}$ with user-given tolerance ϵ . The sets $t^{X,i}$ and $s^{X,i}$ are the row and column pivots chosen by the ACA. The search spaces of the pivots for a particular cluster are illustrated in Figure 6. Similarly, perform ACA on the matrix $K_{\tilde{t}^{X,o}, \tilde{s}^{X,o}}$ to obtain the other two sets of pivots $t^{X,o}$ and $s^{X,o}$. Once we have the pivots, we construct the operators as in Subsection 3.6.4. We denote this nested hierarchical representation as \tilde{K}_b .

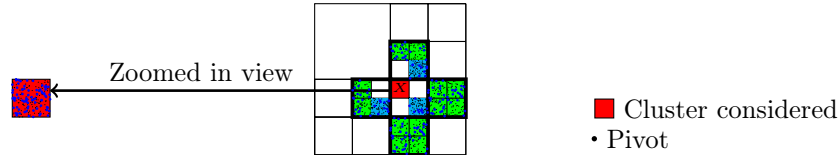


FIG. 6. Illustration of search spaces of the pivots in B2T NCA to construct a nested bases algorithm based on our *weak admissibility* condition in higher dimensions, which leads to poor approximation. The green and cyan-colored regions represent the interaction list of X , i.e., $\mathcal{IL}_*(X)$.

We have shown in [25] that for user-given tolerance ϵ , the rank of interaction between two d dimensional vertex-sharing hyper-cubes containing N uniformly distributed particles scales $\mathcal{O}\left(\log(N) \log^d(\log(N)/\epsilon)\right)$. In our *weak admissibility* condition in higher dimensions (Subsection 3.5), the admissible clusters are the far-field and the vertex-sharing clusters, so the maximum rank scales as $\mathcal{O}\left(\log(N) \log^d(\log(N))\right)$. If we apply B2T NCA on the *weak admissibility* condition in higher dimensions, the size of the sets $\tilde{t}^{X,i}$, $\tilde{s}^{X,i}$, $\tilde{t}^{X,o}$ and $\tilde{s}^{X,o}$ decrease as we traverse the tree from bottom to top. However, as we ascend from bottom to top of the tree, the actual size of the simulation cluster becomes larger. Consequently, the number of particles within a cluster X increases and the actual vertex-sharing interaction rank grows as $\mathcal{O}\left(\log(\#(X)) \log^d(\log(\#(X)))\right)$. Therefore, the pivots obtained from the reduced sets ($\tilde{t}^{X,i}$, $\tilde{s}^{X,i}$, $\tilde{t}^{X,o}$ and $\tilde{s}^{X,o}$) are not enough to get a good approximation of the vertex-sharing interaction matrix. We will see the effect on the rank of a vertex-sharing admissible cluster if we apply the B2T pivot selection. For our convenience, we assume that the N particles are uniformly distributed inside the computational domain. Consider two leaf-level vertex-sharing admissible clusters containing n_{max} particles. Let $R^{(l)}$ be the rank estimate of a vertex-sharing block interaction matrix

at a level l of the tree. At the leaf level, κ , ACA is applied to the global row and column index sets, and $R^{(\kappa)}$ scales as $\mathcal{O}\left(\log(n_{max})\log^d(\log(n_{max}))\right)$. At a non-leaf level, two vertex-sharing admissible clusters (Figure 7a) can be interpreted as $(2^d - 1)$ far-field clusters at the child level (Figure 7c), with a single vertex-sharing cluster at the child level (Figure 7d) as in Figure 7. Considering $F_r^{(l)}$ as the rank of interaction between far-field (or well-separated) clusters and $V_r^{(l)}$ as the rank of interaction between vertex-sharing clusters at level l , the following recurrence relation governs a rough estimate of $R^{(l)}$ at the non-leaf level l .

$$(4.5) \quad R^{(l)} \approx (2^d - 1)F_r^{(l+1)} + V_r^{(l+1)}, \quad l = \kappa - 1 : -1 : 1$$

where $F_r^{(l)} \in \mathcal{O}(1)$ and $V_r^{(l)} \in \mathcal{O}\left(\log(R^{(l)})\log^d(\log(R^{(l)}))\right)$. From (4.5), it is clear that as we traverse the tree from bottom to top, $V_r^{(l)}$ scales as a nested “log” expression, which yields a diminutive value. But the actual vertex-sharing rank grows as $\mathcal{O}\left(\log(N/2^{dl})\log^d(\log(N/2^{dl}))\right)$; the term $N/2^{dl}$ increase as l decrease (as we go bottom to top the l decrease). Thus, if we apply the B2T NCA to the **entire** interaction list, the rank’s diminutive value is insufficient to get a good approximation of the vertex-sharing interaction block matrix. The interaction list of a cluster ($\mathcal{IL}_*(X)$) may contain multiple vertex-sharing clusters, exacerbating the issue. So, it is clear that picking the pivots in B2T traversal is insufficient to get a good nested hierarchical representation based on the *weak admissibility* in higher dimensions.



FIG. 7. We can divide the vertex-sharing interaction like above in 2D to get a rank estimate in B2T approach.

Hence, we show that applying B2T NCA to the **entire** interaction list of a cluster ($\mathcal{IL}_*(X)$) will not yield a *well-approximated* nested hierarchical representation.

To verify it numerically, we consider $N = 160000$ particles (same source and target) to be uniformly distributed inside the domain $[-1, 1]^2$ and set the maximum particles at leaf-clusters $n_{max} = 400$. The kernel matrix $K \in \mathbb{R}^{N \times N}$ is formed using the kernel function $1/r$, where r is the Euclidean distance between source and target. If $r = 0$, we set the value of the kernel function as 1. We construct the nested hierarchical representation, denoted as \tilde{K}_b , based on the B2T pivot selection applied to the **entire** interaction list (search spaces of pivots are illustrated in Figure 6). The maximum rank, minimum rank, and average rank obtained from the NCA at each level of the quad tree are tabulated in Table 1. We also report the relative error in the matrix approximation, i.e., $\|K - \tilde{K}_b\|_2 / \|K\|_2$ with different NCA tolerance (ϵ). From the relative errors of Table 1, it is clear that applying the B2T pivot selection naively to the **entire** interaction list ($\mathcal{IL}_*(X)$) does not result in a well-approximated nested hierarchical representation.

Level of the tree	Level wise rank in B2T ($\epsilon = 10^{-10}$)			Relative error in Matrix approximation (2-norm)	Level wise rank in B2T ($\epsilon = 10^{-12}$)			Relative error in Matrix approximation (2-norm)
	Max. rank	Min. Rank	Avg. rank		Max. Rank	Min. rank	Avg. rank	
1	70	60	63	5.3697E-04	96	80	86	8.784E-05
2	154	73	113		213	108	158	
3	155	80	129		222	108	182	
4	147	75	126		202	108	167	
5	139	64	85		181	64	97	

TABLE 1

Level-wise rank and the relative error in the kernel matrix approximation, i.e., $\|K - \tilde{K}_b\|_2 / \|K\|_2$. The relative errors indicate that the approximation is poor. We choose the kernel function $1/r$ with $N = 160000$ and set $n_{max} = 400$.

4.2. T2B NCA on our *weak admissibility* condition. In contrast to B2T pivot selection, in the T2B pivot selection, the pivots of a cluster at a child level are obtained from its own index set and the pivots at its parent level. Therefore, one needs to traverse the 2^d tree from top to bottom direction to generate all

the required sets of pivots for all the clusters. We discuss the T2B NCA on our *weak admissibility* condition in higher dimensions (Subsection 3.5) in detail as follows.

- If X has no parent, i.e., $\text{parent}(X) = \text{NULL}$ (parentless), then construct the following four sets

$$(4.6) \quad \tilde{t}^{X,i} := t^X \quad \text{and} \quad \tilde{s}^{X,i} := \bigcup_{Y \in \mathcal{IL}_*(X)} s^Y$$

$$(4.7) \quad \tilde{t}^{X,o} := \bigcup_{Y \in \mathcal{IL}_*(X)} t^Y \quad \text{and} \quad \tilde{s}^{X,o} := s^X$$

- If X has parent, i.e., $\text{parent}(X) \neq \text{NULL}$, then construct the following four sets

$$(4.8) \quad \tilde{t}^{X,i} := t^X \quad \text{and} \quad \tilde{s}^{X,i} := \bigcup_{Y \in \mathcal{IL}_*(X)} s^Y \bigcup s^{\text{parent}(X),i}$$

$$(4.9) \quad \tilde{t}^{X,o} := \bigcup_{Y \in \mathcal{IL}_*(X)} t^Y \bigcup t^{\text{parent}(X),o} \quad \text{and} \quad \tilde{s}^{X,o} := s^X$$

We perform ACA on the matrix $K_{\tilde{t}^{X,i}, \tilde{s}^{X,i}}$ with user-given tolerance ϵ . The sets $t^{X,i}$ and $s^{X,i}$ are the row and column pivots chosen by the ACA. The search spaces of the pivots for a particular cluster are illustrated in Figure 8. Similarly, perform ACA on the matrix $K_{\tilde{t}^{X,o}, \tilde{s}^{X,o}}$ to obtain the other two sets of pivots $t^{X,o}$ and $s^{X,o}$. Once we have the pivots, we construct the operators as in Subsection 3.6.4.

The T2B pivot selection does not suffer from the **reduced sets problem**, as it involves appending the parent level pivots with the admissible cluster's global index set. Hence, it possesses a larger search space from which ACA can choose the pivots, leading to a good approximation. We denote this nested hierarchical representation as \tilde{K}_t .

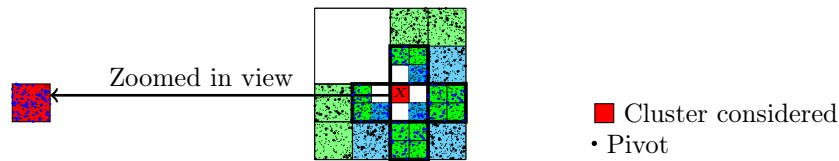


FIG. 8. Illustration of search spaces of the pivots in T2B NCA to construct a nested bases algorithm based on our weak admissibility condition in higher dimensions, which leads to a good approximation. The lighter shade colors represent the interaction list at the parent level.

To provide numerical evidence of the effectiveness of the T2B pivot selection, we develop the nested hierarchical representation \tilde{K}_t based on the T2B NCA and consider the last numerical example ($N = 160000$ uniformly distributed particles and $1/r$ kernel) as in Subsection 4.1. We tabulate the maximum rank, minimum rank, and average rank obtained from the NCA at each level of the quad tree in Table 2. We also report the relative error in the matrix approximation, i.e., $\|K - \tilde{K}_t\|_2 / \|K\|_2$ with different NCA tolerance (ϵ). From the relative errors of Table 2, it is clear that applying the T2B pivot selection to the **entire** interaction list ($\mathcal{IL}_*(X)$) leads to a well-approximated nested hierarchical representation, which is based on the *weak admissibility* condition in higher dimensions.

Level of the tree	Level wise rank in T2B ($\epsilon = 10^{-10}$)			Relative error in Matrix approximation (2-norm)	Level wise rank in T2B ($\epsilon = 10^{-12}$)			Relative error in Matrix approximation (2-norm)
	Max. rank	Min. Rank	Avg. rank		Max. Rank	Min. rank	Avg. rank	
1	102	92	95	5.24526E-10	127	114	123	3.24098E-12
2	234	75	153		335	142	218	
3	222	88	168		288	106	226	
4	187	89	143		253	119	185	
5	150	64	88		199	64	99	

TABLE 2

Level-wise rank and the relative error in the kernel matrix approximation, i.e., $\|K - \tilde{K}_t\|_2 / \|K\|_2$. The relative errors indicate that the approximation is good. We choose the kernel function $1/r$ with $N = 160000$ and set $n_{max} = 400$.

Since \tilde{K}_t is a well-approximated nested hierarchical representation, it is possible to develop a fast MVP algorithm based on it, i.e., $\tilde{K}_t \times \mathbf{q}$. The MVP is performed by following the upward, transverse and downward tree traversal. We denote this algorithm as $\mathcal{H}_*^2(t)$. The detailed algorithm can be found in [Appendix C](#).

Despite the good accuracy and quasi-linear complexity of the T2B NCA, the associated constant in the complexity estimate is very large, leading to a significant time consumption during the initialization of the representation. We demonstrate in [Section 6](#) that the initialization cost of the $\mathcal{H}_*^2(t)$ algorithm is high. However, there is room for improvement, leading to **better** and **efficient** algorithms, which is the main goal of this article. We discuss the proposed algorithms in the next section.

Remark 4.1. From the [Table 1](#) and [Table 2](#), it is evident that the average rank of both the B2T and T2B are almost the same at the leaf level (level 5 of the tree). This is because, in the B2T pivot selection, the ACA is applied directly to the global index sets of the clusters. However, in the B2T pivot selection, as we traverse the tree upward, the pivots are selected from the *reduced sets*, resulting in poor approximation. The substantial difference in the average rank between B2T and T2B pivot selection is apparent from the [Table 1](#) and [Table 2](#) at the coarser levels (level 1 – 4 of the tree) of the tree.

5. Proposed algebraic hierarchical matrix algorithms for fast MVP. This section discusses two main algorithms in this article: efficient \mathcal{H}_*^2 and $(\mathcal{H}^2 + \mathcal{H})_*$. The efficient \mathcal{H}_*^2 and the $(\mathcal{H}^2 + \mathcal{H})_*$ are the **fully** and the **semi/ partially** nested bases algorithms, respectively. Both of these proposed hierarchical matrix algorithms are based on our *weak admissibility* condition in higher dimensions.

We introduce some notations in [Table 3](#), which will be used to explain the proposed algorithms.

\mathcal{C}	Cluster of particles inside a hyper-cube at a level l of the 2^d uniform tree.
$\mathcal{F}(\mathcal{C})$	Set of clusters that are in far-field of \mathcal{C} , i.e., hyper-cubes which are at least one hyper-cube away from \mathcal{C} or the clusters that are well-separated from \mathcal{C} .
$HS_{d'}(\mathcal{C})$	Set of clusters such that their corresponding hyper-cubes share d' hyper-surface with the hyper-cube corresponding to \mathcal{C} ($0 \leq d' \leq d-1$). For example, $HS_0(\mathcal{C})$ is the set of clusters such that their hyper-cubes share a vertex ($d' = 0$) with the hyper-cube corresponding to \mathcal{C} and $HS_1(\mathcal{C})$ is the set of clusters such that their hyper-cubes share an edge ($d' = 1$) with the hyper-cube corresponding to \mathcal{C} .
$child(\mathcal{C})$	Set of clusters such that their hyper-cubes are children of the coarser hyper-cube corresponding to \mathcal{C} .
$parent(\mathcal{C})$	Set of cluster (at coarser level) with child as \mathcal{C} (at finer level)
$siblings(\mathcal{C})$	$child(parent(\mathcal{C})) \setminus \mathcal{C}$
$clan(\mathcal{C})$	$\{siblings(\mathcal{C})\} \cup \{child(P) : P \in \bigcup_{d'=0}^{d-1} HS_{d'}(parent(\mathcal{C}))\}$
$\mathcal{IL}_*(\mathcal{C})$	The interaction list of a cluster \mathcal{C} , based on our <i>weak admissibility</i> condition in higher dimensions (refer to Subsection 3.5), is defined as $\mathcal{IL}_*(\mathcal{C}) = clan(\mathcal{C}) \cap (HS_0(\mathcal{C}) \cup \mathcal{F}(\mathcal{C}))$. These are the admissible clusters for \mathcal{H}_*^2 and $(\mathcal{H}^2 + \mathcal{H})_*$ representations.
$\mathcal{N}_*(\mathcal{C})$	The near-field (neighbor+self) list of a cluster \mathcal{C} with our <i>weak admissibility</i> condition in higher dimensions, is defined as $\mathcal{N}_*(\mathcal{C}) = \bigcup_{d'=1}^{d-1} HS_{d'}(\mathcal{C}) \cup \mathcal{C}$. These are the inadmissible clusters for \mathcal{H}_*^2 and $(\mathcal{H}^2 + \mathcal{H})_*$ representations.
n_{max}	Maximum number of particles at leaf-clusters.
\tilde{K}	\tilde{K} represent the hierarchical low-rank representation of the original kernel matrix K .

TABLE 3

Notations used to describe the \mathcal{H}_*^2 and $(\mathcal{H}^2 + \mathcal{H})_*$ hierarchical matrix algorithm.

5.1. $\mathcal{H}_*^2(\mathbf{b}+\mathbf{t})$: The proposed efficient \mathcal{H}_*^2 matrix algorithm. The \mathcal{H}_*^2 is a hierarchical matrix algorithm with nested bases, which is based on our *weak admissibility* condition in higher dimensions as described in [Subsection 3.5](#).

The admissibility criteria of \mathcal{H}_*^2 delineates that certain far-field (or well-separated) and vertex-sharing clusters are the admissible clusters, i.e., the interaction list of a cluster X ($\mathcal{IL}_*(X)$) consists of both the far-

field and the vertex-sharing clusters. In the [Subsection 4.1](#), we have shown that if we naively apply the B2T NCA to the **entire** interaction list of a cluster (i.e., to $\mathcal{IL}_*(X)$), it will not yield a **well-approximated** and **efficient** nested hierarchical representation because the vertex-sharing interaction rank grows polylogarithmically. Also, we know that B2T NCA works for the $\mathcal{H}_{\sqrt{d}}^2$ matrix ([Subsection 3.6.2](#)), where the admissible clusters are the far-field clusters. So, instead of applying the B2T pivot selection to the **entire** interaction list, if we can separate the far-field interaction from the vertex-sharing interaction, we can apply it specifically to the far-field interaction. Therefore, to construct an efficient \mathcal{H}_*^2 representation, we first partition the interaction list $\mathcal{IL}_*(X)$ into the *far-field* interaction list denoted as $\mathcal{IL}_{far}(X)$ and the *vertex-sharing* interaction list denoted as $\mathcal{IL}_{ver}(X)$, i.e., $\mathcal{IL}_*(X) = \mathcal{IL}_{far}(X) \cup \mathcal{IL}_{ver}(X)$ with $\mathcal{IL}_{far}(X) \cap \mathcal{IL}_{ver}(X) = \phi$. The visual representation of this partitioning corresponding to a cluster X is illustrated in [Figure 9](#).

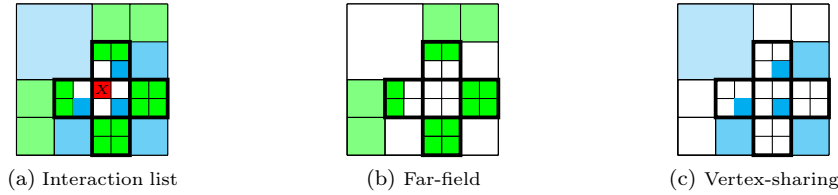


FIG. 9. Partitioning of the interaction list corresponding to cluster X at level 3 of the quad tree in 2D. The interaction list of X ($\mathcal{IL}_*(X)$) consists of green and cyan colored clusters enclosed by a noticeable **black** border. The lighter shade colors represent the interaction list at the coarser levels of the tree (parent or grandparent of X).

To initialize the efficient \mathcal{H}_*^2 representation, we apply the B2T NCA to the $\mathcal{IL}_{far}(X)$ and the T2B NCA to the $\mathcal{IL}_{ver}(X)$. Therefore, we need to independently traverse the 2^d tree twice in reverse directions with different interaction lists (B2T with far-field interaction and T2B with vertex-sharing interaction). Since we use both the B2T NCA (to far-field) and T2B NCA (to vertex-sharing), we abbreviate this algorithm as $\mathcal{H}_*^2(\text{b+t})$. Once we have all the required sets of pivots, we construct the P2M/M2M, M2L, L2L/L2P operators. After forming the $\mathcal{H}_*^2(\text{b+t})$ representation (or structure), we perform the MVP by following upward, transverse and downward tree traversal. We discuss our $\mathcal{H}_*^2(\text{b+t})$ hierarchical matrix algorithm for fast MVP in two steps:

1. Initialization of $\mathcal{H}_*^2(\text{b+t})$ representation. ([Subsection 5.1.1](#))
2. Calculation of the potential (MVP). ([Subsection 5.1.2](#))

5.1.1. Initialization of $\mathcal{H}_*^2(\text{b+t})$ representation. The initialization procedure is described in detail as follows:

1. *B2T NCA for far-field interaction.* Since we partition the far-field and the vertex-sharing interactions associated with a cluster X , i.e., $\mathcal{IL}_*(X) = \mathcal{IL}_{far}(X) \cup \mathcal{IL}_{ver}(X)$, we can apply the B2T NCA only to the far-field interactions ($\mathcal{IL}_{far}(X)$). The detailed procedure to obtain the pivots corresponding to a cluster X is given below.

- If X is a leaf cluster (childless), then construct the following four sets

$$(5.1) \quad \tilde{t}^{X,i} := t^X \quad \text{and} \quad \tilde{s}^{X,i} := \bigcup_{Y \in \mathcal{IL}_{far}(X)} s^Y$$

$$(5.2) \quad \tilde{t}^{X,o} := \bigcup_{Y \in \mathcal{IL}_{far}(X)} t^Y \quad \text{and} \quad \tilde{s}^{X,o} := s^X$$

- If X is a non-leaf cluster, then construct the following four sets

$$(5.3) \quad \tilde{t}^{X,i} := \bigcup_{X_c \in \text{child}(X)} t^{X_c,i} \quad \text{and} \quad \tilde{s}^{X,i} := \bigcup_{Y \in \mathcal{IL}_{far}(X)} \bigcup_{Y_c \in \text{child}(Y)} s^{Y_c,o}$$

$$(5.4) \quad \tilde{t}^{X,o} := \bigcup_{Y \in \mathcal{IL}_{far}(X)} \bigcup_{Y_c \in \text{child}(Y)} t^{Y_c,i} \quad \text{and} \quad \tilde{s}^{X,o} := \bigcup_{X_c \in \text{child}(X)} s^{X_c,o}$$

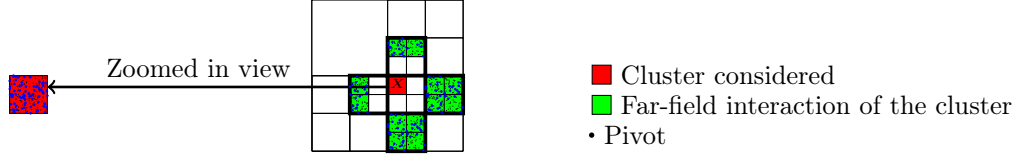


FIG. 10. Illustration of search spaces of the pivots in B2T NCA for $\mathcal{H}_*^2(b+t)$ construction. Note that we consider only the far-field interaction here, i.e., $\mathcal{IL}_{far}(X) \subset \mathcal{IL}_*(X)$.

We perform ACA on the matrix $K_{\tilde{t}^{X,i}, \tilde{s}^{X,i}}$ with user-given tolerance ϵ_{far} . The sets $t^{X,i}$ and $s^{X,i}$ are the row and column pivots chosen by the ACA. The search spaces of the pivots for a particular cluster are illustrated in Figure 10. Similarly, perform ACA on the matrix $K_{\tilde{t}^{X,o}, \tilde{s}^{X,o}}$ to obtain the other two sets of pivots $t^{X,o}$ and $s^{X,o}$. This process recursively goes from bottom to top of the 2^d tree and generates the pivots for all the clusters of the tree. As discussed earlier, the main components for constructing the operators are the four sets: $t^{X,i}$, $s^{X,i}$, $t^{X,o}$ and $s^{X,o}$. We construct different operators as described in Subsection 3.6.4. Therefore, we get the following sets of operators corresponding to far-field interaction:

- (a) P2M $\left(V_X^{far}\right)$ / M2M $\left(\tilde{V}_{X X_c}^{far}\right)$, $X_c \in child(X)$.
- (b) M2L $\left(T_{X,Y}^{far}\right)$, $Y \in \mathcal{IL}_{far}(X)$.
- (c) L2L $\left(\tilde{U}_{X_c X}^{far}\right)$, $X \in parent(X_c)$ / L2P $\left(U_X^{far}\right)$.

2. **T2B NCA for vertex-sharing interaction.** As demonstrated in Subsection 4.2, the T2B NCA is well-suited for our hierarchical representation. However, instead of applying the T2B NCA to the entire interaction list of a cluster X ($\mathcal{IL}_*(X)$), we employ it solely to the vertex-sharing interactions, i.e., only to the $\mathcal{IL}_{ver}(X)$. The detailed procedure for obtaining the pivots corresponding to a cluster X is below.
 - If X has no parent, i.e., $parent(X) = \text{NULL}$ (parentless), then construct the following four sets

$$(5.5) \quad \tilde{t}^{X,i} := t^X \quad \text{and} \quad \tilde{s}^{X,i} := \bigcup_{Y \in \mathcal{IL}_{ver}(X)} s^Y$$

$$(5.6) \quad \tilde{t}^{X,o} := \bigcup_{Y \in \mathcal{IL}_{ver}(X)} t^Y \quad \text{and} \quad \tilde{s}^{X,o} := s^X$$

- If X has parent, i.e., $parent(X) \neq \text{NULL}$, then construct the following four sets

$$(5.7) \quad \tilde{t}^{X,i} := t^X \quad \text{and} \quad \tilde{s}^{X,i} := \bigcup_{Y \in \mathcal{IL}_{ver}(X)} s^Y \bigcup s^{parent(X),i}$$

$$(5.8) \quad \tilde{t}^{X,o} := \bigcup_{Y \in \mathcal{IL}_{ver}(X)} t^Y \bigcup t^{parent(X),o} \quad \text{and} \quad \tilde{s}^{X,o} := s^X$$

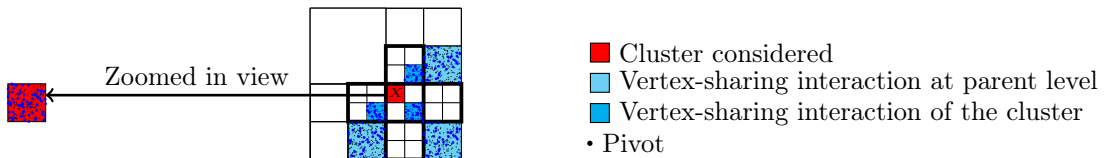


FIG. 11. Illustration of search spaces of the pivots in T2B NCA for $\mathcal{H}_*^2(b+t)$ construction.

We perform ACA on the matrix $K_{\tilde{t}^{X,i}, \tilde{s}^{X,i}}$ with user-given tolerance ϵ_{ver} . The sets $t^{X,i}$ and $s^{X,i}$ are the row and column pivots chosen by the ACA. The search spaces of the pivots for a particular cluster are illustrated in [Figure 11](#). Similarly, perform ACA on the matrix $K_{\tilde{t}^{X,o}, \tilde{s}^{X,o}}$ to obtain the other two sets of pivots $t^{X,o}$ and $s^{X,o}$. These four sets are the main components for constructing the operators. We construct the different operators corresponding to vertex-sharing interaction as described in [Subsection 3.6.4](#). Therefore, we get the following sets of operators corresponding to vertex-sharing interaction:

- (a) P2M (V_X^{ver}) / M2M ($\tilde{V}_{XX_c}^{ver}$), $X_c \in child(X)$.
- (b) M2L ($T_{X,Y}^{ver}$), $Y \in \mathcal{IL}_{ver}(X)$.
- (c) L2L ($\tilde{U}_{X_c X}^{ver}$), $X \in parent(X_c)$ / L2P (U_X^{ver}).

Remark 5.1. The B2T NCA and T2B NCA are performed completely independently with different interaction lists. There is no interdependency of pivots between these two methods.

Therefore, after performing the B2T NCA (to the far-field interaction) and T2B NCA (to the vertex-sharing interaction) for all the clusters, we get two different sets of operators as given in [Table 4](#).

	Far-field	Vertex-sharing
P2M Operators	V_X^{far}	V_X^{ver}
M2M Operators	$\tilde{V}_{XX_c}^{far}$	$\tilde{V}_{XX_c}^{ver}$
M2L Operators	$T_{X,Y}^{far}$	$T_{X,Y}^{ver}$
L2L Operators	$\tilde{U}_{X_c X}^{far}$	$\tilde{U}_{X_c X}^{ver}$
L2P Operators	U_X^{far}	U_X^{ver}

TABLE 4

Two different sets of operators are readily available after performing B2T NCA and T2B NCA.

Pseudocodes of $\mathcal{H}_*^2(\mathbf{b}+\mathbf{t})$ initialization. The pseudocodes outlining the initialization of the $\mathcal{H}_*^2(\mathbf{b}+\mathbf{t})$ representation are presented here.

Initialization step I ([Algorithm 5.1](#)), Initialization step II ([Algorithm 5.2](#)).

Algorithm 5.1 B2T NCA for far-field interaction (Initialization step I)

```

1: procedure B2T-PIVOT-SELECTION( $\epsilon_{far}$ )
2:   for  $l = \kappa - 1 : 2$  do                                      $\triangleright$  Traverse the  $2^d$  tree from bottom to top
3:     for  $i = 1 : 2^{dl}$  do
4:        $X \leftarrow i^{th}$  cluster at level  $l$  of tree.
5:        $I.clear()$ 
6:        $J.clear()$ 
7:       if  $l \neq \kappa$  then
8:          $I.insert(\bigcup t^{X_c,i})$                                 $\triangleright X_c \in child(X), c = 1 : 2^d$ 
9:         for  $Y \in \mathcal{IL}_{far}(X)$  do
10:           $J.insert(\bigcup s^{Y_c,o})$                              $\triangleright Y_c \in child(Y), c = 1 : 2^d$ 
11:        end for
12:       else
13:          $I = t^X$                                             $\triangleright t^X = \text{global index set of } X$ 
14:         for  $Y \in \mathcal{IL}_{far}(X)$  do
15:           $J.insert(s^Y)$                                      $\triangleright s^Y = \text{global index set of } Y$ 
16:        end for
17:       end if
18:        $[t^{X,i}, s^{X,i}] = \text{ACA}(I, J, \epsilon_{far})$                  $\triangleright$  Perform ACA on the matrix  $K_{I,J}$  with tolerance  $\epsilon_{far}$ 
19:       end for
20:   end for
21: end procedure
22: procedure CONSTRUCTION-OF-FAR-FIELD-OPERATORS
23:   One can get the other two sets of pivots  $t^{X,o}$  and  $s^{X,o}$  in a similar fashion. After that, all the operators corresponding to far-field are readily available (Subsection 3.6.4).
24: end procedure

```

Algorithm 5.2 T2B NCA for vertex-sharing interaction (Initialization step II)

```

1: procedure T2B-PIVOT-SELECTION( $\epsilon_{ver}$ )
2:   for  $l = 1 : \kappa$  do ▷ Traverse the  $2^d$  tree from top to bottom
3:     for  $i = 1 : 2^{dl}$  do
4:        $X \leftarrow i^{th}$  cluster at level  $l$  of tree.
5:        $I = t^X$  ▷  $t^X =$  global index set of  $X$ 
6:       for  $Y \in \mathcal{IL}_{ver}(X)$  do
7:          $J = s^Y$  ▷  $s^Y =$  global index set of  $Y$ 
8:         if  $l > 1$  then
9:            $J_{insert}(s^{parent(X),i})$  ▷ If column pivots of the parent exist, add it to  $J$ 
10:        end if
11:        end for
12:         $[t^{X,i}, s^{X,i}] = \text{ACA}(I, J, \epsilon_{ver})$  ▷ Perform ACA on the matrix  $K_{I,J}$  with tolerance  $\epsilon_{ver}$ 
13:      end for
14:    end for
15: end procedure
16: procedure CONSTRUCTION-OF-VERTEX-SHARING-OPERATORS
17:   One can get the other two sets of pivots  $t^{X,o}$  and  $s^{X,o}$  in a similar fashion. After that, all the operators corresponding to
   vertex-sharing interaction are readily available (Subsection 3.6.4).
18: end procedure

```

5.1.2. Calculation of the potential (MVP). $\tilde{\phi} = \tilde{K}q$. All the required operators (Table 4) will be available after the initialization process. The final step is to discuss how to calculate the potential (MVP). Since we obtain two different sets of P2M, M2M, M2L, L2L, and L2P operators (Table 4), we use two different sets of vectors to keep track of the potential corresponding to the far-field and vertex-sharing interaction. We independently compute the potentials corresponding to the far-field and vertex-sharing interactions by following upward, transverse and downward tree traversal. We denote the potential corresponding to the far-field interaction as *far-field potential* and the potential corresponding to the vertex-sharing interaction as *vertex-sharing potential*. The final potential is given by adding the far-field and vertex-sharing potentials to the near-field potential. Let the column vector $q_{X_i^{(\kappa)}}$ denotes the charge corresponding to the i^{th} leaf cluster, i.e., $q = [q_{X_1^{(\kappa)}}; q_{X_2^{(\kappa)}}; \dots; q_{X_{2^{d\kappa}}^{(\kappa)}}]$ (MATLAB notation) and $X_i^{(l)}$ denotes the i^{th} cluster at the level l of the tree. Sometimes we omit the subscripts and superscripts from the cluster notation to improve the readability in the hope that the cluster id and the level of the tree can be understood easily from the context, i.e., instead of $X_i^{(l)}$ we use X_i or $X^{(l)}$ or X . The procedure to compute the far-field and vertex-sharing potentials is as follows:

1. Upward traversal:

- Particles to multipole (*P2M*) at leaf level κ : For all leaf clusters X , calculate

$$v_{X, far}^{(\kappa)} = V_X^{far*} q_X^{(\kappa)}, \quad (\text{Far-field})$$

$$v_{X, ver}^{(\kappa)} = V_X^{ver*} q_X^{(\kappa)}, \quad (\text{Vertex-sharing})$$
- Multipole to multipole (*M2M*) at non-leaf level : For all non-leaf X clusters, calculate

$$v_{X, far}^{(l)} = \sum_{X_c \in \text{child}(X)} \tilde{V}_{XX_c}^{far*} v_{X_c, far}^{(l+1)}, \quad \kappa - 1 \geq l \geq 2. \quad (\text{Far-field})$$

$$v_{X, ver}^{(l)} = \sum_{X_c \in \text{child}(X)} \tilde{V}_{XX_c}^{ver*} v_{X_c, ver}^{(l+1)}, \quad \kappa - 1 \geq l \geq 1. \quad (\text{Vertex-sharing})$$

2. Transverse traversal:

- Multipole to local (*M2L*) at all levels and for all clusters : For all cluster X , calculate

$$u_{X, far}^{(l)} = \sum_{Y \in \mathcal{IL}_{far}(X)} T_{X,Y}^{far} v_{Y, far}^{(l)}, \quad 2 \leq l \leq \kappa. \quad (\text{Far-field})$$

$$u_{X, ver}^{(l)} = \sum_{Y \in \mathcal{IL}_{ver}(X)} T_{X,Y}^{ver} v_{Y, ver}^{(l)}, \quad 1 \leq l \leq \kappa. \quad (\text{Vertex-sharing})$$

3. Downward traversal:

- Local to local (*L2L*) at non-leaf level : For all non-leaf clusters X , calculate

$$u_{X_c, far}^{(l+1)} := u_{X_c, far}^{(l)} + \tilde{U}_{X_c X}^{far} u_{X, far}^{(l)}, \quad 2 \leq l \leq \kappa - 1 \text{ and } X \in \text{parent}(X_c). \quad (\text{Far-field})$$

$$u_{X_c, ver}^{(l+1)} := u_{X_c, ver}^{(l)} + \tilde{U}_{X_c X}^{ver} u_{X, ver}^{(l)}, \quad 1 \leq l \leq \kappa - 1 \text{ and } X \in \text{parent}(X_c). \quad (\text{Vertex-sharing})$$
- Local to particles (*L2P*) at leaf level κ : For all leaf clusters X , calculate

$$\begin{aligned}\phi_{X, far}^{(\kappa)} &= U_X^{far} u_{X, far}^{(\kappa)}, & (\text{Far-field}) \\ \phi_{X, ver}^{(\kappa)} &= U_X^{ver} u_{X, ver}^{(\kappa)}, & (\text{Vertex-sharing})\end{aligned}$$

Near-field potential and the total potential at leaf level. For each leaf cluster X , we add the near-field (neighbor+self) potential, which is a direct computation to the far-field and vertex-sharing potentials. Hence, the final computed potential of a leaf cluster X is given by

$$(5.9) \quad \phi_X^{(\kappa)} = \underbrace{\phi_{X, far}^{(\kappa)}}_{\text{Far-field potential (nested)}} + \underbrace{\phi_{X, ver}^{(\kappa)}}_{\text{Vertex-sharing potential (nested)}} + \underbrace{\sum_{X' \in \mathcal{N}_*(X)} K_{tX, sX'} q_{X'}^{(\kappa)}}_{\text{Near-field potential (direct)}}$$

If $\kappa = 1$, then no far-field interaction exists so $\phi_{X, far}^{(\kappa)} = 0$. We know that X_i is the i^{th} leaf cluster and $\phi_{X_i}^{(\kappa)}$ represents the potential corresponding to it, $1 \leq i \leq 2^{d\kappa}$.

Therefore, the computed potential is given by $\tilde{\phi} = [\phi_{X_1}^{(\kappa)}; \phi_{X_2}^{(\kappa)}; \dots; \phi_{X_{2^{d\kappa}}}^{(\kappa)}]$ (MATLAB notation). The schematic representation of the proposed $\mathcal{H}_*^2(\text{b+t})$ algorithm is given in Figure 12.

Remark 5.2. The difference between $\mathcal{H}_*^2(\text{b+t})$ and $\mathcal{H}_*^2(\text{t})$ (refer to Subsection 4.2 and Appendix C) lies in their construction techniques. (Figure 10, Figure 11) and Figure 8 illustrate this. Since the search spaces for the pivots are small in $\mathcal{H}_*^2(\text{b+t})$, it takes less time to initialize the representation and is more efficient. This enhancement is illustrated in Section 6.

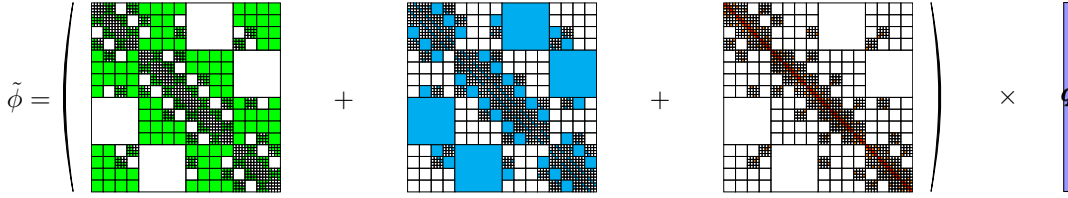


FIG. 12. In the efficient $\mathcal{H}_*^2/\mathcal{H}_*^2(\text{b+t})$ algorithm, the operators (P2M/M2M, M2L and L2L/L2P) corresponding to the far-field and the vertex-sharing interaction are constructed separately using B2T NCA and T2B NCA, respectively. After that, we calculate the far-field and vertex-sharing potentials independently by following Upward, Transverse and Downward tree traversal. We get the final potential by adding the far-field and vertex-sharing potentials to the near-field potential.

5.1.3. Complexity analysis of $\mathcal{H}_*^2(\text{b+t})$. We construct the $\mathcal{H}_*^2(\text{b+t})$ hierarchical representation using B2T NCA and T2B NCA. For a particular cluster X , its far-field interaction $\mathcal{I}\mathcal{L}_{far}(X)$ and vertex-sharing interaction $\mathcal{I}\mathcal{L}_{ver}(X)$ are compressed using the B2T NCA (Algorithm 5.1) and T2B NCA (Algorithm 5.2), respectively.

Time complexity. The time complexity of the initialization steps and the potential calculation steps are given below

- *Far-field interaction compression:* Let the leaf cluster size be bounded by p_1 and we also assume $p_1 = \mathcal{O}(n_{max})$. Let c_{far} be the maximum of the far-field interaction list size of a cluster (in 2D and 3D for the \mathcal{H}_*^2 hierarchical representation $c_{far} = 12$ and 126 , respectively, refer to (3.12)). For a non-leaf cluster, we choose the row indices from the row pivots of the children clusters and column indices from the column pivots of the children of the admissible far-field blocks. After that, the partially pivoted ACA [5] is applied to the row and column indices. The cost for applying ACA for a non-leaf cluster at level l is bounded by $(2^d p_1 + c_{far} 2^d p_1) p_1^2$. By taking all the levels, the cost for the far-field compression is bounded by $\sum_{l=2}^{\kappa} 2^{dl} (2^d p_1 + c_{far} 2^d p_1) p_1^2 \approx \mathcal{O}(N)$. So, the complexity of

Algorithm 5.1 is $\mathcal{O}(N)$.

- *Vertex-sharing interaction compression:* Let c_{ver} be the maximum of the vertex-sharing interaction list size of a cluster (in 2D and 3D for the \mathcal{H}_*^2 hierarchical representation $c_{ver} = 3$ and 7 , respectively, refer to (3.12)). For a cluster (with a parent), we choose the row indices from its index set and column

indices from its index set, along with column pivots of the parent of the admissible vertex-sharing blocks. After that, the partially pivoted ACA [5] is applied to the row and column indices. Let p_2 be the maximum size of parent level pivots across the tree to be added, where p_2 scales at most polylogarithmically with N [25] and this is a loose upper bound of p_2 . Hence, the cost for applying ACA for a particular cluster is bounded by $\left(\frac{N}{2^{dl}} + c_{ver} \frac{N}{2^{dl}} + p_2\right) p_2^2$. By taking all the levels, the cost for the vertex-sharing interaction compression is bounded by $\sum_{l=1}^{\kappa} 2^{dl} \left(\frac{N}{2^{dl}} + c_{ver} \frac{N}{2^{dl}} + p_2\right) p_2^2 = \sum_{l=1}^{\kappa} (N + c_{ver} N + p_2) p_2^2 \approx \mathcal{O}(p_2 N \log(N))$. So, the complexity of Algorithm 5.2 is $\mathcal{O}(p_2 N \log(N))$.

Thus, the overall time complexity to initialize the $\mathcal{H}_*^2(\text{b+t})$ representation scales as $\mathcal{O}(N + p_2 N \log(N))$.

The time required for each step in the calculation of the far-field and vertex-sharing potentials (Subsection 5.1.2) exhibits linear and quasi-linear scaling, respectively. Therefore, the overall time complexity for the potential calculation (MVP) is quasi-linear for non-oscillatory kernels.

Space complexity. For a cluster X , we store two different sets of operators as in Table 4. The total cost for storing all the P2M/M2M, M2L, and L2L/L2P operators is $\mathcal{O}(Np_1^2 + Np_2^2)$. The cost of storing the dense near-field operators at leaf level is $\mathcal{O}(Nn_{max}^2)$. Therefore, the overall memory cost scales at most quasi-linearly.

Remark 5.3. The quasi-linear complexity is an overestimation because the far-field part scales linearly. The $\mathcal{H}_*^2(\text{b+t})$ exhibits similar scaling when comparing its actual performance with the standard $\mathcal{H}^2/\mathcal{H}_{\sqrt{d}}^2$ algorithms [36]. In fact, in the Section 6, we show that $\mathcal{H}_*^2(\text{b+t})$ is competitive with the $\mathcal{H}_{\sqrt{d}}^2$ algorithms (Appendix A, Appendix B) with respect to memory and MVP time. The step-by-step costs of $\mathcal{H}_*^2(\text{b+t})$, along with a comparison of the same in algebraic $\mathcal{H}_{\sqrt{d}}^2$, are presented in Table 5.

STEP	2D ($d = 2$)		3D ($d = 3$)	
	$\mathcal{H}_*^2(\text{b+t})$ in 2D	$\mathcal{H}_{\sqrt{d}}^2$ in 2D	$\mathcal{H}_*^2(\text{b+t})$ in 3D	$\mathcal{H}_{\sqrt{d}}^2$ in 3D
P2M+M2M	$\mathcal{O}(Np_1^2 + Np_2^2)$	$\mathcal{O}(Np^2)$	$\mathcal{O}(Np_1^2 + Np_2^2)$	$\mathcal{O}(Np^2)$
M2L	$\mathcal{O}(12Np_1^2 + 3Np_2^2)$	$\mathcal{O}(27Np^2)$	$\mathcal{O}(126Np_1^2 + 7Np_2^2)$	$\mathcal{O}(189Np^2)$
L2L+L2P	$\mathcal{O}(Np_1^2 + Np_2^2)$	$\mathcal{O}(Np^2)$	$\mathcal{O}(Np_1^2 + Np_2^2)$	$\mathcal{O}(Np^2)$
Near-field	$\mathcal{O}(5Nn_{max}^2)$	$\mathcal{O}(9Nn_{max}^2)$	$\mathcal{O}(19Nn_{max}^2)$	$\mathcal{O}(27Nn_{max}^2)$

TABLE 5

Comparison of complexities between $\mathcal{H}_*^2(\text{b+t})$ and $\mathcal{H}_{\sqrt{d}}^2$ for $d = 2, 3$, where p_1 and p scales as $\mathcal{O}(1)$ but p_2 scales at most polylogarithmically with N . The constants corresponding to Near-field and M2L steps are discussed in (3.11) and (3.12).

5.2. $(\mathcal{H}^2 + \mathcal{H})_*$: The proposed semi-nested hierarchical matrix algorithm. The $(\mathcal{H}^2 + \mathcal{H})_*$ is a hierarchical matrix algorithm with semi-nested (or partially nested) bases. It is also based on our *weak admissibility* condition in higher dimensions (Subsection 3.5). We term this algorithm *semi-nested* because we employ both the nested and non-nested bases in the representation. Therefore, $(\mathcal{H}^2 + \mathcal{H})_*$ differs from the $\mathcal{H}_*^2(\text{b+t})$ algorithm in that it is not a **fully** nested algorithm. Let X be a cluster at a particular level of the tree. We know that the interaction list of X consists of far-field and vertex-sharing interactions; and it can be partitioned, i.e., $\mathcal{I}\mathcal{L}_*(X) = \mathcal{I}\mathcal{L}_{far}(X) \cup \mathcal{I}\mathcal{L}_{ver}(X)$ (refer to Figure 9). To initialize the $(\mathcal{H}^2 + \mathcal{H})_*$ representation, we apply the B2T NCA to $\mathcal{I}\mathcal{L}_{far}(X)$ and partially pivoted ACA to $\mathcal{I}\mathcal{L}_{ver}(X)$. It is to be noted that the far-field interaction compression routine is the same as the proposed $\mathcal{H}_*^2(\text{b+t})$ algorithm. The main difference between the $\mathcal{H}_*^2(\text{b+t})$ and the $(\mathcal{H}^2 + \mathcal{H})_*$ representations is the vertex-sharing interaction compression routine. Once we have the $(\mathcal{H}^2 + \mathcal{H})_*$ representation, i.e., all the required operators are available, we calculate the potential or MVP. The potential corresponding to the far-field interaction, i.e., the far-field potential, is obtained through upward, transverse and downward tree traversal. The potential corresponding to the vertex-sharing interaction, i.e., the vertex-sharing potential, is derived using \mathcal{H} matrix-like algorithm (non-nested approach). We discuss our $(\mathcal{H}^2 + \mathcal{H})_*$ hierarchical matrix

algorithm for fast MVP in the following steps:

1. Initialization of $(\mathcal{H}^2 + \mathcal{H})_*$ representation. (Subsection 5.2.1)
2. Calculation of the potential (MVP). (Subsection 5.2.2)

5.2.1. Initialization of $(\mathcal{H}^2 + \mathcal{H})_*$ representation. The initialization procedure is described in detail as follows:

1. *B2T NCA for far-field interaction.* We apply the B2T NCA only to the $\mathcal{IL}_{far}(X)$. This step is analogous to the first step of $\mathcal{H}_*^{2(b+t)}$ initialization (Item 1). So, upon completion of the B2T NCA, we will get the following sets of operators:

- (a) P2M (V_X^{far}) / M2M $(\tilde{V}_{XX_c}^{far})$, $X_c \in child(X)$.
- (b) M2L $(T_{X,Y}^{far})$, $Y \in \mathcal{IL}_{far}(X)$.
- (c) L2L $(\tilde{U}_{X_cX}^{far})$, $X \in parent(X_c)$ / L2P (U_X^{far}) .

2. *ACA-based compression for vertex-sharing interaction.* We compress the vertex-sharing interaction using partially pivoted ACA [5]. For each pair of clusters X and $Y \in \mathcal{IL}_{ver}(X)$ at all the levels of the 2^d tree, the vertex-sharing interaction matrix (K_{t^X, s^Y}) is compressed by partially pivoted ACA with user-given tolerance ϵ_{ver} as follows:

$$(5.10) \quad K_{t^X, s^Y} \approx UV^*, \quad t^X \text{ and } s^Y \text{ are the global index sets of the clusters } X \text{ and } Y, \text{ respectively.}$$

Therefore, after performing the B2T NCA (to the far-field) and ACA (to the vertex-sharing) for all the clusters, we get two different sets of operators as given in Table 6.

Far-field	
P2M Operators	V_X^{far}
M2M Operators	$\tilde{V}_{XX_c}^{far}$
M2L Operators	$T_{X,Y}^{far}$
L2L Operators	$\tilde{U}_{X_cX}^{far}$
L2P Operators	U_X^{far}

(a) Far-field operators

Vertex-sharing	
U	
V	

(b) Vertex-sharing operators

TABLE 6

Different operators after performing the B2T NCA on far-field and ACA on vertex-sharing interaction.

Pseudocodes of $(\mathcal{H}^2 + \mathcal{H})_*$ initialization. The pseudocodes for initializing $(\mathcal{H}^2 + \mathcal{H})_*$ representation are given here.

Initialization step I (Algorithm 5.1), Initialization step II (Algorithm 5.3)

Algorithm 5.3 Compression of the vertex-sharing interaction using only ACA (Initialization step II)

```

1: procedure VERTEX-SHARING-INTERACTION-COMPRESSION( $\epsilon_{ver}$ )
2:   for  $l = 1 : \kappa$  do
3:     for  $i = 1 : 2^{dl}$  do
4:        $X \leftarrow i^{th}$  cluster at level  $l$  of tree.
5:        $I = t^X$  ▷  $t^X =$  global index set of  $X$ 
6:       for  $Y \in \mathcal{IL}_{ver}(X)$  do
7:          $J = s^Y$  ▷  $s^Y =$  global index set of  $Y$ 
8:          $[U, V] = \text{ACA}(I, J, \epsilon_{ver})$  ▷ Perform ACA on the matrix  $K_{I,J}$ ,  $K_{I,J} \approx UV^*$ 
9:       end for
10:    end for
11:  end for
12: end procedure

```

5.2.2. Calculation of the potential (MVP). $\tilde{\phi} = \tilde{K}\mathbf{q}$. After the initialization process, all the required operators (Table 6) will be available, and the final step is to discuss the calculation of the potential (MVP). We compute the far-field potential using upward, transverse and downward tree traversal, which is similar to the far-field potential computation of the $\mathcal{H}_*^{2(b+t)}$ algorithm. The vertex-sharing potential is

calculated using a single tree traversal in a manner analogous to the \mathcal{H} matrix-like algorithms. Thus, the $(\mathcal{H}^2 + \mathcal{H})_*$ algorithm can be thought of as a cross of \mathcal{H}^2 and \mathcal{H} matrix-like algorithms. The final potential is given by adding the far-field, vertex-sharing and near-field potentials.

The procedure to compute the far-field potential is as follows:

1. **Upward traversal:**

- Particles to multipole ($P2M$) at leaf level κ : For all leaf clusters X , calculate $v_{X, far}^{(\kappa)} = V_X^{far*} q_X^{(\kappa)}$, (Far-field)
- Multipole to multipole ($M2M$) at non-leaf level : For all non-leaf X clusters, calculate $v_{X, far}^{(l)} = \sum_{X_c \in \text{child}(X)} \tilde{V}_{XX_c}^{far*} v_{X_c, far}^{(l+1)}$, $\kappa - 1 \geq l \geq 2$. (Far-field)

2. **Transverse traversal:**

- Multipole to local ($M2L$) at all levels and for all clusters : For all cluster X , calculate $u_{X, far}^{(l)} = \sum_{Y \in \mathcal{IL}_{far}(X)} T_{X,Y}^{far} v_{Y, far}^{(l)}$, $2 \leq l \leq \kappa$. (Far-field)

3. **Downward traversal:**

- Local to local ($L2L$) at non-leaf level : For all non-leaf clusters X , calculate $u_{X_c, far}^{(l+1)} := u_{X_c, far}^{(l+1)} + \tilde{U}_{X_c X}^{far} u_{X, far}^{(l)}$, $2 \leq l \leq \kappa - 1$ and $X \in \text{parent}(X_c)$. (Far-field)
- Local to particles ($L2P$) at leaf level κ : For all leaf clusters X , calculate $\phi_{X, far}^{(\kappa)} = U_X^{far} u_{X, far}^{(\kappa)}$, (Far-field)

The calculation of the vertex-sharing potential ϕ_{ver} is executed in a non-nested manner, as given in [Algorithm 5.4](#).

Pseudocode of calculating the vertex-sharing potential in $(\mathcal{H}^2 + \mathcal{H})_*$ algorithm. The pseudocode outlining the calculation of the vertex-sharing potential (ϕ_{ver}) is presented here.

Algorithm 5.4 Compute the vertex-sharing potential in $(\mathcal{H}^2 + \mathcal{H})_*$

```

1: procedure VERTEX-SHARING POTENTIAL( $\phi_{ver}$ )
2:   for  $l = 1 : \kappa$  do
3:     for  $i = 1 : 2^{dl}$  do
4:        $X \leftarrow i^{th}$  cluster at level  $l$  of tree.
5:       for  $Y \in \mathcal{IL}_{ver}(X)$  do.
6:          $\phi_{ver}(X) := \phi_{ver}(X) + U(V^* q_Y^{(l)})$  ▷ Low-rank MVP, MATLAB notation is applied to  $\phi_{ver}$ 
7:       end for
8:     end for
9:   end for
10:  return  $\phi_{ver}$ 
11: end procedure
    
```

Near-field potential and the total potential at leaf level. For each leaf cluster X , we add the near-field (neighbor+self) potential, which is a direct computation with the far-field and vertex-sharing potential. Hence, the final computed potential of a leaf cluster is given by

$$(5.11) \quad \phi_X^{(\kappa)} = \underbrace{\phi_{X, far}^{(\kappa)}}_{\text{Far-field potential (nested)}} + \underbrace{\phi_{ver}(X)}_{\text{Vertex-sharing potential (non-nested)}} + \underbrace{\sum_{X' \in \mathcal{N}_*(X)} K_{tX, sX'} q_{X'}^{(\kappa)}}_{\text{Near-field potential (direct)}}$$

If $\kappa = 1$, then no far-field interaction exists so $\phi_{X, far}^{(\kappa)} = 0$. We know that X_i is the i^{th} leaf cluster and $\phi_{X_i}^{(\kappa)}$ represents the potential corresponding to it, $1 \leq i \leq 2^{d\kappa}$.

Therefore, the computed potential is given by $\tilde{\phi} = \left[\phi_{X_1}^{(\kappa)}; \phi_{X_2}^{(\kappa)}; \dots; \phi_{X_{2^{d\kappa}}}^{(\kappa)} \right]$ (MATLAB notation). The visual representation of the $(\mathcal{H}^2 + \mathcal{H})_*$ algorithm is given in [Figure 13](#).

$$\tilde{\phi} = \left(\begin{array}{c} \text{Green Matrix} \\ \text{Blue Matrix} \\ \text{Brown Matrix} \end{array} \right) + \left(\text{Blue Matrix} \right) + \left(\text{Brown Matrix} \right) \times \mathbf{q}$$

FIG. 13. In the $(\mathcal{H}^2 + \mathcal{H})_*$ algorithm, the operators (P2M/M2M, M2L and L2L/L2P) corresponding to the far-field interaction are constructed using B2T NCA and the operators (U, V) corresponding to vertex-sharing interaction are constructed using partially pivoted ACA. After that, we calculate the far-field potential by following the Upward, Transverse and Downward tree traversal. The vertex-sharing potential is calculated independently following a single tree traversal. We get the final potential by adding the far-field, vertex-sharing and near-field potentials.

5.2.3. Complexity analysis of $(\mathcal{H}^2 + \mathcal{H})_*$. We construct the $(\mathcal{H}^2 + \mathcal{H})_*$ hierarchical representation using B2T NCA and the ACA.

Time complexity. The time complexity of the initialization steps and the potential calculation steps are given below

- *Far-field interaction compression:* The far-field compression cost of this algorithm is the same as the $\mathcal{H}_*^2(\text{b+t})$ algorithm. Let the leaf cluster size be bounded by p_1 , and we also assume $p_1 = \mathcal{O}(n_{max})$. Let c_{far} be the maximum of the far-field interaction list size (in 2D and 3D for this hierarchical representation $c_{far} = 12$ and 126, respectively). Considering all the levels, the cost is bounded by

$$\sum_{l=2}^{\kappa} 2^{dl} (2^d p_1 + c_{far} 2^d p_1) p_1^2 \approx \mathcal{O}(N).$$

- *Vertex-sharing interaction compression:* Let c_{ver} be the maximum of the vertex-sharing interaction list size of a cluster (in 2D and 3D for this hierarchical representation $c_{ver} = 3$ and 7, respectively). The partially pivoted ACA [5] is applied to a cluster's global row and column indices. Let p_3 be the maximum rank (vertex-sharing blocks) and $p_3 \in \mathcal{O}(\log(N) \log^d(\log(N)))$ [25]. Then the cost for applying ACA for a particular cluster is bounded by $\left(\frac{N}{2^{dl}} + c_{ver} \frac{N}{2^{dl}}\right) p_3^2$. By taking all the levels,

$$\text{the cost for the vertex-sharing interaction compression is bounded by } \sum_{l=1}^{\kappa} 2^{dl} \left(\frac{N}{2^{dl}} + c_{ver} \frac{N}{2^{dl}}\right) p_3^2 =$$

$$\sum_{l=1}^{\kappa} (N + c_{ver} N) p_3^2 \approx \mathcal{O}(p_3 N \log(N)).$$

Therefore, the overall time complexity to initialize the $(\mathcal{H}^2 + \mathcal{H})_*$ hierarchical representation scales asymptotically $\mathcal{O}(N + p_3 N \log(N))$, $p_3 \in \mathcal{O}(\log(N) \log^d(\log(N)))$ [25].

The time required to compute the far-field and vertex-sharing potentials calculation exhibits a scaling of $\mathcal{O}(N)$ and $\mathcal{O}(p_3 N \log(N))$, respectively. Therefore, the overall time complexity for potential calculation (MVP) scales quasi-linearly for the non-oscillatory kernels.

Space complexity. The cost of storing the far-field P2M/M2M, M2L, and L2L/L2P operators is $\mathcal{O}(N)$, same as in the $\mathcal{H}_*^2(\text{b+t})$ algorithm. The cost of storing the vertex-sharing U and V operators is roughly $\mathcal{O}(p_3 N \log(N))$. So, the overall storage cost of the $(\mathcal{H}^2 + \mathcal{H})_*$ algorithm scales quasi-linearly.

Remark 5.4. It is noteworthy that the compression routines of the far-field and vertex-sharing interactions are independent and operate separately for both the proposed algorithms. Hence, one has the flexibility to opt for different values of tolerances, i.e., ϵ_{far} and ϵ_{ver} , to achieve improved compression and, consequently, enhanced relative error control. However, we set $\epsilon_{far} = \epsilon_{ver} = \epsilon$ throughout this article.

Remark 5.5. Despite having the same asymptotic complexities as the \mathcal{H}_* algorithm [25], the proposed $(\mathcal{H}^2 + \mathcal{H})_*$ algorithm demonstrates improved time and storage efficiency due to the use of nested bases for partial interaction list. This enhancement is illustrated in numerical results (Section 6).

Remark 5.6. Note that in 1D ($d = 1$), $\mathcal{H}_*^2 \equiv \text{HSS}$, and $(\mathcal{H}^2 + \mathcal{H})_* \equiv \text{HODLR [2]} \equiv \mathcal{H}_*$.

6. Numerical results. This section presents various numerical experiments to demonstrate the performance of the proposed algorithms. We also compare the proposed algorithms with other related existing **algebraic** fast MVP algorithms and present various benchmarks. Notably, all the algorithms are developed using NCA/ACA-based compression.

For convenience, we discuss a few abbreviations in [Table 7](#) corresponding to the different algebraic fast algorithms discussed in this article. The notation $b+t$ in the parenthesis signifies the utilization of both the B2T NCA and T2B NCA. On the other hand, b or t denotes the exclusive application of either B2T NCA or T2B NCA, respectively.

We perform the following experiments for different algorithms in 2D and 3D, report their performance, scalability, and plot various benchmarks.

- (1) Fast MVP for the kernel matrix arises from different kernel functions. We choose the single layer Laplacian ($\log(r)$) in 2D. In 3D, we select single layer Laplacian ($1/r$), Matérn covariance kernel ($\exp(-r)$) and Helmholtz kernel ($\exp(ir)/r$).
- (2) Fast iterative solver (GMRES) for the Fredholm integral equation of the second kind.
- (3) Fast iterative solver (GMRES) for RBF interpolation.

Abbreviation	Description of the fast MVP algorithm	Admissible clusters	Compression technique(s)	Type of bases
$\mathcal{H}_*^2(b+t)$	The proposed efficient \mathcal{H}_*^2 algorithm. (Subsection 5.1)	Far-field and Vertex-sharing	B2T NCA and T2B NCA	Nested
$(\mathcal{H}^2 + \mathcal{H})_*$	The proposed $(\mathcal{H}^2 + \mathcal{H})_*$ algorithm. (Subsection 5.2)	Far-field and Vertex-sharing	B2T NCA and ACA	Semi-nested
$\mathcal{H}_*^2(t)$	The nested algorithm, where T2B NCA is used upon the entire interaction list ($\mathcal{I}\mathcal{L}_*(X)$). (Subsection 4.2/ Appendix C)	Far-field and Vertex-sharing	T2B NCA	Nested
$\mathcal{H}_{\sqrt{d}}^2(b)$	The standard algebraic \mathcal{H}^2 matrix algorithm, where B2T NCA is used. (Subsection 3.6.2/ Appendix A)	Far-field	B2T NCA	Nested
$\mathcal{H}_{\sqrt{d}}^2(t)$	The standard algebraic \mathcal{H}^2 matrix algorithm, where T2B NCA is used. (Subsection 3.6.3/ Appendix B)	Far-field	T2B NCA	Nested
\mathcal{H}_*	The HODLRdD algorithm in [24 , 25]. In this article, we call it \mathcal{H}_* .	Far-field and Vertex-sharing	ACA	Non-nested
$\mathcal{H}_{\sqrt{d}}$	The standard algebraic \mathcal{H} matrix algorithm. (Subsection 3.3)	Far-field	ACA	Non-nested

TABLE 7

Abbreviations of the algebraic fast MVP algorithms used in this section for various numerical experiments.

It is worth noting that the *initialization time* of the $\mathcal{O}(N)$ NCA discussed in [[36](#), [19](#)] is faster than that of the $\mathcal{O}(N \log(N))$ NCA discussed in [[6](#)]. However, the storage and MVP time scales are similar. The article [[19](#)] also verifies it numerically. Therefore, we believe that it would be sufficient to compare the proposed algorithms with $\mathcal{H}_{\sqrt{d}}^2(b)$ and $\mathcal{H}_{\sqrt{d}}^2(t)$ from [[36](#)].

All the algorithms are developed in a similar fashion in C++ and performed on an Intel Xeon Gold 2.5GHz processor with 8 OpenMP threads within the same environment configuration. We want to emphasize that high-performance implementation is not the goal of this article. The central theme here is to maintain consistency in implementing all the fast algorithms, thereby allowing for meaningful comparisons.

Further, we introduce some other notations in [Table 8](#), which are used in this section.

N	Total number of particles (we consider the same source and target) in the domain
\tilde{K}	\tilde{K} represent the hierarchical low-rank representation of the original kernel matrix K .
Memory (Mem.)	The total memory (in GB) needed to store the hierarchical low-rank representation (\tilde{K}). This refers to the total memory for storing all the operators, including the near-field operators.
Initialization time (t_{init})	The time taken (in seconds) to create the hierarchical low-rank representation \tilde{K} (Initialization routine). This refers to the overall execution time, excluding the time spent on the matrix-vector product operation.
Fast MVP time (t_{MVP})	The time taken (in seconds) to compute the MVP using the hierarchical low-rank representation, i.e., time for fast MVP ($\tilde{K}\mathbf{q}$).
Total time (t_{total})	Total time taken (in seconds), i.e., $t_{total} = t_{init} + t_{mvp}$.
Direct MVP time (t_{direct})	The time taken (in seconds) to compute the direct matrix-vector product, i.e., time for naive MVP.
Solution time (t_{sol})	Total time (in seconds) to solve the system $K\boldsymbol{\sigma} = \mathbf{f}$ using the fast iterative solver GMRES [30]. In the GMRES routine, the MVP is accelerated using the hierarchical low-rank representation (\tilde{K})
n_{max}	Maximum number of particles in leaf-clusters. We set $n_{max} = 100$ and 125 for the experiments in 2D and 3D, respectively.
Relative error in MVP (RE_{MVP})	Let \mathbf{q} be a random column vector and the exact matrix-vector product $\tilde{\boldsymbol{\phi}} = K\mathbf{q}$ (exact up to round-off). The computed column vector $\hat{\boldsymbol{\phi}}$ is given by $\hat{\boldsymbol{\phi}} = \tilde{K}\mathbf{q}$. The 2-norm relative error in the matrix-vector product is given by $\ \hat{\boldsymbol{\phi}} - \tilde{\boldsymbol{\phi}}\ _2 / \ \tilde{\boldsymbol{\phi}}\ _2$
Relative error in solution (RE_{sol})	Let \mathbf{q} be a random column vector and the exact matrix-vector product $\mathbf{b} = K\mathbf{q}$ (exact up to round-off). We set \mathbf{b} as RHS and solve the system $K\boldsymbol{\lambda} = \mathbf{b}$ using the iterative solver, GMRES. The 2-norm relative error in the solution of the system is given by $\ \boldsymbol{\lambda} - \mathbf{q}\ _2 / \ \mathbf{q}\ _2$
NCA/ACA tolerance (ϵ)	The NCA/ACA tolerance. We set $\epsilon = \epsilon_{ver} = \epsilon_{far}$ for all the experiments.
GMRES stopping condition	We use GMRES [30] without restart, and GMRES routine will terminate if the relative residual is less than ϵ_{GMRES} . The matrix-vector product part in the GMRES routine is accelerated using various fast MVP algorithms (Table 7). We set $\epsilon_{GMRES} = 10^{-12}$ and 10^{-10} for the experiments in 2D and 3D, respectively.
$\#iter$	The number of iterations of the fast iterative solver (GMRES) to reach the stopping condition.

TABLE 8

Notations used in this section for various numerical experiments.

6.1. Experiments in two dimensions ($d = 2$). In this subsection, we perform various experiments in 2D, and we consider the same source and target for all the experiments.

6.1.1. Fast MVP in 2D. Let us consider N uniformly distributed particles with location at $\{\mathbf{x}_i\}_{i=1}^N$ in the square $[-1, 1]^2$. We choose the kernel function as the single layer Laplacian in 2D. The $(i, j)^{th}$ entry of the kernel matrix $K \in \mathbb{R}^{N \times N}$ arises from the kernel function $\log(r)$ is given by

$$(6.1) \quad K(i, j) = \begin{cases} \log(r) = \log(\|\mathbf{x}_i - \mathbf{x}_j\|_2) & \text{if } i \neq j \\ 0 & \text{otherwise} \end{cases}$$

We compare the proposed algorithms with the $\mathcal{H}_{\sqrt{d}}^2(\mathbf{b})$, \mathcal{H}_* and $\mathcal{H}_{\sqrt{d}}$ algorithms. Note that the initialization time of $\mathcal{H}_{\sqrt{d}}^2(\mathbf{b})$ is better than $\mathcal{H}_{\sqrt{d}}^2(\mathbf{t})$, and the scaling of memory and MVP time are the same for both (refer to [36]). Hence, it is sufficient to compare the proposed algorithms with $\mathcal{H}_{\sqrt{d}}^2(\mathbf{b})$, i.e., the better one in terms of initialization time. We choose the non-nested algorithms, \mathcal{H}_* and $\mathcal{H}_{\sqrt{d}}$, to demonstrate the improvement over memory (Mem.) and MVP time (t_{MVP}) achieved in the nested algorithms.

We randomly select 5 different column vectors (\mathbf{q}) and perform the fast MVPs ($\tilde{K}\mathbf{q}$) using $\mathcal{H}_*^2(\mathbf{b}+\mathbf{t})$, $(\mathcal{H}^2 + \mathcal{H})_*$, $\mathcal{H}_{\sqrt{d}}^2(\mathbf{b})$, \mathcal{H}_* and $\mathcal{H}_{\sqrt{d}}$ algorithms. The average memory (Mem.), initialization time (t_{init}), MVP time (t_{MVP}), and relative error in MVP (RE_{MVP}) with respect to different tolerances ($\epsilon = 10^{-08}, 10^{-10}, 10^{-12}$) are tabulated in Table 9, Table 10, and Table 11. We also report the direct MVP time (t_{direct}).

	N	Mem. (GB)	t_{init} (s)	t_{MVP} (s)	t_{direct} (s)	Rel. error (RE_{MVP})
$\mathcal{H}_*^{(b+t)}$	102400	0.42	2.94	0.01	63.05	1.82E-08
	409600	1.72	12.66	0.04	1006.78	8.04E-08
	1638400	6.90	61.19	0.16	16116.5	2.01E-07
	6553600	27.61	296.31	0.62	257863.7	1.03E-06
$(\mathcal{H}^2 + \mathcal{H})_*$	102400	0.66	1.83	0.01	63.05	3.91E-08
	409600	3.05	8.17	0.07	1006.78	4.89E-08
	1638400	13.55	38.98	0.38	16116.5	5.36E-08
	6553600	59.70	158.44	1.70	257863.7	1.12E-07
$\mathcal{H}_{\sqrt{d}}^2(b)$	102400	0.56	2.56	0.02	63.05	1.36E-08
	409600	2.32	10.16	0.08	1006.78	1.29E-08
	1638400	9.31	43.23	0.28	16116.5	8.36E-08
	6553600	37.30	172.28	1.11	257863.7	3.22E-07
\mathcal{H}_*	102400	1.02	3.05	0.03	63.05	8.14E-08
	409600	4.92	12.81	0.15	1006.78	1.24E-07
	1638400	23.22	65.12	0.72	16116.5	8.59E-07
	6553600	108.23	313.25	3.59	257863.7	1.51E-07
$\mathcal{H}_{\sqrt{d}}$	102400	1.26	2.92	0.04	63.05	2.07E-09
	409600	6.22	12.71	0.23	1006.78	3.18E-08
	1638400	29.58	64.42	1.09	16116.5	6.73E-08
	6553600	136.44	308.83	5.19	257863.7	5.35E-08

TABLE 9

Comparison between the proposed algorithms and other **algebraic** algorithms as mentioned in Table 7 for the single layer Laplacian in 2D with tolerance $\epsilon = 10^{-08}$. Rel. error refers to 2-norm relative error in MVP, i.e., RE_{MVP} (refer to Table 8).

	N	Mem. (GB)	t_{init} (s)	t_{MVP} (s)	t_{direct} (s)	Rel. error (RE_{MVP})
$\mathcal{H}_*^{(b+t)}$	102400	0.49	3.96	0.01	63.05	7.67E-10
	409600	2.02	15.93	0.05	1006.78	2.40E-09
	1638400	8.18	74.03	0.21	16116.5	1.37E-09
	6553600	32.63	392.58	0.86	257863.7	4.81E-09
$(\mathcal{H}^2 + \mathcal{H})_*$	102400	0.77	2.61	0.02	63.05	3.41E-11
	409600	3.57	12.35	0.11	1006.78	7.58E-11
	1638400	16.25	50.02	0.47	16116.5	1.44E-10
	6553600	71.02	228.27	2.11	257863.7	8.14E-10
$\mathcal{H}_{\sqrt{d}}^2(b)$	102400	0.62	2.71	0.02	63.05	9.37E-11
	409600	2.46	12.52	0.08	1006.78	3.53E-10
	1638400	10.28	51.66	0.35	16116.5	3.84E-10
	6553600	41.20	232.39	1.41	257863.7	2.17E-09
\mathcal{H}_*	102400	1.21	4.04	0.05	63.05	6.26E-10
	409600	5.88	16.44	0.21	1006.78	1.99E-09
	1638400	28.55	80.12	0.99	16116.5	1.40E-09
	6553600	131.8	398.17	5.11	257863.7	4.60E-09
$\mathcal{H}_{\sqrt{d}}$	102400	1.47	4.01	0.06	63.05	1.98E-11
	409600	7.34	16.87	0.23	1006.78	2.08E-11
	1638400	35.09	82.23	1.21	16116.5	8.64E-11
	6553600	162.62	395.71	6.08	257863.7	5.31E-10

TABLE 10

Comparison between the proposed algorithms and other **algebraic** algorithms as mentioned in Table 7 for the single layer Laplacian in 2D with tolerance $\epsilon = 10^{-10}$. Rel. error refers to 2-norm relative error in MVP, i.e., RE_{MVP} (refer to Table 8).

	N	Mem. (GB)	t_{init} (s)	t_{MVP} (s)	t_{direct} (s)	Rel. error (RE_{MVP})
$\mathcal{H}_*^2(\text{b+t})$	102400	0.56	4.94	0.02	63.05	1.63E-12
	409600	2.33	22.33	0.06	1006.78	1.06E-11
	1638400	9.44	102.08	0.25	16116.5	3.93E-11
	6553600	37.75	495.43	1.01	257863.7	1.15E-10
$(\mathcal{H}^2 + \mathcal{H})_*$	102400	0.88	3.36	0.04	63.05	7.86E-13
	409600	4.12	15.65	0.2	1006.78	1.36E-12
	1638400	18.89	68.01	1.01	16116.5	1.36E-11
	6553600	86.49	288.72	4.50	257863.7	2.49E-11
$\mathcal{H}_{\sqrt{d}}^2(\text{b})$	102400	0.69	3.25	0.02	63.05	7.09E-12
	409600	2.82	15.46	0.09	1006.78	2.93E-11
	1638400	11.21	69.47	0.39	16116.5	3.34E-11
	6553600	45.99	294.3	1.64	257863.7	1.13E-11
\mathcal{H}_*	102400	1.41	3.57	0.08	63.05	1.76E-11
	409600	6.91	21.19	0.41	1006.78	2.63E-11
	1638400	33.07	109.33	2.05	16116.5	7.37E-11
	6553600	-	-	-	-	-
$\mathcal{H}_{\sqrt{d}}$	102400	1.68	3.66	0.10	63.05	1.35E-13
	409600	8.41	26.84	0.42	1006.78	1.43E-13
	1638400	40.47	121.10	2.32	16116.5	6.69E-12
	6553600	-	-	-	-	-

TABLE 11

Comparison between the proposed algorithms and other **algebraic** algorithms as mentioned in Table 7 for the single layer Laplacian in 2D with tolerance $\epsilon = 10^{-12}$. Rel. error refers to 2-norm relative error in MVP, i.e., RE_{MVP} (refer to Table 8).

The job either exceeds the specified wall time or is out of the memory corresponding to the cells with “-” in the tables.

From the Table 9, Table 10, and Table 11, the following conclusions can be drawn.

1. The scaling of the memory (Mem.) and MVP time (t_{MVP}) of the $\mathcal{H}_*^2(\text{b+t})$ algorithm is similar to that of $\mathcal{H}_{\sqrt{d}}^2(\text{b})$. Notably, $\mathcal{H}_*^2(\text{b+t})$ shows slightly less storage usage and improved MVP time.
2. In 2D, the initialization time (t_{init}) of $\mathcal{H}_*^2(\text{b+t})$ is slightly higher than that of $\mathcal{H}_{\sqrt{d}}^2(\text{b})$. This is due to the fact that in $\mathcal{H}_*^2(\text{b+t})$, the *vertex-sharing* interactions are compressed using T2B NCA, which scales quasi-linearly, while in $\mathcal{H}_{\sqrt{d}}^2(\text{b})$, the initialization time scales roughly $\mathcal{O}(N)$. Overall, the initialization time of the $\mathcal{H}_*^2(\text{b+t})$ scales quasi-linearly.
3. $\mathcal{H}_*^2(\text{b+t})$ and $\mathcal{H}_{\sqrt{d}}^2(\text{b})$ are the nested versions of \mathcal{H}_* and $\mathcal{H}_{\sqrt{d}}$ algorithms, respectively. We can see that the nested versions require much less storage and improved MVP time than the non-nested ones.
4. The initialization time of $(\mathcal{H}^2 + \mathcal{H})_*$ is the fastest and scales similar to the initialization time of $\mathcal{H}_{\sqrt{d}}^2(\text{b})$.
5. The *semi-nested* $(\mathcal{H}^2 + \mathcal{H})_*$ is better than the \mathcal{H}_* and $\mathcal{H}_{\sqrt{d}}$ matrix algorithms due to the use of semi/partially nested bases. Thus, $(\mathcal{H}^2 + \mathcal{H})_*$ demonstrates a nice balance between nested and non-nested algorithms in 2D.

We arrange the above fast algorithms in ascending order with respect to memory usage and MVP time.

Memory: $\mathcal{H}_*^2(\text{b+t}) < \mathcal{H}_{\sqrt{d}}^2(\text{b}) < (\mathcal{H}^2 + \mathcal{H})_* < \mathcal{H}_* < \mathcal{H}_{\sqrt{d}}$

MVP time: $\mathcal{H}_*^2(\text{b+t}) < \mathcal{H}_{\sqrt{d}}^2(\text{b}) < (\mathcal{H}^2 + \mathcal{H})_* < \mathcal{H}_* < \mathcal{H}_{\sqrt{d}}$

Therefore, though we do not have a strict theoretical error bound, the above numerical experiment demonstrates that the proposed $\mathcal{H}_*^2(\text{b+t})$ algorithm shows slightly less memory usage and improved MVP time than the $\mathcal{H}_{\sqrt{d}}^2$ matrix algorithm with comparable accuracy.

6.1.2. Fast MVP accelerated GMRES for integral equation in 2D. In this experiment, Our goal is to compare the performance of the proposed algorithms with various nested algorithms from Table 7.

Consider the Fredholm integral equation of the second kind over $C = [-1, 1]^2 \subset \mathbb{R}^2$, which is given by

$$(6.2) \quad \sigma(\mathbf{x}) + \int_C F(\mathbf{x}, \mathbf{y}) \sigma(\mathbf{y}) d\mathbf{y} = f(\mathbf{x}) \quad \mathbf{x}, \mathbf{y} \in C$$

with $F(\mathbf{x}, \mathbf{y}) = -\frac{1}{2\pi} \log(\|\mathbf{x} - \mathbf{y}\|_2)$ (Green's function for Laplace equation in 2D). We follow a piece-wise constant collocation method with collocation points on a uniform grid in $C = [-1, 1]^2$ to discretize (6.2) and set the RHS \mathbf{f} as described in the 11th cell of Table 8. Therefore, the following linear system can be obtained

$$(6.3) \quad K\boldsymbol{\sigma} = \mathbf{f}$$

The Equation (6.3) is solved using **fast** GMRES, i.e., the MVP part of GMRES is accelerated using the $\mathcal{H}_*^2(\text{b+t})$, $(\mathcal{H}^2 + \mathcal{H})_*$, $\mathcal{H}_{\sqrt{d}}^2(\text{b})$, $\mathcal{H}_*^2(\text{t})$ and $\mathcal{H}_{\sqrt{d}}^2(\text{t})$ algorithms. We set $\epsilon = 10^{-10}$ and $\epsilon_{GMRES} = 10^{-12}$ and report the memory, initialization time, solution time and number of iterations in Table 12. The relative error in solution (RE_{sol}) is of order 10^{-12} in all cases. We also plot the memory (Figure 14a), initialization time (Figure 14b) and solution time (Figure 14c) in Figure 14.

N	Memory (GB)					Initialization time (s)					Solution time (s)					#iter
	$\mathcal{H}_*^2(\text{b+t})$	$(\mathcal{H}^2 + \mathcal{H})_*$	$\mathcal{H}_{\sqrt{d}}^2(\text{b})$	$\mathcal{H}_*^2(\text{t})$	$\mathcal{H}_{\sqrt{d}}^2(\text{t})$	$\mathcal{H}_*^2(\text{b+t})$	$(\mathcal{H}^2 + \mathcal{H})_*$	$\mathcal{H}_{\sqrt{d}}^2(\text{b})$	$\mathcal{H}_*^2(\text{t})$	$\mathcal{H}_{\sqrt{d}}^2(\text{t})$	$\mathcal{H}_*^2(\text{b+t})$	$(\mathcal{H}^2 + \mathcal{H})_*$	$\mathcal{H}_{\sqrt{d}}^2(\text{b})$	$\mathcal{H}_*^2(\text{t})$	$\mathcal{H}_{\sqrt{d}}^2(\text{t})$	
25600	0.11	0.15	0.14	0.12	0.14	0.62	0.45	0.54	1.22	1.2	0.03	0.04	0.04	0.03	0.06	6
102400	0.48	0.74	0.60	0.55	0.60	4.02	2.11	3.18	9.11	7.625	0.14	0.19	0.17	0.17	0.22	6
409600	2.03	3.56	2.52	2.34	2.52	18.57	10.22	13.51	60.79	42.11	0.59	0.90	0.75	0.72	1.02	6
1638400	8.25	16.29	10.33	9.45	10.33	101.05	44.2	61.39	402.29	219.66	2.29	3.98	2.79	2.75	4.10	6
2250000	10.15	22.74	13.18	12.19	13.17	182.42	72.85	101.67	615.54	347.74	3.82	7.02	4.74	4.39	7.27	6

TABLE 12

Performance of the proposed and the nested algorithms as mentioned in Table 7. We set $\epsilon = 10^{-10}$ and $\epsilon_{GMRES} = 10^{-12}$.

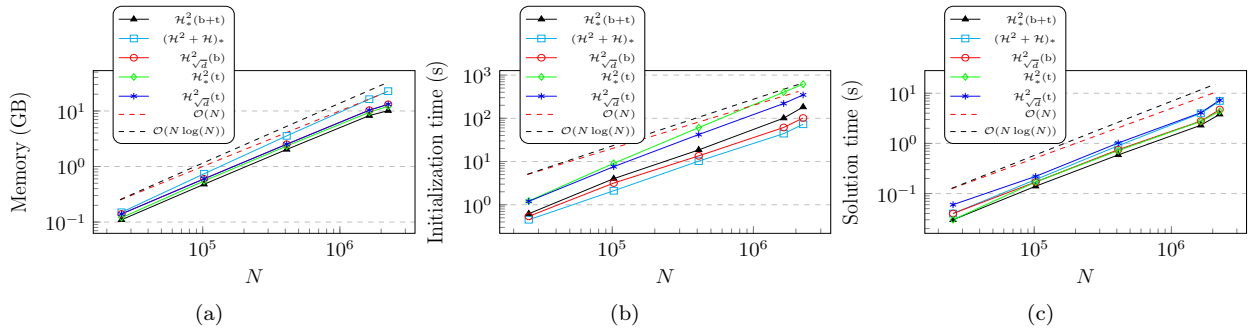


FIG. 14. Plots of Memory, Initialization time and Solution time of the fast MVP algorithms.

Let us arrange the fast algorithms in ascending order with respect to memory usage and solution time.

Memory: $\mathcal{H}_*^2(\text{b+t}) < \mathcal{H}_*^2(\text{t}) < \mathcal{H}_{\sqrt{d}}^2(\text{b}) \leq \mathcal{H}_{\sqrt{d}}^2(\text{t}) < (\mathcal{H}^2 + \mathcal{H})_*$

Solution time: $\mathcal{H}_*^2(\text{b+t}) < \mathcal{H}_*^2(\text{t}) < \mathcal{H}_{\sqrt{d}}^2(\text{b}) < \mathcal{H}_{\sqrt{d}}^2(\text{t}) < (\mathcal{H}^2 + \mathcal{H})_*$

6.1.3. Fast MVP accelerated GMRES for RBF interpolation in 2D. Let the location of the particles $\{\mathbf{x}_i\}_{i=1}^N$ be the $\sqrt{N} \times \sqrt{N}$ Chebyshev grid on the domain $[-1, 1]^2$. We consider the Chebyshev distribution of particles to study the performance of the nested algorithms over slightly non-uniformly distributed particles. However, we use the uniform 2^d tree (quad tree in 2D) as described in Subsection 3.1. Let us consider the following radial basis function

$$(6.4) \quad G(r) = \begin{cases} a/r & \text{if } r \geq a \\ r/a & \text{if } r < a \end{cases}$$

Below is the dense linear system generated by the radial basis function G

$$(6.5) \quad \alpha \lambda_i + \sum_{j=1, j \neq i}^N G(\|\mathbf{x}_i - \mathbf{x}_j\|_2) \lambda_j = b_i, \quad i = 1, 2, \dots, N.$$

We set $a = 0.0001$ and $\alpha = N^{1/4}$. By setting \mathbf{b} as described in the 11th cell of Table 8, the Equation (6.5) can be written in the form

$$(6.6) \quad K\lambda = \mathbf{b}$$

The Equation (6.6) is solved using **fast** GMRES. We set $\epsilon = 10^{-10}$ and $\epsilon_{GMRES} = 10^{-12}$ and report the memory, initialization time and solution time in Table 13 for all the nested algorithms. The relative error in solution (RE_{sol}) is of order 10^{-9} in all cases. We also plot the memory (Figure 15a), initialization time (Figure 15b) and solution time (Figure 15c) in Figure 15.

N	Memory (GB)					Initialization time (s)					Solution time (s)				#iter
	$\mathcal{H}_*^2(\mathbf{b}+\mathbf{t})$	$(\mathcal{H}^2 + \mathcal{H})_*$	$\mathcal{H}_{\sqrt{d}}^2(\mathbf{b})$	$\mathcal{H}_*^2(\mathbf{t})$	$\mathcal{H}_{\sqrt{d}}^2(\mathbf{t})$	$\mathcal{H}_*^2(\mathbf{b}+\mathbf{t})$	$(\mathcal{H}^2 + \mathcal{H})_*$	$\mathcal{H}_{\sqrt{d}}^2(\mathbf{b})$	$\mathcal{H}_*^2(\mathbf{t})$	$\mathcal{H}_{\sqrt{d}}^2(\mathbf{t})$	$\mathcal{H}_*^2(\mathbf{b}+\mathbf{t})$	$(\mathcal{H}^2 + \mathcal{H})_*$	$\mathcal{H}_{\sqrt{d}}^2(\mathbf{b})$	$\mathcal{H}_*^2(\mathbf{t})$	
25600	0.16	0.20	0.18	0.17	0.18	0.64	0.28	0.37	1.26	1.03	0.07	0.08	0.08	0.07	0.09
102400	0.83	2.06	0.94	0.92	0.94	4.57	2.06	2.24	12.12	7.48	0.50	0.59	0.57	0.63	
409600	4.08	5.55	4.67	4.52	4.67	28.68	10.22	12.67	100.06	45.09	3.65	4.18	3.98	4.01	
1638400	19.31	28.47	22.43	22.09	22.41	182.27	61.95	74.50	709.76	268.86	26.27	35.09	30.11	28.78	
2250000	21.43	34.64	24.61	24.12	24.60	310.58	105.48	145.85	1054.3	577.35	38.15	50.57	42.32	40.55	

TABLE 13

Performance of the proposed and the nested algorithms as mentioned in Table 7. We set $\epsilon = 10^{-10}$ and $\epsilon_{GMRES} = 10^{-12}$.

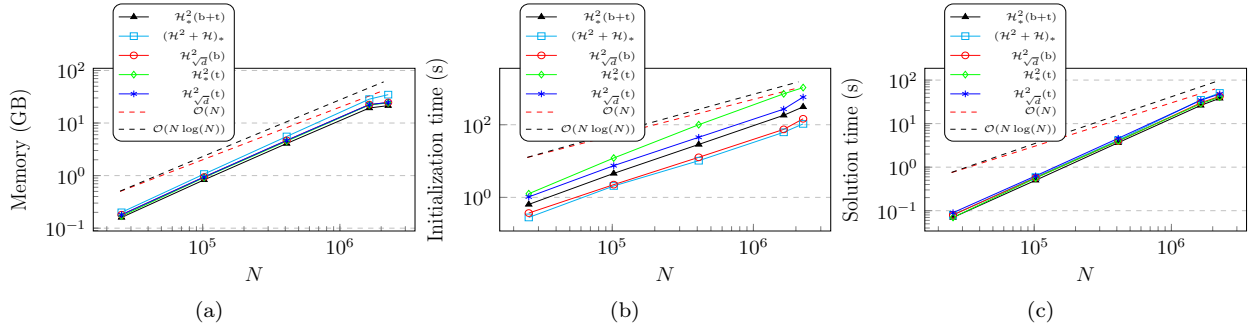


FIG. 15. Plots of Memory, Initialization time and Solution time of the fast MVP algorithms.

Let us arrange the fast algorithms in ascending order with respect to memory usage and solution time.

Memory: $\mathcal{H}_*^2(\mathbf{b}+\mathbf{t}) < \mathcal{H}_*^2(\mathbf{t}) < \mathcal{H}_{\sqrt{d}}^2(\mathbf{b}) \leq \mathcal{H}_{\sqrt{d}}^2(\mathbf{t}) < (\mathcal{H}^2 + \mathcal{H})_*$

Solution time: $\mathcal{H}_*^2(\mathbf{b}+\mathbf{t}) < \mathcal{H}_*^2(\mathbf{t}) < \mathcal{H}_{\sqrt{d}}^2(\mathbf{b}) < \mathcal{H}_{\sqrt{d}}^2(\mathbf{t}) < (\mathcal{H}^2 + \mathcal{H})_*$

Summary of the experiments in 2D. Here is a summary of the results obtained from all the experiments performed in 2D.

1. In all the experiments, the proposed $\mathcal{H}_*^2(\mathbf{b}+\mathbf{t})$ outperforms all the other algebraic algorithms (Table 7) in terms of memory and MVP/Solution time.
2. The initialization time of the $\mathcal{H}_*^2(\mathbf{t})$ algorithm (Subsection 4.2) is the highest and the proposed $\mathcal{H}_*^2(\mathbf{b}+\mathbf{t})$ performs way better than the $\mathcal{H}_*^2(\mathbf{t})$ algorithm.
3. The $(\mathcal{H}^2 + \mathcal{H})_*$ is the fastest among the other algorithms in terms of the initialization time and it performs better than the non-nested algorithms.
4. The initialization time of $\mathcal{H}_{\sqrt{d}}^2(\mathbf{b})$ is better than the $\mathcal{H}_{\sqrt{d}}^2(\mathbf{t})$, and the scaling of the memory and MVP time are almost the same, which was shown in [36] also.

6.2. Experiments in three dimensions ($d = 3$). In this subsection, we perform various experiments in 3D. We consider the same source and target for all the experiments.

6.2.1. Fast MVP in 3D. Let us consider N uniformly distributed particles with location at $\{\mathbf{x}_i\}_{i=1}^N$ in the cube $[-1, 1]^3$. We choose the kernel function as the single layer Laplacian in 3D. The $(i, j)^{th}$ entry of the kernel matrix $K \in \mathbb{R}^{N \times N}$ arises from the kernel function $1/r$ is given by

$$(6.7) \quad K(i, j) = \begin{cases} \frac{1}{r} = \frac{1}{\|\mathbf{x}_i - \mathbf{x}_j\|_2} & \text{if } i \neq j \\ 0 & \text{otherwise} \end{cases}$$

We compare the proposed algorithms with the $\mathcal{H}_{\sqrt{d}}^2(\text{b})$ (the better \mathcal{H}^2 matrix algorithm in terms of initialization time), \mathcal{H}_* and $\mathcal{H}_{\sqrt{d}}$ algorithms. Again, we choose the non-nested algorithms, \mathcal{H}_* and $\mathcal{H}_{\sqrt{d}}$, to demonstrate the improvement over memory (Mem.) and MVP time (t_{MVP}) achieved in the nested algorithms.

We randomly select 5 different column vectors (\mathbf{q}) and perform the fast MVPs ($\tilde{K}\mathbf{q}$) using $\mathcal{H}_{\sqrt{d}}^2(\text{b}+\text{t})$, $(\mathcal{H}^2 + \mathcal{H})_*$, $\mathcal{H}_{\sqrt{d}}^2(\text{b})$, \mathcal{H}_* and $\mathcal{H}_{\sqrt{d}}$ algorithms. The average memory (Mem.), initialization time (t_{init}), MVP time (t_{MVP}), and relative error in MVP (RE_{MVP}) with respect to different tolerances ($\epsilon = 10^{-4}, 10^{-6}, 10^{-8}$) are tabulated in [Table 14](#), [Table 15](#), and [Table 16](#). We also report the direct MVP time (t_{direct}).

	N	Mem. (GB)	t_{init} (s)	t_{MVP} (s)	t_{direct} (s)	Rel. error (RE_{MVP})
$\mathcal{H}_{\sqrt{d}}^2(\text{b}+\text{t})$	64000	0.91	2.76	0.03	13.18	1.94E-04
	512000	9.18	51.78	0.41	851.35	3.85E-04
	1000000	21.36	131.65	1.03	3829.64	7.15E-04
	1728000	39.07	237.65	2.25	11575.3	1.08E-03
$(\mathcal{H}^2 + \mathcal{H})_*$	64000	1.04	1.56	0.04	13.18	8.41E-05
	512000	10.68	37.81	0.57	851.35	1.24E-04
	1000000	25.41	117.32	1.83	3829.64	1.38E-04
	1728000	46.71	210.51	3.12	11575.3	1.67E-03
$\mathcal{H}_{\sqrt{d}}^2(\text{b})$	64000	1.16	4.11	0.04	13.18	7.57E-05
	512000	12.64	60.06	0.79	851.35	5.85E-04
	1000000	27.56	150.51	1.88	3829.64	1.24E-04
	1728000	50.79	267.6	3.61	11575.3	1.86E-03
\mathcal{H}_*	64000	1.59	1.41	0.07	13.18	3.85E-05
	512000	20.07	45.67	0.88	851.35	4.89E-04
	1000000	50.21	109.16	4.18	3829.64	2.97E-04
	1728000	86.94	192.64	7.78	11575.3	1.99E-03
$\mathcal{H}_{\sqrt{d}}$	64000	1.83	2.11	0.07	13.18	3.44E-05
	512000	23.77	47.23	1.06	851.35	2.98E-04
	1000000	59.75	103.54	4.92	3829.64	2.43E-04
	1728000	103.07	197.46	7.91	11575.3	5.69E-04

TABLE 14

Comparison between the proposed algorithms and other **algebraic** algorithms as mentioned in [Table 7](#) for the single layer Laplacian in 3D with tolerance $\epsilon = 10^{-4}$. Rel. error refers to 2-norm relative error in MVP, i.e., RE_{MVP} (refer to [Table 8](#)).

	N	Mem. (GB)	t_{init} (s)	t_{MVP} (s)	t_{direct} (s)	Rel. error (RE_{MVP})
$\mathcal{H}_*^2(\text{b}+\text{t})$	64000	2.07	10.71	0.07	13.18	1.69E-06
	512000	22.98	237.27	0.67	851.35	4.41E-06
	1000000	43.38	528.45	1.34	3829.64	5.34E-06
	1728000	76.35	951.12	2.75	11575.3	1.30E-05
$(\mathcal{H}^2 + \mathcal{H})_*$	64000	2.27	8.73	0.10	13.18	5.91E-07
	512000	26.20	211.44	1.26	851.35	1.04E-06
	1000000	51.14	477.23	2.65	3829.64	1.64E-06
	1728000	91.67	863.76	5.21	11575.3	1.76E-05
$\mathcal{H}_*^2(\text{b})$	64000	2.47	12.27	0.11	13.18	2.02E-06
	512000	28.38	265.71	1.41	851.35	8.44E-06
	1000000	54.39	641.85	2.77	3829.64	1.41E-05
	1728000	96.25	1121.62	5.89	11575.3	3.91E-05
\mathcal{H}_*	64000	2.78	5.78	0.24	13.18	2.95E-06
	512000	36.69	78.41	2.25	851.35	4.25E-06
	1000000	98.93	255.34	5.36	3829.64	8.33E-06
	1728000	172.26	589.91	11.35	11575.3	1.56E-05
$\mathcal{H}_{\sqrt{d}}$	64000	3.07	5.87	0.25	13.18	8.54E-07
	512000	41.91	89.41	2.87	851.35	1.27E-06
	1000000	113.34	257.31	5.88	3829.64	3.51E-06
	1728000	-	-	-	-	-

TABLE 15

Comparison between the proposed algorithms and other **algebraic** algorithms as mentioned in Table 7 for the single layer Laplacian in 3D with tolerance $\epsilon = 10^{-6}$. Rel. error refers to 2-norm relative error in MVP, i.e., RE_{MVP} (refer to Table 8).

	N	Mem. (GB)	t_{init} (s)	t_{MVP} (s)	t_{direct} (s)	Rel. error (RE_{MVP})
$\mathcal{H}_*^2(\text{b}+\text{t})$	64000	2.94	21.16	0.10	13.18	7.96E-09
	512000	35.17	540.01	1.38	851.35	1.85E-08
	1000000	77.47	1260.17	2.84	3829.64	5.45E-08
	1728000	143.20	2502.12	5.11	11575.3	1.68E-07
$(\mathcal{H}^2 + \mathcal{H})_*$	64000	3.19	17.34	0.12	13.18	4.95E-08
	512000	39.52	498.17	1.43	851.35	5.12E-08
	1000000	88.22	1104.75	3.45	3829.64	1.03E-07
	1728000	165.07	2111.28	6.58	11575.3	1.33E-07
$\mathcal{H}_*^2(\text{b})$	64000	3.44	30.07	0.12	13.18	4.79E-08
	512000	42.99	645.32	1.68	851.35	8.53E-08
	1000000	96.54	1672.41	4.79	3829.64	1.27E-07
	1728000	-	-	-	-	-
\mathcal{H}_*	64000	4.32	10.12	0.23	13.18	1.63E-08
	512000	58.89	195.06	3.42	851.35	2.60E-08
	1000000	153.92	565.13	8.78	3829.64	2.50E-07
	1728000	-	-	-	-	-
$\mathcal{H}_{\sqrt{d}}$	64000	4.71	9.15	0.25	13.18	8.47E-09
	512000	66.16	172.22	3.85	851.35	1.20E-08
	1000000	180.43	511.13	10.55	3829.64	4.15E-08
	1728000	-	-	-	-	-

TABLE 16

Comparison between the proposed algorithms and other **algebraic** algorithms as mentioned in Table 7 for the single layer Laplacian in 3D with tolerance $\epsilon = 10^{-8}$. Rel. error refers to 2-norm relative error in MVP, i.e., RE_{MVP} (refer to Table 8).

From the [Table 14](#), [Table 15](#), and [Table 16](#), the following conclusions can be drawn.

1. The scaling of the memory and MVP time of the $\mathcal{H}_*^2(\text{b+t})$ algorithm is similar to that of $\mathcal{H}_{\sqrt{d}}^2(\text{b})$, and notably, $\mathcal{H}_*^2(\text{b+t})$ shows less storage and improved MVP time. [Table 16](#) indicates that we get output for $N = 1728000$ in the proposed algorithms $(\mathcal{H}_*^2(\text{b+t}), (\mathcal{H}^2 + \mathcal{H})_*)$. However, outputs corresponding to $N = 1728000$ are unavailable for the other algorithms as they ran out of memory.
2. In 3D, the initialization time of $\mathcal{H}_*^2(\text{b+t})$ is better than that of $\mathcal{H}_{\sqrt{d}}^2(\text{b})$ for a reasonably large value of N (up to $N \leq 1728000$, the maximum value of N achievable in our system), even though the initialization of $\mathcal{H}_{\sqrt{d}}^2(\text{b})$ scales linearly. The reason is as we go for the higher dimensional problems, the interaction list size as well as the far-field rank value, grow exponentially with the underlying dimension (the far-field rank scales as $\mathcal{O}(1)$ with N , but the value of the constant is large), and the $\mathcal{H}_{\sqrt{d}}^2(\text{b})$ has a larger interaction list compared to the $\mathcal{H}_*^2(\text{b+t})$ (refer to [Table 5](#)).
3. $\mathcal{H}_*^2(\text{b+t})$ and $\mathcal{H}_{\sqrt{d}}^2(\text{b})$ are the nested versions of \mathcal{H}_* and $\mathcal{H}_{\sqrt{d}}$ algorithms, respectively. We can see that the nested versions require much less storage and improved MVP time than the non-nested ones.
4. It is noteworthy that in 3D, the *semi-nested* $(\mathcal{H}^2 + \mathcal{H})_*$ is slightly better than the $\mathcal{H}_{\sqrt{d}}^2(\text{b})$ in terms of both memory and time.

We arrange the above algorithms in ascending order with respect to memory and MVP time.

Memory: $\mathcal{H}_*^2(\text{b+t}) < (\mathcal{H}^2 + \mathcal{H})_* < \mathcal{H}_{\sqrt{d}}^2(\text{b}) < \mathcal{H}_* < \mathcal{H}_{\sqrt{d}}$

MVP time: $\mathcal{H}_*^2(\text{b+t}) < (\mathcal{H}^2 + \mathcal{H})_* < \mathcal{H}_{\sqrt{d}}^2(\text{b}) < \mathcal{H}_* < \mathcal{H}_{\sqrt{d}}$

Therefore, though we do not have a strict theoretical error bound, the above numerical experiment demonstrates that in 3D, the proposed $\mathcal{H}_*^2(\text{b+t})$ and $(\mathcal{H}^2 + \mathcal{H})_*$ algorithms show less memory usage and improved MVP time than the standard \mathcal{H}^2 matrix algorithm with comparable accuracy.

We also perform the fast MVPs for the Matérn and Helmholtz kernels with the performance analysis of both the proposed and various nested algorithms as mentioned in [Table 7](#). Please refer to [Appendix D.1](#) for more details.

6.2.2. Fast MVP accelerated GMRES for integral equation in 3D. We consider the Fredholm integral equation of the second kind over $C = [-1, 1]^3 \subset \mathbb{R}^3$, which is given by

$$(6.8) \quad \sigma(\mathbf{x}) + \int_C F(\mathbf{x}, \mathbf{y}) \sigma(\mathbf{y}) d\mathbf{y} = f(\mathbf{x}) \quad \mathbf{x}, \mathbf{y} \in C$$

with $F(\mathbf{x}, \mathbf{y}) = \frac{1}{4\pi \|\mathbf{x} - \mathbf{y}\|_2}$ (Green's function for Laplace equation in 3D). We follow a piece-wise constant collocation method with collocation points on a uniform grid in $C = [-1, 1]^3$ to discretize (6.8) and set the RHS \mathbf{f} as described in [Table 8](#). Therefore, we obtain the following linear system

$$(6.9) \quad K\boldsymbol{\sigma} = \mathbf{f}$$

The [Equation \(6.9\)](#) is solved using **fast** GMRES, i.e., the MVP part of GMRES is accelerated using the $\mathcal{H}_*^2(\text{b+t})$, $(\mathcal{H}^2 + \mathcal{H})_*$, $\mathcal{H}_{\sqrt{d}}^2(\text{b})$, $\mathcal{H}_*^2(\text{t})$ and $\mathcal{H}_{\sqrt{d}}^2(\text{t})$ algorithms. We set $\epsilon = 10^{-6}$ and $\epsilon_{GMRES} = 10^{-10}$ and report the memory, initialization time, and solution time in [Table 17](#). The relative error in solution (RE_{sol}) is of order 10^{-10} in all cases. We also plot the memory ([Figure 16a](#)), initialization time ([Figure 16b](#)) and solution time ([Figure 16c](#)) in [Figure 16](#).

N	Memory (GB)					Initialization time (s)					Solution time (s)					#iter
	$\mathcal{H}_*^2(\text{b+t})$	$(\mathcal{H}^2 + \mathcal{H})_*$	$\mathcal{H}_{\sqrt{d}}^2(\text{b})$	$\mathcal{H}_*^2(\text{t})$	$\mathcal{H}_{\sqrt{d}}^2(\text{t})$	$\mathcal{H}_*^2(\text{b+t})$	$(\mathcal{H}^2 + \mathcal{H})_*$	$\mathcal{H}_{\sqrt{d}}^2(\text{b})$	$\mathcal{H}_*^2(\text{t})$	$\mathcal{H}_{\sqrt{d}}^2(\text{t})$	$\mathcal{H}_*^2(\text{b+t})$	$(\mathcal{H}^2 + \mathcal{H})_*$	$\mathcal{H}_{\sqrt{d}}^2(\text{b})$	$\mathcal{H}_*^2(\text{t})$	$\mathcal{H}_{\sqrt{d}}^2(\text{t})$	
64000	2.07	2.17	2.47	2.26	2.46	17.6	13.66	18.5	25.22	20.81	0.52	0.55	0.72	0.78	0.7	5
125000	4.19	4.49	5.09	4.68	5.06	47.81	38.84	52.27	67.97	57.6	1.10	1.16	1.80	1.78	1.35	4
512000	22.99	24.64	28.33	26.54	28.25	271.53	230.77	311.19	510.19	412.39	5.54	7.23	8.25	7.15	8.07	5
1000000	43.34	48.30	54.38	50.40	54.11	601.7	512.91	760.36	1296.93	1001.32	10.44	13.09	17.22	14.81	15.02	5
1728000	76.12	85.52	95.56	91.11	95.49	1021.61	861.95	1278.25	2952.32	2049.52	16.03	21.68	25.06	22.08	24.47	4

TABLE 17

Performance of the proposed and the nested algorithms as mentioned in [Table 7](#). We set $\epsilon = 10^{-6}$ and $\epsilon_{GMRES} = 10^{-10}$.

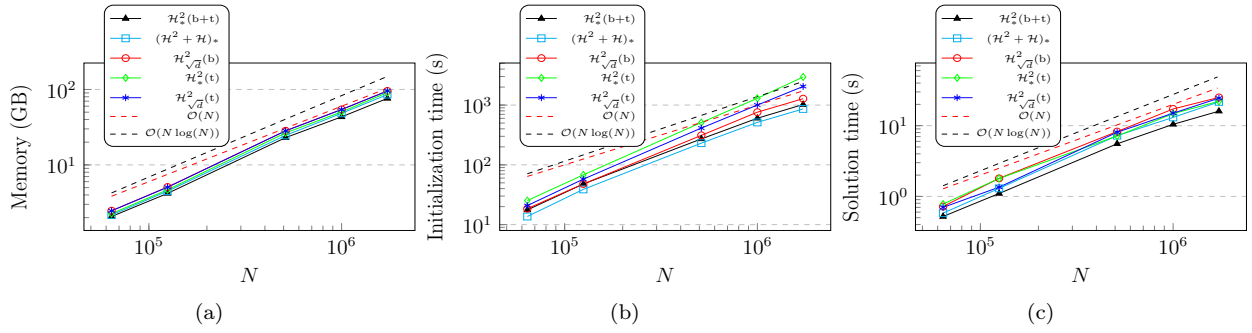


FIG. 16. Plots of Memory, Initialization time and Solution time of the fast MVP algorithms.

We arrange the above algorithms in ascending order with respect to memory and solution time.

Memory: $\mathcal{H}_*^2(\mathbf{b}+\mathbf{t}) < (\mathcal{H}^2 + \mathcal{H})_* < \mathcal{H}_*^2(\mathbf{t}) < \mathcal{H}_{\sqrt{d}}^2(\mathbf{b}) \leq \mathcal{H}_{\sqrt{d}}^2(\mathbf{t})$

Solution time: $\mathcal{H}_*^2(\mathbf{b}+\mathbf{t}) < (\mathcal{H}^2 + \mathcal{H})_* < \mathcal{H}_*^2(\mathbf{t}) < \mathcal{H}_{\sqrt{d}}^2(\mathbf{t}) < \mathcal{H}_{\sqrt{d}}^2(\mathbf{b})$

6.2.3. Fast MVP accelerated GMRES for RBF interpolation in 3D. Let the location of the particles $\{\mathbf{x}_i\}_{i=1}^N$ be the $N^{1/3} \times N^{1/3} \times N^{1/3}$ Chebyshev grid on the domain $[-1, 1]^3$. We choose the Chebyshev distribution of particles to study the performance of the nested algorithms over non-uniformly distributed particles. However, we use the uniform 2^d tree (oct tree in 3D) as described in Subsection 3.1. In this experiment, we consider the following non-translation invariant (NTI) scaled multiquadric radial basis function [10]

$$(6.10) \quad F(\mathbf{x}, \mathbf{y}) = \left(\|\mathbf{x} - \mathbf{y}\|_2^2 + (c(\mathbf{x}) - c(\mathbf{y}))^2 + 1 \right)^{3/2}$$

where $c(\mathbf{x}) = \exp(-(\mathbf{x}(1) + \mathbf{x}(3)))$ and $\mathbf{x} = (\mathbf{x}(1), \mathbf{x}(2), \mathbf{x}(3))$.

Consider the following linear system generated by the above NTI kernel function F

$$(6.11) \quad \lambda_i \sqrt{N} + \sum_{j=1}^N F(\mathbf{x}_i, \mathbf{x}_j) \lambda_j = b_i, \quad i = 1, 2, \dots, N.$$

By setting \mathbf{b} as described in the 11th cell of Table 8, the Equation (6.11) can be written in the form

$$(6.12) \quad K\boldsymbol{\lambda} = \mathbf{b}$$

The Equation (6.12) is solved using fast GMRES. We set $\epsilon = 10^{-6}$ and $\epsilon_{GMRES} = 10^{-10}$ and tabulate the memory, initialization time and solution time in Table 18 for all the nested algorithms. The relative error in solution (RE_{sol}) is of order 10^{-6} in all cases. We also plot the memory (Figure 17a), initialization time (Figure 17b) and solution time (Figure 17c) in Figure 17.

N	Memory (GB)					Initialization time (s)					Solution time (s)					#iter
	$\mathcal{H}_*^2(\mathbf{b}+\mathbf{t})$	$(\mathcal{H}^2 + \mathcal{H})_*$	$\mathcal{H}_{\sqrt{d}}^2(\mathbf{b})$	$\mathcal{H}_*^2(\mathbf{t})$	$\mathcal{H}_{\sqrt{d}}^2(\mathbf{t})$	$\mathcal{H}_*^2(\mathbf{b}+\mathbf{t})$	$(\mathcal{H}^2 + \mathcal{H})_*$	$\mathcal{H}_{\sqrt{d}}^2(\mathbf{b})$	$\mathcal{H}_*^2(\mathbf{t})$	$\mathcal{H}_{\sqrt{d}}^2(\mathbf{t})$	$\mathcal{H}_*^2(\mathbf{b}+\mathbf{t})$	$(\mathcal{H}^2 + \mathcal{H})_*$	$\mathcal{H}_{\sqrt{d}}^2(\mathbf{b})$	$\mathcal{H}_*^2(\mathbf{t})$	$\mathcal{H}_{\sqrt{d}}^2(\mathbf{t})$	
64000	0.69	0.69	0.79	0.76	0.79	26.25	25.12	30.32	27.86	39.97	1.03	1.11	1.57	1.14	1.56	34
125000	0.92	0.92	1.08	1.07	1.12	52.21	49.79	62.04	68.54	134.92	2.96	3.18	4.31	3.26	3.88	37
512000	7.53	7.65	8.73	8.39	9.02	243.02	205.45	277.25	417.53	562.48	12.11	17.06	20.98	14.49	19.02	42
1000000	7.79	8.69	9.81	9.59	11.01	326.58	288.06	382.72	828.57	1070.25	32.46	40.50	46.58	43.48	45.32	46
1728000	17.51	19.56	21.15	20.88	23.66	552.26	492.06	656.43	1754.62	1879.72	57.48	68.81	76.97	72.96	74.46	52

TABLE 18

Performance of the proposed and the nested algorithms as mentioned in Table 7. We set $\epsilon = 10^{-6}$ and $\epsilon_{GMRES} = 10^{-10}$.

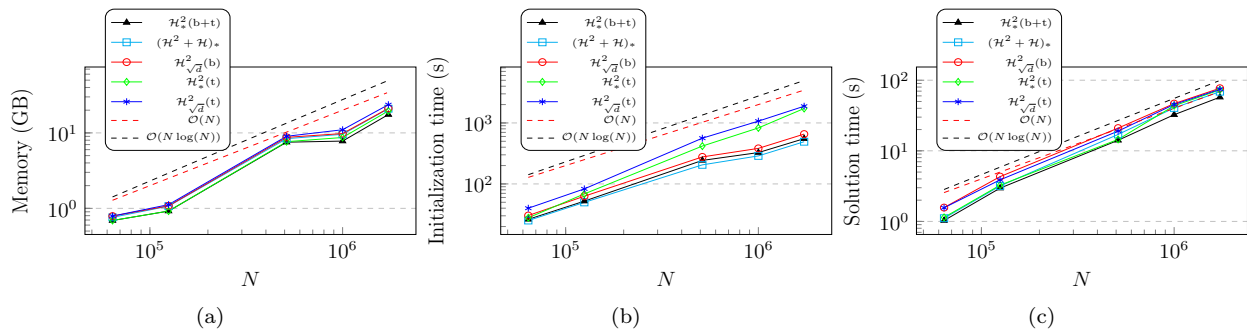


FIG. 17. Plots of Memory, Initialization time and Solution time of the fast MVP algorithms.

The kinks in the plots are due to the additional levels in the oct tree structure. We arrange the above algorithms in ascending order with respect to memory and solution time.

Memory: $\mathcal{H}_*^2(b+t) < (\mathcal{H}^2 + \mathcal{H})_* < \mathcal{H}_*^2(t) < \mathcal{H}_{\sqrt{d}}^2(b) < \mathcal{H}_{\sqrt{d}}^2(t)$

Solution time: $\mathcal{H}_*^2(b+t) < (\mathcal{H}^2 + \mathcal{H})_* < \mathcal{H}_*^2(t) < \mathcal{H}_{\sqrt{d}}^2(t) < \mathcal{H}_{\sqrt{d}}^2(b)$

Summary of the experiments in 3D. Here is a summary of the results obtained from all the experiments performed in 3D.

1. In all the experiments, the proposed $\mathcal{H}_*^2(b+t)$ outperforms all the other algebraic algorithms (Table 7) in terms of memory and MVP/Solution time. Also, the $\mathcal{H}_*^2(b+t)$ has the least initialization time among the fully nested algorithms. Hence, $\mathcal{H}_*^2(b+t)$ could be an attractive alternative to the standard \mathcal{H}^2 matrix algorithm.
2. The initialization time of the $\mathcal{H}_*^2(t)$ algorithm (Subsection 4.2) is the highest and the proposed $\mathcal{H}_*^2(b+t)$ performs way better than the $\mathcal{H}_*^2(t)$ algorithm.
3. Note that in 3D, the $(\mathcal{H}^2 + \mathcal{H})_*$, $\mathcal{H}_{\sqrt{d}}^2(b)$ and $\mathcal{H}_{\sqrt{d}}^2(t)$ exhibit similar scaling in memory. The numerical results demonstrate that the $(\mathcal{H}^2 + \mathcal{H})_*$ beats the $\mathcal{H}_{\sqrt{d}}^2(b)$ and $\mathcal{H}_{\sqrt{d}}^2(t)$ in terms of memory, initialization time and MVP/Solution time.

Therefore, in both 2D and 3D, the proposed $\mathcal{H}_*^2(b+t)$ algorithm outperforms the NCA-based standard \mathcal{H}^2 matrix algorithms [36] in the context of memory and MVP/Solution time. Also, in 3D, the proposed $(\mathcal{H}^2 + \mathcal{H})_*$ algorithm performs slightly better than the standard \mathcal{H}^2 matrix algorithms.

7. Conclusion. We have presented an efficient *nested* hierarchical matrix algorithm, $\mathcal{H}_*^2(b+t)$, and a *semi-nested* hierarchical matrix algorithm, $(\mathcal{H}^2 + \mathcal{H})_*$. In our proposed hierarchical matrix algorithms, the admissible clusters are the far-field and the vertex-sharing clusters. Due to the use of nested form of the bases, the computational cost is significantly reduced. We evaluate the performance of the proposed algorithms through extensive numerical experiments conducted in both 2D and 3D, which include time taken for various kernel MVPs and solving linear systems using the fast GMRES. We also compare the proposed algorithms with different related algebraic fast MVP algorithms and present various benchmarks. Notably, all these algorithms are developed purely algebraically, making them kernel-independent. To the best of our knowledge, this is the first work to study the performance analysis of a wide range of algebraic fast MVP algorithms in 2D and 3D. Numerical results show that the proposed algorithms are competitive with the standard \mathcal{H}^2 algorithm with respect to the memory and MVP time. Therefore, they could be an attractive alternative to the standard \mathcal{H}^2 matrix algorithm. Finally, we would like to release the implementation of the proposed algorithms made available at <https://github.com/riteshkhan/H2weak/>.

Acknowledgments. We acknowledge the use of the computing resources at HPCE, IIT Madras.

REFERENCES

- [1] S. AMBIKASARAN AND E. DARVE, *An $\mathcal{O}(N \log N)$ fast direct solver for partial hierarchically semi-separable matrices: With application to radial basis function interpolation*, Journal of Scientific Computing, 57 (2013), pp. 477–501.
- [2] S. AMBIKASARAN, K. R. SINGH, AND S. S. SANKARAN, *HODLRlib: A library for hierarchical matrices*, Journal of Open Source Software, 4 (2019), p. 1167.

- [3] J. BARNES AND P. HUT, *A hierarchical $O(N \log N)$ force-calculation algorithm*, nature, 324 (1986), pp. 446–449.
- [4] M. BEBENDORF, *Hierarchical Matrices: A Means to Efficiently Solve Elliptic Boundary Value Problems*, Springer, 2008.
- [5] M. BEBENDORF AND S. RJSANOW, *Adaptive low-rank approximation of collocation matrices*, Computing, 70 (2003), pp. 1–24.
- [6] M. BEBENDORF AND R. VENN, *Constructing nested bases approximations from the entries of non-local operators*, Numerische Mathematik, 121 (2012), pp. 609–635.
- [7] S. BÖRM, *Construction of data-sparse \mathcal{H}^2 -matrices by hierarchical compression*, SIAM Journal on Scientific Computing, 31 (2009), pp. 1820–1839.
- [8] S. BÖRM, L. GRASEDYCK, AND W. HACKBUSCH, *Hierarchical matrices*, Lecture notes, 21 (2003), p. 2003.
- [9] S. BÖRM, L. GRASEDYCK, AND W. HACKBUSCH, *Introduction to hierarchical matrices with applications*, Engineering analysis with boundary elements, 27 (2003), pp. 405–422.
- [10] M. BOZZINI, L. LENARDUZZI, M. ROSSINI, AND R. SCHABACK, *Interpolation with variably scaled kernels*, IMA Journal of Numerical Analysis, 35 (2015), pp. 199–219.
- [11] S. CHANDRASEKARAN, P. DEWILDE, M. GU, W. LYONS, AND T. PALS, *A fast solver for HSS representations via sparse matrices*, SIAM Journal on Matrix Analysis and Applications, 29 (2007), pp. 67–81.
- [12] S. CHANDRASEKARAN AND I. C. IPSEN, *On rank-revealing factorisations*, SIAM Journal on Matrix Analysis and Applications, 15 (1994), pp. 592–622.
- [13] W. FONG AND E. DARVE, *The black-box fast multipole method*, Journal of Computational Physics, 228 (2009), pp. 8712–8725.
- [14] A. GILLMAN, P. M. YOUNG, AND P.-G. MARTINSSON, *A direct solver with $O(N)$ complexity for integral equations on one-dimensional domains*, Frontiers of Mathematics in China, 7 (2012), pp. 217–247.
- [15] L. GRASEDYCK AND W. HACKBUSCH, *Construction and arithmetics of h -matrices*, Computing, 70 (2003), pp. 295–334.
- [16] A. GRAY AND A. MOORE, *N -body problems in statistical learning*, Advances in neural information processing systems, 13 (2000).
- [17] L. GREENGARD AND V. ROKHLIN, *A fast algorithm for particle simulations*, Journal of computational physics, 73 (1987), pp. 325–348.
- [18] L. GREENGARD AND V. ROKHLIN, *A new version of the fast multipole method for the laplace equation in three dimensions*, Acta numerica, 6 (1997), pp. 229–269.
- [19] V. GUJJULA AND S. AMBIKASARAN, *A new nested cross approximation*, arXiv preprint arXiv:2203.14832, (2022).
- [20] W. HACKBUSCH, *Hierarchical Matrices: Algorithms and Analysis*, vol. 49, Springer, 12 2015, <https://doi.org/10.1007/978-3-662-47324-5>.
- [21] W. HACKBUSCH, B. N. KHOROMSKIJ, AND R. KRIEMANN, *Hierarchical matrices based on a weak admissibility criterion*, Computing, 73 (2004), pp. 207–243.
- [22] N. HALKO, P.-G. MARTINSSON, AND J. A. TROPP, *Finding structure with randomness: Probabilistic algorithms for constructing approximate matrix decompositions*, SIAM review, 53 (2011), pp. 217–288.
- [23] K. L. HO AND L. YING, *Hierarchical interpolative factorization for elliptic operators: integral equations*, arXiv preprint arXiv:1307.2666, (2013).
- [24] V. A. KANDAPPAN, V. GUJJULA, AND S. AMBIKASARAN, *HODLR2D: A new class of hierarchical matrices*, SIAM Journal on Scientific Computing, 45 (2023), pp. A2382–A2408.
- [25] R. KHAN, V. A. KANDAPPAN, AND S. AMBIKASARAN, *HODLRdD: A new black-box fast algorithm for N -body problems in d -dimensions with guaranteed error bounds: Applications to integral equations and support vector machines*, Journal of Computational Physics, 501 (2024), p. 112786, <https://doi.org/10.1016/j.jcp.2024.112786>.
- [26] D. MALHOTRA AND G. BIROS, *Pvfm: A parallel kernel independent fmm for particle and volume potentials*, Communications in Computational Physics, 18 (2015), pp. 808–830.
- [27] S. MASSEI, L. ROBOL, AND D. KRESSNER, *Hierarchical adaptive low-rank format with applications to discretized partial differential equations*, Numerical Linear Algebra with Applications, 29 (2022), p. e2448.
- [28] C.-T. PAN, *On the existence and computation of rank-revealing lu factorizations*, Linear Algebra and its Applications, 316 (2000), pp. 199–222.
- [29] C. E. RASMUSSEN, *Gaussian Processes in Machine Learning*, Springer Berlin Heidelberg, Berlin, Heidelberg, 2004, pp. 63–71, https://doi.org/10.1007/978-3-540-28650-9_4.
- [30] Y. SAAD AND M. H. SCHULTZ, *Gmres: A generalized minimal residual algorithm for solving nonsymmetric linear systems*, SIAM Journal on scientific and statistical computing, 7 (1986), pp. 856–869.
- [31] A. K. SAIBABA, S. AMBIKASARAN, J. Y. LI, P. K. KITANIDIS, AND E. F. DARVE, *Application of hierarchical matrices to linear inverse problems in geostatistics*, Oil & Gas Science and Technology—Revue d’IFP Energies nouvelles, 67 (2012), pp. 857–875.
- [32] J. XIA, S. CHANDRASEKARAN, M. GU, AND X. S. LI, *Fast algorithms for hierarchically semiseparable matrices*, Numerical Linear Algebra with Applications, 17 (2010), pp. 953–976.
- [33] C. YANG, R. DURAISWAMI, N. A. GUMEROV, AND L. DAVIS, *Improved fast gauss transform and efficient kernel density estimation*, in Computer Vision, IEEE International Conference on, vol. 2, IEEE Computer Society, 2003, pp. 464–464.
- [34] L. YING, G. BIROS, AND D. ZORIN, *A kernel-independent adaptive fast multipole algorithm in two and three dimensions*, Journal of Computational Physics, 196 (2004), pp. 591–626.
- [35] R. YOKOTA, H. IBEID, AND D. KEYES, *Fast multipole method as a matrix-free hierarchical low-rank approximation*, in International Workshop on Eigenvalue Problems: Algorithms, Software and Applications in Petascale Computing, Springer, 2015, pp. 267–286.
- [36] Y. ZHAO, D. JIAO, AND J. MAO, *Fast nested cross approximation algorithm for solving large-scale electromagnetic problems*, IEEE Transactions on Microwave Theory and Techniques, 67 (2019), pp. 3271–3283.

Appendix A. Purely algebraic $\mathcal{H}_{\sqrt{d}}^2(\mathbf{b})$ algorithm [36, 19]. In this section, we discuss a purely algebraic standard \mathcal{H}^2 MVP algorithm. Since the construction of the standard \mathcal{H}^2 matrix representation is based on the B2T NCA, we denote this algorithm as $\mathcal{H}_{\sqrt{d}}^2(\mathbf{b})$. We discuss $\mathcal{H}_{\sqrt{d}}^2(\mathbf{b})$ MVP algorithm in two steps:

1. Initialization of $\mathcal{H}_{\sqrt{d}}^2(\mathbf{b})$ representation. (Appendix A.1)
2. Calculation of the potential (MVP). (Appendix A.2)

A.1. Initialization of $\mathcal{H}_{\sqrt{d}}^2(\mathbf{b})$ representation. In the B2T pivot selection, the pivots of a cluster at a parent level are obtained from the pivots at its child level. Therefore, one needs to traverse the 2^d uniform tree from bottom to top direction (starting at the leaf level) to find pivots of all clusters of the tree. The detailed procedure to obtain the four sets of pivots corresponding to a cluster X is given below.

- If X is a leaf cluster (childless), then construct the following four sets

$$(A.1) \quad \tilde{t}^{X,i} := t^X \quad \text{and} \quad \tilde{s}^{X,i} := \bigcup_{Y \in \mathcal{IL}_{\sqrt{d}}(X)} s^Y$$

$$(A.2) \quad \tilde{t}^{X,o} := \bigcup_{Y \in \mathcal{IL}_{\sqrt{d}}(X)} t^Y \quad \text{and} \quad \tilde{s}^{X,o} := s^X$$

- If X is a non-leaf cluster, then construct the following four sets

$$(A.3) \quad \tilde{t}^{X,i} := \bigcup_{X_c \in \text{child}(X)} t^{X_c,i} \quad \text{and} \quad \tilde{s}^{X,i} := \bigcup_{Y \in \mathcal{IL}_{\sqrt{d}}(X)} \bigcup_{Y_c \in \text{child}(Y)} s^{Y_c,o}$$

$$(A.4) \quad \tilde{t}^{X,o} := \bigcup_{Y \in \mathcal{IL}_{\sqrt{d}}(X)} \bigcup_{Y_c \in \text{child}(Y)} t^{Y_c,i} \quad \text{and} \quad \tilde{s}^{X,o} := \bigcup_{X_c \in \text{child}(X)} s^{X_c,o}$$

To obtain the pivots $t^{X,i}$, $s^{X,i}$, $t^{X,o}$ and $s^{X,o}$, one needs to perform ACA. We perform ACA on the matrix $K_{\tilde{t}^{X,i}, \tilde{s}^{X,i}}$ with user-given tolerance ϵ . The sets $t^{X,i}$ and $s^{X,i}$ are the row and column pivots chosen by the ACA. The search spaces of the pivots for a particular cluster are illustrated in Figure 18. Similarly, perform ACA on the matrix $K_{\tilde{t}^{X,o}, \tilde{s}^{X,o}}$ to obtain the other two sets of pivots $t^{X,o}$ and $s^{X,o}$.

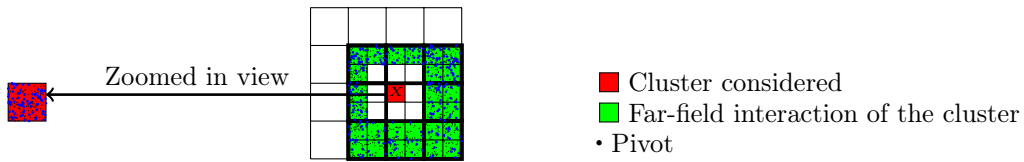


FIG. 18. Illustration of search spaces of the pivots in B2T NCA for $\mathcal{H}_{\sqrt{d}}^2(\mathbf{b})$ construction.

As we discussed before, these four sets are the main components for constructing the operators. We construct different operators as described in Subsection 3.6.4. Therefore, we get the following sets of operators:

1. P2M (V_X) / M2M ($\tilde{V}_{X X_c}$), $X_c \in \text{child}(X)$.
2. M2L ($T_{X,Y}$), $Y \in \mathcal{IL}_{\sqrt{d}}(X)$.
3. L2L ($\tilde{U}_{X_c X}$), $X \in \text{parent}(X_c)$ / L2P (U_X).

A.2. Calculation of the potential (MVP). The procedure to compute the potential is as follows:

1. **Upward traversal:**

- Particles to multipole (P2M) at leaf level κ : For all leaf clusters X , calculate $v_X^{(\kappa)} = V_X^* q_X^{(\kappa)}$

- Multipole to multipole (*M2M*) at non-leaf level : For all non-leaf X clusters, calculate

$$v_X^{(l)} = \sum_{X_c \in \text{child}(X)} \tilde{V}_{XX_c}^* v_{X_c}^{(l+1)}, \quad \kappa - 1 \geq l \geq 2$$
- 2. **Transverse traversal:**
 - Multipole to local (*M2L*) at all levels and for all clusters : For all cluster X , calculate

$$u_X^{(l)} = \sum_{Y \in \mathcal{IL}_{\sqrt{d}}(X)} T_{X,Y} v_Y^{(l)}, \quad 2 \leq l \leq \kappa$$
- 3. **Downward traversal:**
 - Local to local (*L2L*) at non-leaf level : For all non-leaf clusters X , calculate

$$u_{X_c}^{(l+1)} := u_{X_c}^{(l+1)} + \tilde{U}_{X_c X} u_X^{(l)}, \quad 2 \leq l \leq \kappa - 1 \text{ and } X \in \text{parent}(X_c)$$
 - Local to particles (*L2P*) at leaf level κ : For all leaf clusters X , calculate

$$\phi_X^{(\kappa)} = U_X u_X^{(\kappa)}$$

Near-field potential and the total potential at leaf level. For each leaf cluster X , we add the near-field (neighbor+self) potential, which is a direct computation. Hence, the final computed potential of a leaf cluster is given by

$$(A.5) \quad \phi_X^{(\kappa)} := \phi_X^{(\kappa)} + \underbrace{\sum_{X' \in \mathcal{N}_{\sqrt{d}}(X)} K_{tX, sX'} q_{X'}^{(\kappa)}}_{\text{Near-field potential (direct)}}$$

We know that X_i is the i^{th} leaf cluster and $\phi_{X_i}^{(\kappa)}$ represents the potential corresponding to it, $1 \leq i \leq 2^{d\kappa}$.

Therefore, the computed potential is given by $\tilde{\phi} = \left[\phi_{X_1}^{(\kappa)}; \phi_{X_2}^{(\kappa)}; \dots; \phi_{X_{2^{d\kappa}}}^{(\kappa)} \right]$ (MATLAB notation).

We refer the reader to Algorithm 2 of [36] and [19] for more details.

Appendix B. Purely algebraic $\mathcal{H}_{\sqrt{d}}^2(\mathbf{t})$ algorithm [36]. In this section, we discuss a purely algebraic standard \mathcal{H}^2 MVP algorithm. Since the construction of the standard \mathcal{H}^2 matrix representation is based on the T2B NCA, we denote this algorithm as $\mathcal{H}_{\sqrt{d}}^2(\mathbf{t})$. We discuss the $\mathcal{H}_{\sqrt{d}}^2(\mathbf{t})$ MVP algorithm in the following steps:

1. Initialization of $\mathcal{H}_{\sqrt{d}}^2(\mathbf{t})$ representation. (Appendix B.1)
2. Calculation of the potential (MVP). (Appendix B.2)

B.1. Initialization of $\mathcal{H}_{\sqrt{d}}^2(\mathbf{t})$ representation. In the T2B pivot selection, the pivots of a cluster at a child level are obtained from its own index set and the pivots at its parent level. Therefore, one needs to traverse the 2^d uniform tree from top to bottom direction to find pivots of all clusters. The detailed procedure to obtain the four sets of pivots corresponding to a cluster X is given below.

- If X has no parent, i.e., $\text{parent}(X) = \text{NULL}$ (parentless), then construct the following four sets

$$(B.1) \quad \tilde{t}^{X,i} := t^X \quad \text{and} \quad \tilde{s}^{X,i} := \bigcup_{Y \in \mathcal{IL}_{\sqrt{d}}(X)} s^Y$$

$$(B.2) \quad \tilde{t}^{X,o} := \bigcup_{Y \in \mathcal{IL}_{\sqrt{d}}(X)} t^Y \quad \text{and} \quad \tilde{s}^{X,o} := s^X$$

- If X has parent, i.e., $\text{parent}(X) \neq \text{NULL}$, then construct the following four sets

$$(B.3) \quad \tilde{t}^{X,i} := t^X \quad \text{and} \quad \tilde{s}^{X,i} := \bigcup_{Y \in \mathcal{IL}_{\sqrt{d}}(X)} s^Y \bigcup s^{\text{parent}(X),i}$$

$$(B.4) \quad \tilde{t}^{X,o} := \bigcup_{Y \in \mathcal{IL}_{\sqrt{d}}(X)} t^Y \bigcup t^{\text{parent}(X),o} \quad \text{and} \quad \tilde{s}^{X,o} := s^X$$

To obtain the pivots $t^{X,i}$, $s^{X,i}$, $t^{X,o}$ and $s^{X,o}$, one needs to perform ACA [5]. We perform ACA on the matrix $K_{\tilde{t}^{X,i}, \tilde{s}^{X,i}}$ with user-given tolerance ϵ . The sets $t^{X,i}$ and $s^{X,i}$ are the row and column pivots chosen by the ACA. The search spaces of the pivots for a particular cluster are illustrated in Figure 19. Similarly, perform ACA on the matrix $K_{\tilde{t}^{X,o}, \tilde{s}^{X,o}}$ to obtain the other two sets of pivots $t^{X,o}$ and $s^{X,o}$.

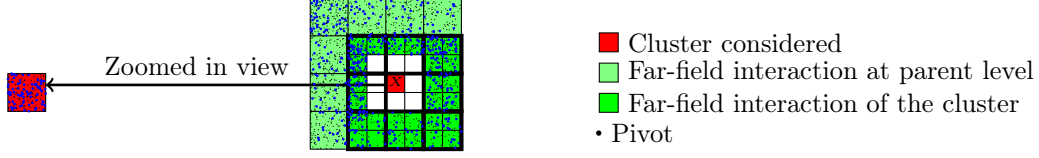


FIG. 19. Illustration of search spaces of the pivots in T2B NCA for $\mathcal{H}^2_{\sqrt{d}}(t)$ construction.

As discussed before, these four sets are the main components for constructing the operators. We construct different operators as described in Subsection 3.6.4. Therefore, we get the following sets of operators:

1. P2M (V_X) / M2M (\tilde{V}_{XX_c}), $X_c \in \text{child}(X)$.
2. M2L ($T_{X,Y}$), $Y \in \mathcal{IL}_{\sqrt{d}}(X)$.
3. L2L ($\tilde{U}_{X_c X}$), $X \in \text{parent}(X_c)$ / L2P (U_X).

B.2. Calculation of the potential (MVP). We perform the potential (MVP) calculation by following upward, transverse and downward tree traversal, which is similar to Appendix A.2.

We refer the reader to Algorithm 1 of [36] for more details.

Appendix C. $\mathcal{H}_*^2(\mathbf{t})$: T2B NCA on our *weak admissibility* condition. This section discusses a fast MVP algorithm when applying the T2B NCA on our *weak admissibility* condition in higher dimensions (Subsection 3.5), i.e., the admissible clusters are the far-field and vertex-sharing clusters. We denote this algorithm as $\mathcal{H}_*^2(\mathbf{t})$. We discuss the $\mathcal{H}_*^2(\mathbf{t})$ algorithm in the following steps:

1. Initialization of $\mathcal{H}_*^2(\mathbf{t})$ representation. (Appendix C.1)
2. Calculation of the potential (MVP). (Appendix C.2)

C.1. Initialization of $\mathcal{H}_*^2(\mathbf{t})$ representation. In the T2B pivot selection, the pivots of a cluster at a child level are obtained from its own index set and the pivots at its parent level. Therefore, one needs to traverse the 2^d uniform tree from top to bottom direction to find pivots of all clusters. The detailed procedure to obtain the pivots corresponding to a cluster X is given below.

- If X has no parent, i.e., $\text{parent}(X) = \text{NULL}$ (parentless), then construct the following four sets

$$(C.1) \quad \tilde{t}^{X,i} := t^X \quad \text{and} \quad \tilde{s}^{X,i} := \bigcup_{Y \in \mathcal{IL}_*(X)} s^Y$$

$$(C.2) \quad \tilde{t}^{X,o} := \bigcup_{Y \in \mathcal{IL}_*(X)} t^Y \quad \text{and} \quad \tilde{s}^{X,o} := s^X$$

- If X has parent, i.e., $\text{parent}(X) \neq \text{NULL}$, then construct the following four sets

$$(C.3) \quad \tilde{t}^{X,i} := t^X \quad \text{and} \quad \tilde{s}^{X,i} := \bigcup_{Y \in \mathcal{IL}_*(X)} s^Y \bigcup s^{\text{parent}(X),i}$$

$$(C.4) \quad \tilde{t}^{X,o} := \bigcup_{Y \in \mathcal{IL}_*(X)} t^Y \bigcup t^{\text{parent}(X),o} \quad \text{and} \quad \tilde{s}^{X,o} := s^X$$

To obtain the pivots $t^{X,i}$, $s^{X,i}$, $t^{X,o}$ and $s^{X,o}$, one needs to perform ACA [5]. We perform ACA on the matrix $K_{\tilde{t}^{X,i}, \tilde{s}^{X,i}}$ with user-given tolerance ϵ . The sets $t^{X,i}$ and $s^{X,i}$ are the row and column pivots chosen

by the ACA. The search spaces of the pivots for a particular cluster are illustrated in [Figure 8](#). Similarly, perform ACA on the matrix $K_{\tilde{t}^{X,o}, \tilde{s}^{X,o}}$ to obtain the other two sets of pivots $t^{X,o}$ and $s^{X,o}$.

These four sets are the main components for constructing the operators. We construct different operators as described in [Subsection 3.6.4](#). Therefore, we get the following sets of operators:

1. P2M (V_X) / M2M ($\tilde{V}_{X X_c}$), $X_c \in \text{child}(X)$.
2. M2L ($T_{X,Y}$), $Y \in \mathcal{IL}_*(X)$.
3. L2L ($\tilde{U}_{X_c X}$), $X \in \text{parent}(X_c)$ / L2P (U_X).

C.2. Calculation of the potential (MVP). The procedure to compute the potential is as follows:

1. **Upward traversal:**

- Particles to multipole (*P2M*) at leaf level κ : For all leaf clusters X , calculate $v_X^{(\kappa)} = V_X^* q_X^{(\kappa)}$
- Multipole to multipole (*M2M*) at non-leaf level : For all non-leaf X clusters, calculate $v_X^{(l)} = \sum_{X_c \in \text{child}(X)} \tilde{V}_{X X_c}^* v_{X_c}^{(l+1)}$, $\kappa - 1 \geq l \geq 1$

2. **Transverse traversal:**

- Multipole to local (*M2L*) at all levels and for all clusters : For all cluster X , calculate $u_X^{(l)} = \sum_{Y \in \mathcal{IL}_*(X)} T_{X,Y} v_Y^{(l)}$, $1 \leq l \leq \kappa$

3. **Downward traversal:**

- Local to local (*L2L*) at non-leaf level : For all non-leaf clusters X , calculate $u_{X_c}^{(l+1)} := u_{X_c}^{(l+1)} + \tilde{U}_{X_c X} u_X^{(l)}$, $1 \leq l \leq \kappa - 1$ and $X \in \text{parent}(X_c)$
- Local to particles (*L2P*) at leaf level κ : For all leaf clusters X , calculate $\phi_X^{(\kappa)} = U_X u_X^{(\kappa)}$

Near-field potential and the total potential at leaf level. For each leaf cluster X , we add the near-field (neighbor+self) potential, which is a direct computation. Hence, the final computed potential of a leaf cluster is given by

$$(C.5) \quad \phi_X^{(\kappa)} := \phi_X^{(\kappa)} + \underbrace{\sum_{X' \in \mathcal{N}_*(X)} K_{t^{X,o}, s^{X',o}} q_{X'}^{(\kappa)}}_{\text{Near-field potential (direct)}}$$

We know that X_i is the i^{th} leaf cluster and $\phi_{X_i}^{(\kappa)}$ represents the potential corresponding to it, $1 \leq i \leq 2^{d\kappa}$.

Therefore, the computed potential is given by $\tilde{\phi} = \left[\phi_{X_1}^{(\kappa)}; \phi_{X_2}^{(\kappa)}; \dots; \phi_{X_{2^{d\kappa}}}^{(\kappa)} \right]$ (MATLAB notation). The visual representation of the $\mathcal{H}_*^2(t)$ algorithm is given in [Figure 20](#).

$$\tilde{\phi} = \left(\begin{array}{c} \text{Matrix 1} \\ \text{Matrix 2} \end{array} \right) + \left(\text{Matrix 3} \right) \times \mathbf{q}$$

FIG. 20. In the $\mathcal{H}_*^2(t)$ algorithm, the operators (*P2M/M2M*, *M2L* and *L2L/L2P*) are constructed using *T2B NCA*. After that, we calculate the potential using *Upward*, *Transverse* and *Downward tree traversal*. The near-field potential is added at the leaf level.

Appendix D. Additional experiments in 3D. In this section, we perform additional experiments using different kernel matrices and compare the performance of the proposed algorithms with the standard \mathcal{H}^2 matrix algorithm [36].

D.1. Fast MVP with different kernel functions. We consider N uniformly distributed particles with location at $\{\mathbf{x}_i\}_{i=1}^N$ in the cube $[-1, 1]^3$. The kernel matrix (K) is generated by the Matérn covariance kernel and Helmholtz kernel. The fast MVP ($\tilde{K}\mathbf{q}$) is performed using different nested hierarchical representations (refer to Table 7).

D.1.1. Matérn covariance kernel with $\nu = 1/2$. We choose the kernel function as the Matérn covariance kernel. The $(i, j)^{th}$ entry of the kernel matrix $K \in \mathbb{R}^{N \times N}$ is given by

$$(D.1) \quad K(i, j) = \exp(-r) = \exp(-\|\mathbf{x}_i - \mathbf{x}_j\|_2)$$

We randomly select 5 different column vectors (\mathbf{q}) and perform the fast MVPs ($\tilde{K}\mathbf{q}$) using $\mathcal{H}_*^2(\text{b+t})$, $(\mathcal{H}^2 + \mathcal{H})_*$, $\mathcal{H}_{\sqrt{d}}^2(\text{b})$, $\mathcal{H}_*^2(\text{t})$ and $\mathcal{H}_{\sqrt{d}}^2(\text{t})$ algorithms. The average initialization time, MVP time, memory and relative error in MVP (RE_{MVP}) are tabulated in Table 19 and Table 20. We also plot the initialization time (Figure 21a), MVP time (Figure 21b), total time (Figure 22a) and memory (Figure 22b). Please refer to Figure 21 and Figure 22.

N	Initialization time (s)					MVP time (s)				
	$\mathcal{H}_*^2(\text{b+t})$	$(\mathcal{H}^2 + \mathcal{H})_*$	$\mathcal{H}_{\sqrt{d}}^2(\text{b})$	$\mathcal{H}_*^2(\text{t})$	$\mathcal{H}_{\sqrt{d}}^2(\text{t})$	$\mathcal{H}_*^2(\text{b+t})$	$(\mathcal{H}^2 + \mathcal{H})_*$	$\mathcal{H}_{\sqrt{d}}^2(\text{b})$	$\mathcal{H}_*^2(\text{t})$	$\mathcal{H}_{\sqrt{d}}^2(\text{t})$
64000	12.04	10.18	16.59	25.15	25.59	0.09	0.09	0.12	0.09	0.11
125000	35.65	30.77	41.58	60.64	57.17	0.22	0.25	0.3	0.24	0.32
512000	195.09	159.19	226.98	448.17	439.29	0.92	1.06	1.25	1.01	1.31
1000000	452.44	385.12	510.36	911.33	879.86	1.85	2.17	2.75	2.15	2.66
1728000	844.16	688.95	958.17	1738.65	1635.63	3.01	3.84	5.78	3.98	5.03

TABLE 19

Performance of the proposed and the nested algorithms as mentioned in Table 7 in terms of the initialization time and MVP time.

N	Memory (GB)					Relative error in MVP (2-norm)				
	$\mathcal{H}_*^2(\text{b+t})$	$(\mathcal{H}^2 + \mathcal{H})_*$	$\mathcal{H}_{\sqrt{d}}^2(\text{b})$	$\mathcal{H}_*^2(\text{t})$	$\mathcal{H}_{\sqrt{d}}^2(\text{t})$	$\mathcal{H}_*^2(\text{b+t})$	$(\mathcal{H}^2 + \mathcal{H})_*$	$\mathcal{H}_{\sqrt{d}}^2(\text{b})$	$\mathcal{H}_*^2(\text{t})$	$\mathcal{H}_{\sqrt{d}}^2(\text{t})$
64000	1.84	1.98	2.21	2.17	2.2	8.13E-07	5.78E-07	4.93E-07	1.10E-06	5.64E-07
125000	3.63	4.07	4.48	4.08	4.48	1.53E-06	7.32E-07	7.89E-07	2.20E-06	8.62E-07
512000	17.56	20.08	21.92	21.89	22.31	2.32E-06	1.10E-06	1.01E-06	3.39E-06	1.13E-06
1000000	33.3	39.83	42.49	42.44	42.51	3.35E-06	1.35E-06	1.34E-06	5.47E-06	1.19E-06
1728000	64.87	77.03	83.12	83.05	83.34	3.86E-06	1.28E-06	1.31E-06	6.23E-06	1.73E-06

TABLE 20

Performance of the proposed and the nested algorithms as mentioned in Table 7 in terms of the memory and relative error. We set the tolerance $\epsilon = 10^{-6}$.

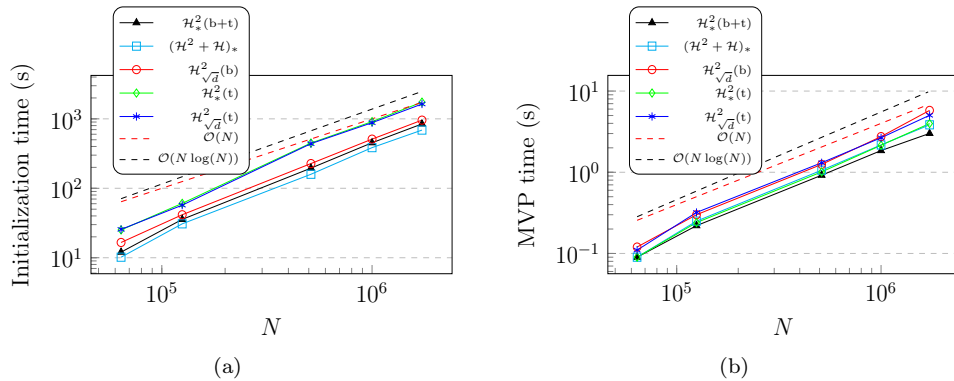


FIG. 21. Plots of Initialization time and MVP time of different fast MVP algorithms.

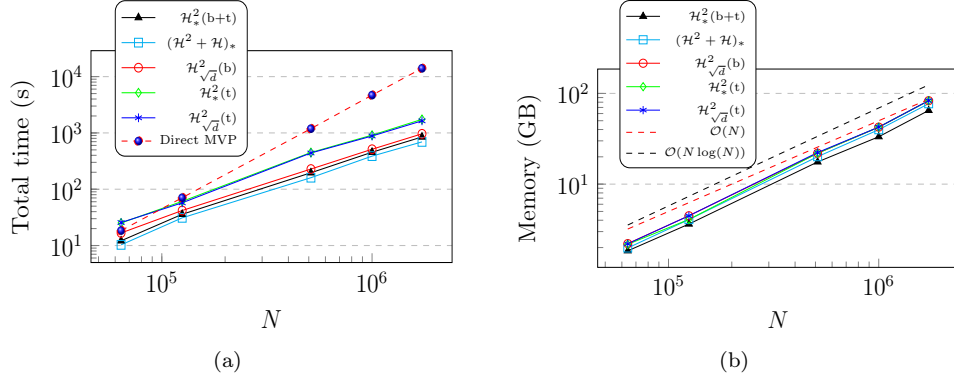


FIG. 22. Plots of total time ($t_{init} + t_{MVP}$) and memory of the algorithms. We also plot the time for Direct MVP.

Let us arrange the above algorithms in ascending order with respect to memory and MVP time.

Memory: $\mathcal{H}_*^2(\text{b+t}) < (\mathcal{H}^2 + \mathcal{H})_* < \mathcal{H}_*^2(\text{t}) < \mathcal{H}_{\sqrt{d}}^2(\text{b}) \leq \mathcal{H}_{\sqrt{d}}^2(\text{t})$

MVP time: $\mathcal{H}_*^2(\text{b+t}) < (\mathcal{H}^2 + \mathcal{H})_* < \mathcal{H}_*^2(\text{t}) < \mathcal{H}_{\sqrt{d}}^2(\text{t}) < \mathcal{H}_{\sqrt{d}}^2(\text{b})$

D.1.2. 3D Helmholtz kernel with $k = 1$. We choose the kernel function as the Helmholtz kernel with wave number $k = 1$. The $(\alpha, \beta)^{th}$ entry of the kernel matrix $K \in \mathbb{C}^{N \times N}$ is given by

$$(D.2) \quad K(\alpha, \beta) = \begin{cases} \frac{\exp(ir)}{r} = \frac{\exp(i \|\mathbf{x}_\alpha - \mathbf{x}_\beta\|_2)}{\|\mathbf{x}_\alpha - \mathbf{x}_\beta\|_2} & \text{if } \alpha \neq \beta \\ 0 & \text{otherwise} \end{cases}$$

We randomly select 5 different column vectors (\mathbf{q}) and perform the fast MVPs ($\tilde{K}\mathbf{q}$) using $\mathcal{H}_*^2(\text{b+t})$, $(\mathcal{H}^2 + \mathcal{H})_*$, $\mathcal{H}_{\sqrt{d}}^2(\text{b})$, $\mathcal{H}_*^2(\text{t})$ and $\mathcal{H}_{\sqrt{d}}^2(\text{t})$ algorithms. The average initialization time, MVP time, memory and relative error in MVP (RE_{MVP}) are tabulated in Table 21 and Table 22. We also plot the initialization time (Figure 23a), MVP time (Figure 23b), total time (Figure 24a) and memory (Figure 24b). Please refer to Figure 23 and Figure 24.

N	Initialization time (s)					MVP time (s)				
	$\mathcal{H}_*^2(\text{b+t})$	$(\mathcal{H}^2 + \mathcal{H})_*$	$\mathcal{H}_{\sqrt{d}}^2(\text{b})$	$\mathcal{H}_*^2(\text{t})$	$\mathcal{H}_{\sqrt{d}}^2(\text{t})$	$\mathcal{H}_*^2(\text{b+t})$	$(\mathcal{H}^2 + \mathcal{H})_*$	$\mathcal{H}_{\sqrt{d}}^2(\text{b})$	$\mathcal{H}_*^2(\text{t})$	$\mathcal{H}_{\sqrt{d}}^2(\text{t})$
27000	10.47	10.12	11.22	13.44	13.26	0.11	0.12	0.11	0.11	0.13
64000	38.65	32.55	40.33	57.54	56.29	0.31	0.38	0.35	0.32	0.43
125000	95.82	88.65	108.59	176.07	168.23	0.65	0.74	0.73	0.75	1.01
512000	640.44	630.25	665.35	1295.68	1219.55	2.51	3.28	3.31	3.25	4.45
1000000	1418.08	1355.88	-	3208.47	-	5.47	7.85	-	6.98	-

TABLE 21

Performance of the proposed and the nested algorithms as mentioned in Table 7 in terms of the initialization time and MVP time.

N	Memory (GB)					Relative error in MVP (2-norm)				
	$\mathcal{H}_*^2(\text{b+t})$	$(\mathcal{H}^2 + \mathcal{H})_*$	$\mathcal{H}_{\sqrt{d}}^2(\text{b})$	$\mathcal{H}_*^2(\text{t})$	$\mathcal{H}_{\sqrt{d}}^2(\text{t})$	$\mathcal{H}_*^2(\text{b+t})$	$(\mathcal{H}^2 + \mathcal{H})_*$	$\mathcal{H}_{\sqrt{d}}^2(\text{b})$	$\mathcal{H}_*^2(\text{t})$	$\mathcal{H}_{\sqrt{d}}^2(\text{t})$
27000	0.66	0.73	0.79	0.66	0.78	5.60E-07	3.26E-07	3.77E-07	8.42E-07	3.41E-07
64000	2.06	2.27	2.48	2.15	2.48	1.25E-06	6.64E-07	5.84E-07	1.74E-06	7.03E-07
125000	4.2	4.75	5.09	4.46	5.08	3.09E-06	8.26E-07	1.02E-06	3.32E-06	1.11E-06
512000	22.75	25.94	28.74	25.35	28.48	4.07E-06	9.99E-07	1.45E-06	6.11E-06	1.34E-06
1000000	43.41	51.12	-	48.45	-	7.19E-06	1.09E-06	-	1.74E-05	-

TABLE 22

Performance of the proposed and the nested algorithms as mentioned in Table 7 in terms of the memory and relative error. We set the tolerance $\epsilon = 10^{-6}$.

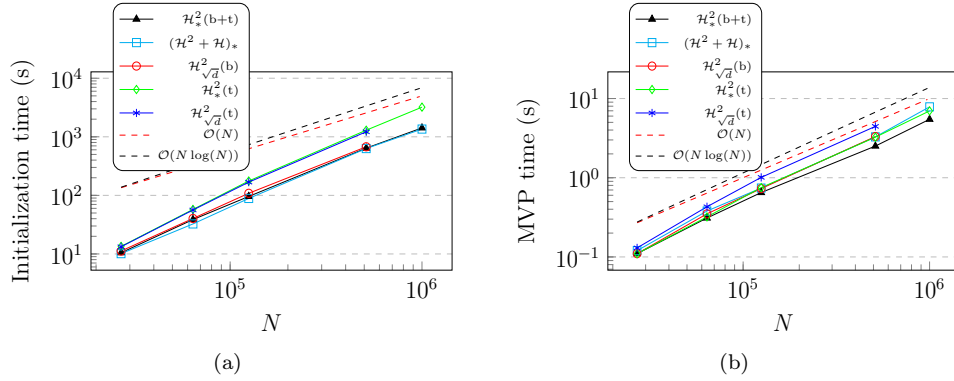
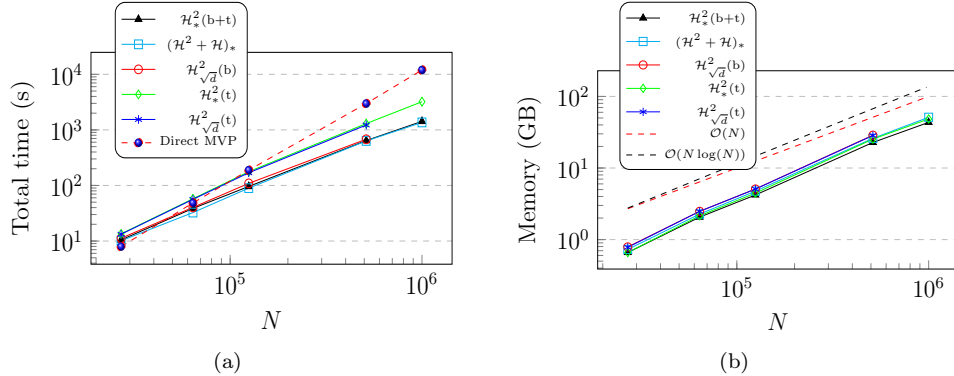


FIG. 23. Plots of Initialization time and MVP time of different fast MVP algorithms.


 FIG. 24. Plots of total time ($t_{init} + t_{MVP}$) and memory of the algorithms. We also plot the time for Direct MVP.

We arrange the above algorithms in ascending order with respect to memory and MVP time.

Memory: $\mathcal{H}_*^2(\text{b+t}) < \mathcal{H}_*^2(\text{t}) < (\mathcal{H}^2 + \mathcal{H})_* < \mathcal{H}_{\sqrt{d}}^2(\text{b}) \leq \mathcal{H}_{\sqrt{d}}^2(\text{t})$

MVP time: $\mathcal{H}_*^2(\text{b+t}) < \mathcal{H}_*^2(\text{t}) < (\mathcal{H}^2 + \mathcal{H})_* < \mathcal{H}_{\sqrt{d}}^2(\text{b}) < \mathcal{H}_{\sqrt{d}}^2(\text{t})$

D.1.3. Fast MVP accelerated GMRES for RBF interpolation. Let the location of the particles $\{\mathbf{x}_i\}_{i=1}^N$ be the $N^{1/3} \times N^{1/3} \times N^{1/3}$ Chebyshev grid on the domain $[-1, 1]^3$. We consider the Chebyshev distribution of particles to study the performance of the nested algorithms over slightly non-uniformly distributed particles. However, we use the uniform 2^d tree (oct tree in 3D) as described in Subsection 3.1.

Let us consider the following radial basis function

$$(D.3) \quad G(r) = \begin{cases} \log r & \text{if } r \geq a \\ \frac{\log a}{r \log r - 1} & \text{if } r < a \end{cases}$$

Consider the linear system (Equation (D.4)) generated by the above kernel function G

$$(D.4) \quad \alpha \lambda_i + \sum_{j=1, j \neq i}^N G(\|\mathbf{x}_i - \mathbf{x}_j\|_2) \lambda_j = b_i, \quad i = 1, 2, \dots, N.$$

We set $a = 0.0001$ and $\alpha = \sqrt{N}$. By setting \mathbf{b} as described in the 11th cell of Table 8, the Equation (D.4) can be written in the form

$$(D.5) \quad K\lambda = \mathbf{b}$$

The Equation (D.5) is solved using **fast** GMRES. We set $\epsilon = 10^{-6}$ and $\epsilon_{GMRES} = 10^{-10}$ and tabulate the memory, initialization time and solution time in Table 23 for all the nested algorithms. The relative error in solution (RE_{sol}) is of order 10^{-6} in all cases. We also plot the memory (Figure 25a), initialization time (Figure 25b) and solution time (Figure 25c) in Figure 25.

N	Memory (GB)					Initialization time (s)					Solution time (s)					#iter
	$\mathcal{H}_*^2(\mathbf{b}+\mathbf{t})$	$(\mathcal{H}^2 + \mathcal{H})_*$	$\mathcal{H}_{\sqrt{d}}^2(\mathbf{b})$	$\mathcal{H}_*^2(\mathbf{t})$	$\mathcal{H}_{\sqrt{d}}^2(\mathbf{t})$	$\mathcal{H}_*^2(\mathbf{b}+\mathbf{t})$	$(\mathcal{H}^2 + \mathcal{H})_*$	$\mathcal{H}_{\sqrt{d}}^2(\mathbf{b})$	$\mathcal{H}_*^2(\mathbf{t})$	$\mathcal{H}_{\sqrt{d}}^2(\mathbf{t})$	$\mathcal{H}_*^2(\mathbf{b}+\mathbf{t})$	$(\mathcal{H}^2 + \mathcal{H})_*$	$\mathcal{H}_{\sqrt{d}}^2(\mathbf{b})$	$\mathcal{H}_*^2(\mathbf{t})$	$\mathcal{H}_{\sqrt{d}}^2(\mathbf{t})$	
64000	1.34	1.45	1.5	1.42	1.51	14.58	15.57	25.81	30.06	25.93	1.01	1.08	2.09	1.32	1.89	
125000	2.68	2.94	3.05	2.96	3.05	35.24	36.98	66.85	91.65	77.34	2.88	2.98	5.74	4.4	5.46	
512000	16.5	18.15	19.4	18.91	19.54	232.01	201.11	431.82	615.79	534.27	15.8	17.25	39.32	25.48	41.97	
1000000	29.85	33.85	36.55	35.95	36.60	613.21	502.63	1011.81	1709.84	1445.45	39.51	45.58	76.31	61.29	78.07	
1728000	57.15	64.87	69.62	69.23	70.13	1038.16	901.72	1641.97	3490.25	2867.08	74.86	82.02	142.17	122.08	145.93	

TABLE 23

Performance of the proposed and the nested algorithms as mentioned in Table 7. We set $\epsilon = 10^{-6}$ and $\epsilon_{GMRES} = 10^{-10}$.

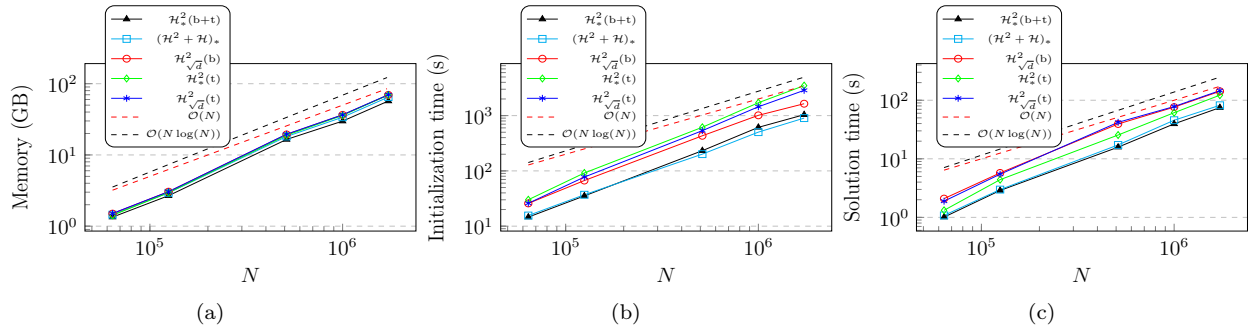


FIG. 25. Plots of Memory, Initialization time and Solution time of the fast MVP algorithms.

We arrange the above algorithms in ascending order with respect to memory and solution time.

Memory: $\mathcal{H}_*^2(\mathbf{b}+\mathbf{t}) < (\mathcal{H}^2 + \mathcal{H})_* < \mathcal{H}_*^2(\mathbf{t}) < \mathcal{H}_{\sqrt{d}}^2(\mathbf{b}) \leq \mathcal{H}_{\sqrt{d}}^2(\mathbf{t})$

Solution time: $\mathcal{H}_*^2(\mathbf{b}+\mathbf{t}) < (\mathcal{H}^2 + \mathcal{H})_* < \mathcal{H}_*^2(\mathbf{t}) < \mathcal{H}_{\sqrt{d}}^2(\mathbf{b}) < \mathcal{H}_{\sqrt{d}}^2(\mathbf{t})$

In all the experiments, the proposed $\mathcal{H}_*^2(\mathbf{b}+\mathbf{t})$ algorithm outperforms the NCA-based standard \mathcal{H}^2 matrix algorithms [36] in the context of memory and MVP/Solution time. Also, $\mathcal{H}_*^2(\mathbf{b}+\mathbf{t})$ has the least initialization time among the fully nested algorithms. Therefore, the proposed $\mathcal{H}_*^2(\mathbf{b}+\mathbf{t})$ could be an attractive alternative to the standard \mathcal{H}^2 matrix algorithms. Additionally, in 3D, the proposed $(\mathcal{H}^2 + \mathcal{H})_*$ algorithm performs slightly better than the standard \mathcal{H}^2 matrix algorithms.